EFFECTS OF CHANGING RCS AND ANTENNA ARRAY PATTERN ON RADAR PERFORMANCE

Submitted By

Major Mohammad Ali Khan, Student No - 200716011
Afia Binte Rahman, Student No - 200816026
Jannatul Fardous Popy, Student No - 200816035

Supervised By

Wg Cdr Dr. Mohammed Hossam-E-Haider

Department of Electrical, Electronics and Communication Engineering (EECE)
MILITARY INSTITUTE OF SCIENCE AND TECHNOLOGY (MIST)
Mirpur Cantonment, Dhaka-1216.

EFFECTS OF CHANGING RCS AND ANTENNA ARRAY PATTERN ON RADAR PERFORMANCE

This thesis is submitted to the Department of Electrical, Electronic and Communication Engineering (EECE) of MILITARY INSTITUTE OF SCIENCE AND TECHNOLOGY (MIST), Mirpur Cantonment, Dhaka – 1216 for partial fulfillment of the requirements for the degree of B.Sc. in Electrical, Electronic & Communication Engineering.

Submitted By

Major Mohammad Ali Khan, Student No - 200716011
Afia Binte Rahman, Student No - 200816026
Jannatul Fardous Popy, Student No - 200816035

Supervised By

Wg Cdr Dr. Mohammed Hossam-E-Haider
Instructor Class - A
Department of Electrical, Electronic and Communication Engineering
Military Institute of Science and Technology
Mirpur Cantonment, Dhaka-1216.

December 2011

Department of Electrical, Electronics and Communication Engineering (EECE)
MILITARY INSTITUTE OF SCIENCE AND TECHNOLOGY (MIST)
Mirpur Cantonment, Dhaka-1216.

CERTIFICATION

The thesis titled "EFFECTS OF CHANGING RCS AND ANTENNA ARRAY PATTERN ON RADAR PERFORMANCE." is submitted by the group as under mentioned has been accepted as satisfactory in partial fulfillment of the requirement for the degree of Bachelor of Science in Electrical, Electronic and Communication Engineering on December 2011.

Group Members

Major Mohammad Ali Khan

Afia Binte Rahman

Jannatul Fardous Popy

Supervisor

Wg Cdr Dr. Mohammed Hossam-E-Haider

Instructor Class - A

Department of Electrical, Electronic and Communication Engineering (EECE)

Military Institute of Science and Technology

Mirpur Cantonment, Dhaka-1216.

DECLARATION

This is to certify that, the work presented in this thesis is the outcome of the investigation carried out by the following students under the supervision of Wg Cdr Dr. Mohammed Hossam-E-Haider, Instructor Class–A, Department of Electrical Electronic and communication Engineering (EECE), Military Institute of Science and Technology (MIST)

It is also declared that neither of this paper nor any part therefore has been submitted anywhere else for the award of any degree, diploma or other qualifications.

———————————————
Major Mohammad Ali Khan

———————————————
Afia Binte Rahman

———————————————
Jannatul Fardous Popy

ACKNOWLEDGEMENT

ABSTRACT

Radio Detection and Ranging (RADAR) is totally a matter of technology and engineering with immense practical consequences. Because of radar, astronomers can map the contours of far-off planets, physicians can see images of internal organs, meteorologists can measure rain falling in distant places, air travel is hundreds of times safer than travel by road. Due to its reasonably larger practical applications, the mono-static pulse radar system is the main focus of our thesis.

The main goal of this thesis was to carry out a detail study of the basic nature of the mono-static pulse radar system with an aim to find out its performance under changing radar cross section and antenna configurations. In this regard, various radar parameters were taken into consideration, their effects on radar performance were simulated and best option was identified.

Thereafter, the significant affect of shape changes of elementary static target cross sections were studied with a small introduction to complex target RCS. The significance of operating frequency and aspect angle on radar detection range has also been illustrated.

The effect of earth and atmosphere on the wave propagation has been calculated in order to provide a reliable prediction method under the adverse atmospheric effects.

An elaborate and exhaustive effort is taken to examine various antenna patterns to suggest the best possible array antenna configuration for better radar performance.

In this regard, various correlated mathematical equations were taken into consideration; those were simulated using MATLAB to provide relevant plots for study. The extensive use of this tool has made the thesis extremely interesting with valuable results drawing important conclusions about the behavior of radar under changing conditions.

Table of Contents

Chapter 1: Introduction

1.1 Radar in General

1.2 Continuous Wave (CW) and Pulsed Radars

1.3 Radar Terminologies

1.4 Radar Losses

Chapter 6: Conclusion and Future Work

LIST OF FIGURES

Chapter 03

LIST OF TABLES

LIST OF ABBREVIATIONS

RADAR   Radio Detection and Ranging

CW   Continuous Wave

PRF   Pulse Repetition Frequency

PRI   Pulse Repetition Interval

IPP   Inter Pulse Period

SNR   Signal to Noise Ratio

CI   Coherent Integration

NCI   Non-coherent Integration

dB   Decibel

SSJ   Self-screening Jammers

SOJ   Stand-off Jammers

RRF   Range Reduction Factor

RCS   Radar Cross Section

IEEE   Institute of Electrical and Electronic Engineering

AF   Array Factor

DFT   Discrete Fourier Transform

PP   Principle Polarization

OP   Orthogonal polarization

Chapter 1

INTRODUCTION

1.1 Radar in General

1.1.1 Definition and Basic Principle

The word RADAR stands for Radio Detection and Ranging. From the name itself we can define radar as an electromagnetic device that can detect an object at long ranges and determine its specific location.

The transmitter part of the device radiates electromagnetic energy in space, a portion of which after being reflected from the target is received as an echo signal by the receiver part of the device. This small echo signal along with noise is processed by high sensitivity signal processor to determine the exact location, range, velocity, angular position, size and other information varying according to the type of Radar used. The most important functions that radar can perform are

- Resolution
- Detection
- Measurement

Resolution corresponds to radar's ability to resolve (separate) one target signal from another. Larger bandwidths give better resolution in the range parameter, while long transmitted pulses give better resolution in frequency.

Detection function is the ability of the radar to be able to sense the presence of the reflected target signal in the radar receiver. The function is complicated by the unwanted reflected signal (clutter) and the receiver noise.

- Noise is reduced by better receiver design and transmitting signals with larger energy per pulse.
- Clutter is reduced by proper signal design and appropriate signal-processing methods.

Modern radars measures much more than radial range; they measure a targets position in 3-D space, its velocity vector, angular direction, and vector angular velocity. Advanced radars even can measure target extent (size), shape, and classification (truck, tank etc.). With the advancement of technology classification of target may become the fourth most important function of radar.

The basic principle of the mono-static radar is illustrated in Figure 1.1 where the transmitter and the receiver are in same place. In fact the transmitting and the receiving parts may remain separated (bi-static) as we will see later on.
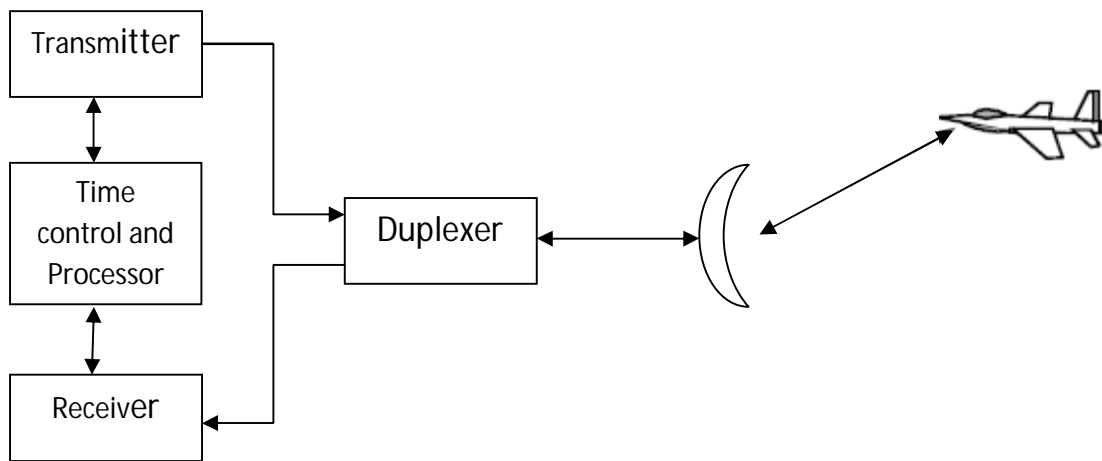
Figure 1.1: Mono-static Radar Block Diagram (Pulsed radar system)

1.1.2 History

The history of radar starts with experiments by Heinrich Hertz in the late 19th century that showed that radio waves were reflected by metallic objects. This possibility was suggested in James Clerk Maxwell's seminal work on electromagnetism.

However, it was not until the early 20th century that systems able to use these principles were becoming widely available, and it was German engineer Christian Huelsmeyer who first used them to build a simple ship detection device intended to help avoid collisions in fog.

Numerous similar systems were developed over the next two decades. Extensive development of radar took place during the two world wars.

1.1.3 Classification

According to the configuration variations radars can be classified as following:

- Mono-static and Bi-static radars.
- Continuous-wave radar.
- Doppler radar.
- FM-CW radar
- Mono-pulse radar.
- Passive radar.
- Planar array radar.
- Pulse-Doppler.
- Synthetic aperture radar.

According to Function radars can be further classified as following:

- Detection and Search radars
- Targeting radar
    - Battlefield and Reconnaissance radar
    - Missile guidance system
    - Target Tracking (TT) system
    - Fire Control (FC) system
    - Airborne Intercept (AI) radars
- Triggers
- Weather radar
- Navigational radar
    - Air Traffic Control Navigation
    - Space and Range Instrumentation radar system
- Mapping radar
- Road radar
- Radars for biological research

1.1.4 Radar Frequency Bands

The table below has the radar classification based on the operating frequency:

Letter designation	Frequency (GHz)	Usage
HF	0.003-0.03	Over the horizon radar
VHF	0.03-0.3	Very-long-range surveillance
UHF	0.3-1	Very-long-range surveillance
L-band	1.0-2.0	Long-range surveillance, Enroute traffic control
S-band	2.0-4.0	Moderate range surveillance, Terminal air traffic control, Long range weather (200 nmi)
C-band	4.0-8.0	Long range tracking, Airborne weather detection
X-band	8.0-12.5	Airborne intercept & weather radar, Short range tracking, Missile guidance, Mapping marine radar
Ku-band	12.5-18.0	High resolution mapping, satellite altimetry
K-band	18.0-26.5	Little Used (water vapor)
Ka-band	26.5-40.0	Very High resolution mapping, Short range tracking, Airport surveillance
V, W	40-110	Smart munitions, remote sensing
MMW	110+	Experimental, remote sensing

TABLE 1.1:   Radar Frequency Bands

1.2   Continuous Wave (CW) and Pulsed Radars

1.2.1   CW Radar

Continuous-wave radar systems are those which use a stable frequency continuous wave for transmission and reception.

The main advantages of the CW radars are:

- Simple to manufacture.

- No minimum or maximum range (broadcast power level imposes a practical limit on range).
- Maximize power on a target due to continuous broadcasting.

However they also have the following disadvantages:

- They can only detect moving targets, as stationary targets (along the line of sight) will not cause a Doppler shift.
- They cannot measure range. Range is normally measured by timing the delay between a pulse being sent and received, but as CW radars are always broadcasting, there is no delay to measure. Ranging can be implemented, however, by use of a technique known as frequency modulated continuous-wave radar.

1.2.2 Pulsed Radar

Pulsed Radars use a train of pulsed waveforms with modulation. Basing on pulse repetition frequency or PRF (definition given in the next section), Pulsed radars are classified as low PRF, medium PRF and High PRF. Low PRF radars are used primarily for ranging where target velocity is not needed. High PRF radars are used for measuring target velocity (Doppler Shift).

This paper is developed for mono-static pulsed radar since they are widely used.

1.3 Radar Terminologies

1.3.1 PRF

Pulsed radar uses a train of pulse for transmission and reception as illustrated Figure 1.2. The time interval between any two transmitted pulses is known as the Pulse Repetition Interval (PRI) or Inter Pulse Period (IPP) denoted by T. The inverse of PRI is called Pulse Repetition Frequency (PRF) denoted by f_r.

During each PRI radar radiates energy only for τ (pulse width) seconds and listens for target returns for rest of the PRI. Here

$$f_r = \frac{1}{PRI} = \frac{1}{T} \tag{1.1}$$

Radar transmitting duty cycle is

$$d_t = \frac{\tau}{T} \tag{1.2}$$

And the radar average transmitted power is

$$P_{ave} = P_t \times d_t \tag{1.3}$$
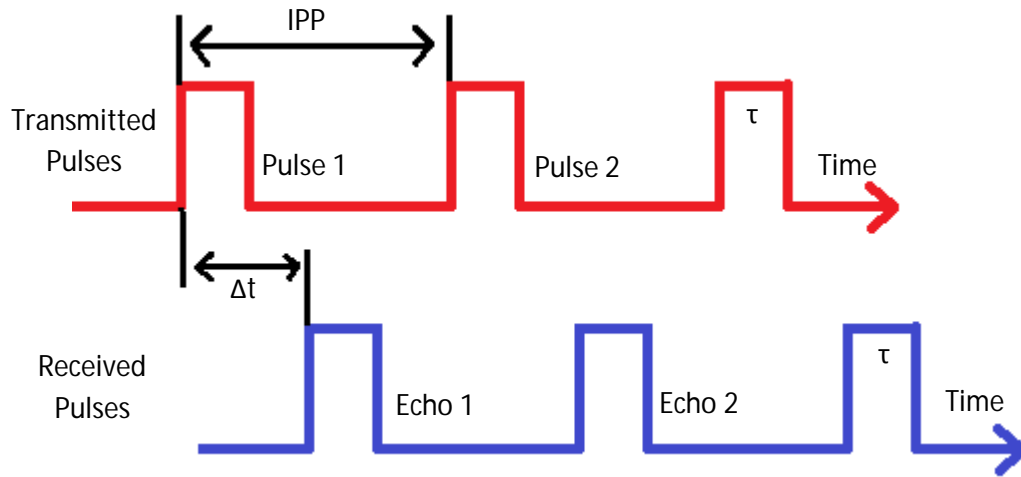
Figure 1.2: PRF and IPP

From the above equations it is clear that increasing the pulse width means increasing the transmitting duty cycle which in turn increases the radar average transmitted power thereby increasing the SNR.

Figure 1.3 is a plot generated by MATLAB simulation that shows the increase in SNR with the increasing pulse width. When pulse width is increased from 0.15 µsec to 1.7 µsec the increase in SNR is sufficient to detect the target from a distance of even 150 km instead of 75 km.

Detail of the code is listed in Appendix A.
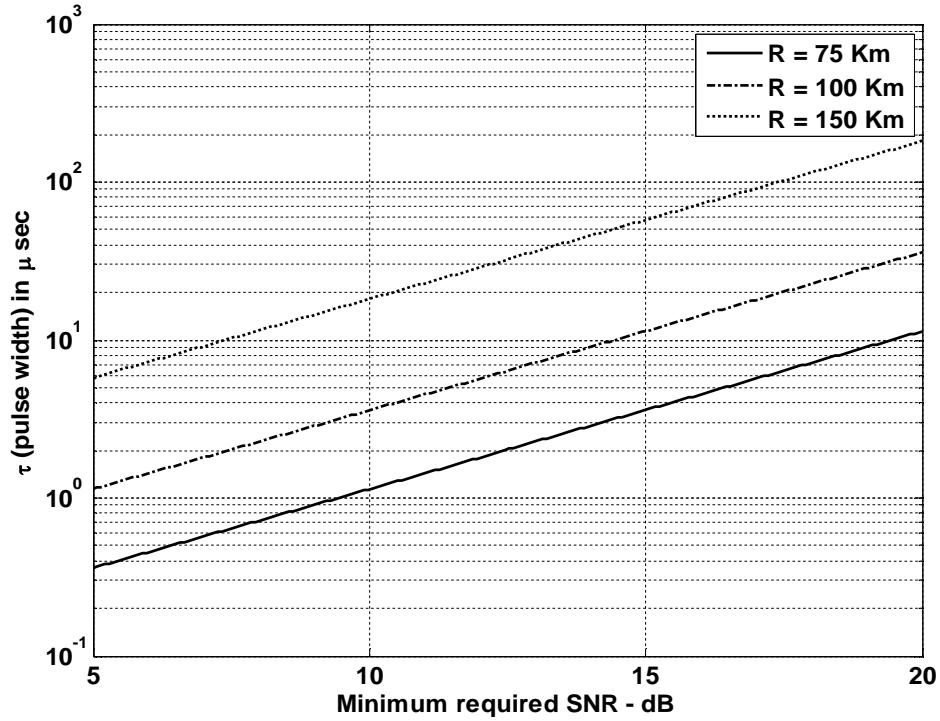
Figure 1.3: Pulse width versus SNR

1.3.2   Maximum Unambiguous Range

Once a pulse is transmitted the radar transmitter must wait for sufficient time for the receiver to receive the echo signal for that particular transmitted signal before it sends out the next pulse to avoid ambiguity. Therefore the maximum unambiguous range (R_u) must correspond to half of PRI

$$R_u = c\frac{T}{2} = \frac{c}{2f_r} \tag{1.4}$$

1.3.3   Range Resolution (ΔR)

It is the radar`s ability to detect targets in close proximity to each other as distinct objects. Radars have a minimum range R_{min} and a maximum range R_{max}. The whole range area is divided into number of range bins or gates (M) each of width ΔR.

Targets separated by at least ΔR can be completely resolved in range. Targets within the same range bin can be resolved in cross range (horizontally) utilizing signal processing techniques.

7

To find the minimum ∆R let us assume two targets separated by cτ/4 as shown in Figure 1.4 (a).In this case, when the pulse trailing edge strikes target 2 the leading-edge would have traveled backwards a distance cτ, and the returned pulse would be composed of returns from both targets.
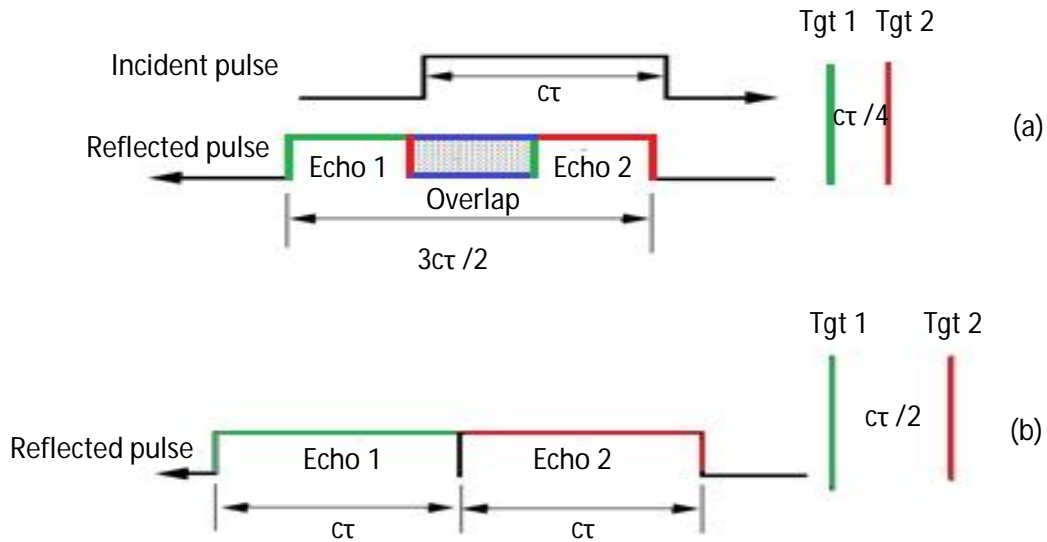
Figure 1.4: Range resolutions: (a) Two unresolved targets, (b) Two resolved targets

However, if the two targets are at least cτ/2 apart, then as the pulse trailing edge strikes the first target the leading edge will start to return from target 2, and two distinct returned pulses will be produced, as illustrated by Figure 1.4 (b). Thus, ∆R should be greater or equal to cτ/2. And since the radar bandwidth B is equal to 1/τ, then

$$\Delta R = \frac{c\tau}{2} = \frac{c}{2B} \tag{1.5}$$

In general, radar users and designers alike seek to minimize in order to enhance the radar performance. As suggested by Eq. 1.5, in order to achieve fine range resolution one must minimize the pulse width. However, this will reduce the average transmitted power and increase the operating bandwidth. Achieving fine range resolution while maintaining adequate average transmitted power can be accomplished by using pulse compression techniques.

1.3.4 Doppler Shift

Doppler shift is an apparent change in frequency (or wavelength) due to the relative motion of two objects. When the two objects are approaching each other, the Doppler shift causes a shortening of wavelength - or increase in frequency. When the two objects are moving away from each other, the Doppler shift causes a lengthening of wavelength - or decrease in frequency. For a Doppler radar system to measure speed, an accurate sample of the original phase of the transmitted signal must be maintained for comparison against the reflected signal. Consider Figure 1.5.
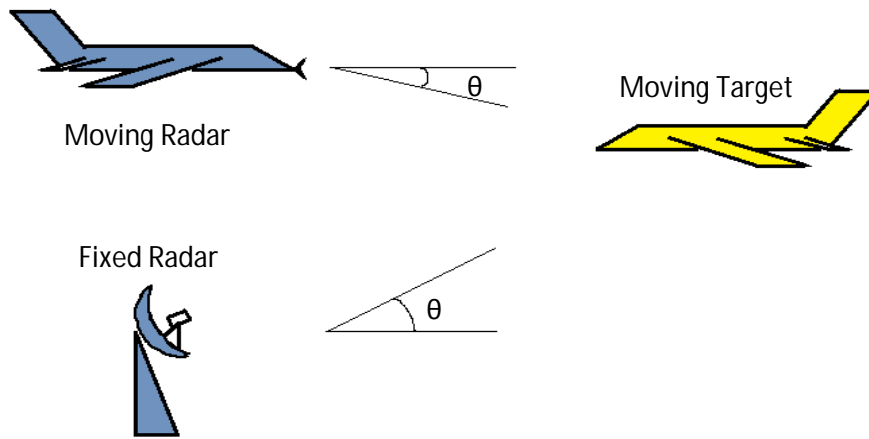
Figure 1.5: Doppler shift due to moving radar and targets

Angle shown (θ) is for elevation differences only; if there is also an azimuthal angle, it must be factored into the equation as cos (α), where α is the azimuth angle relative to the radar antenna bore sight direction. For fixed radar with moving target:

$$f_{D} = 2 * V_T * \cos\theta * \frac{f_T}{c} \tag{1.6a}$$

For moving radar with moving target:

$$f_{D} = 2 *(V_R + V_T) * \cos\theta * \frac{f_T}{c} \tag{1.6b}$$

Where f_D= Doppler frequency, f_T = Transmitted frequency, V_T = Target velocity, V_R = Radar velocity, c=speed of light.

1.3.5 Coherence

A radar is coherent if there is continuity in phase from one transmitted pulse to another. It is radar's ability to maintain an integer multiple of wavelengths between the equiphase wave fronts of any two successive pulses. Coherence is a requirement to measure (extract) the received signal phase. Since Doppler represents a frequency shift in the received signal, then only coherent or coherent-on-receive radars can extract Doppler information. This is because the instantaneous frequency of a signal is proportional to the time derivative of the signal phase. More precisely, if f_i the instantaneous frequency, and $\varphi(t)$ is the signal phase.

$$f_i = \frac{1}{2\pi}\frac{d\varphi(t)}{dt} \tag{1.7}$$
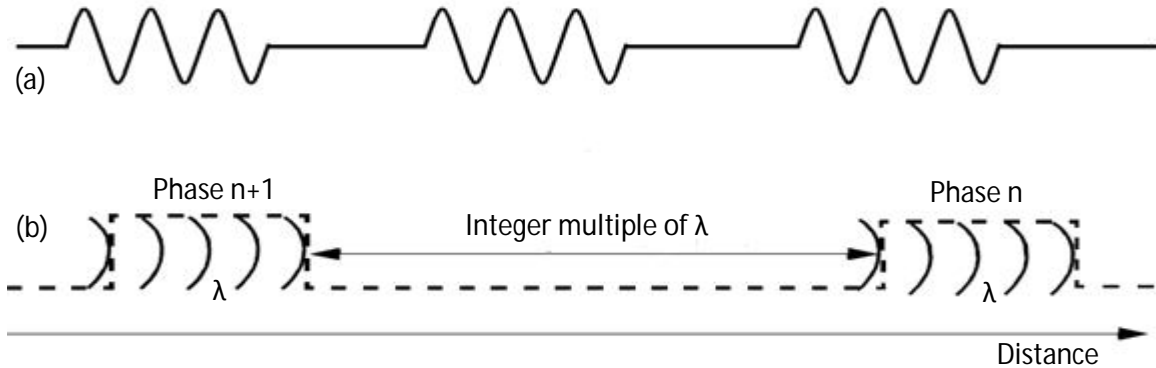
Figure 1.6: (a) Phase continuity between consecutive pulses. (b) Maintaining an integer multiple of wavelengths between the equiphase wave fronts of any two successive pulses guarantees coherency.

The increase in SNR and the detection range of radar due to coherent pulse integration will be clear from the following MATLAB simulation. The detail MATLAB code is listed in Appendix A. The plots generated by the simulation is given as Figure 1.7 and Figure 1.8 below which clearly reveal that

- Single pulse radar has minimum SNR and detection range.
- Non-coherent Integration (NCI) of number of pulses increases the SNR and the detection range.
- Coherent Integration (CI) of same number of pulses gives highest SNR and maximum detection range.
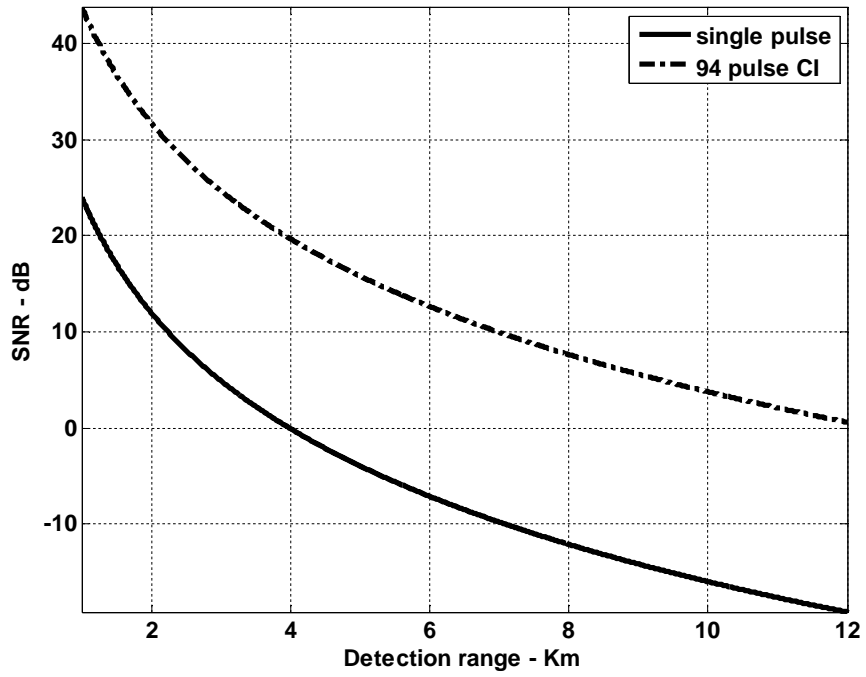
Figure 1.7: SNR versus number of single pulses and CI
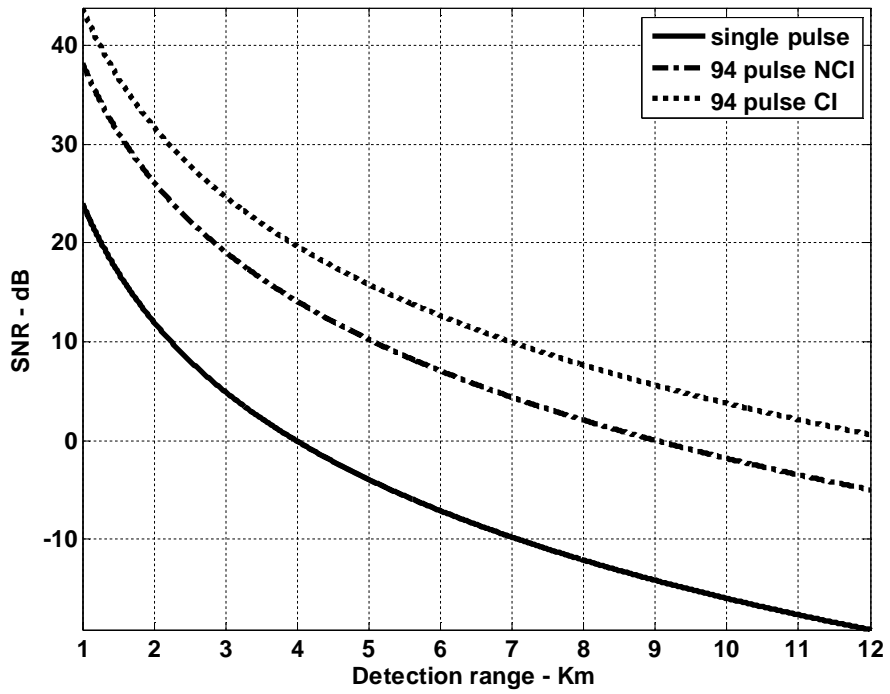
Figure 1.8: Change in SNR and detection range due to NCI and CI

1.4   Radar Losses

From the basic equation of radar we see that radar losses are inversely proportional to SNR. Hence, any increase in radar loss causes a drop in SNR, thus decreasing the probability of detection. These losses include ohmic losses and statistical losses.

1.4.1   Transmit and Receive Loss or Plumbing Loss

It occurs between the radar transmitter and antenna port, and between the antenna output port and the receiver front end. It is limited to 1 to 2 dBs.

1.4.2   Antenna Pattern Loss and Scan Loss

Since radar keeps scanning an area for a target, depending on antennas radiation pattern the antenna gain in the direction of the target is usually less than maximum whereas in the basic equation for radar we assume maximum antenna gain. Loss in SNR for not having maximum antenna gain on the target at all times is called the antenna pattern loss.

A typical sinx/x antenna radiation pattern is plotted in Figure 1.9 below to show the variation of gain with change of angle from the bore sight axis.
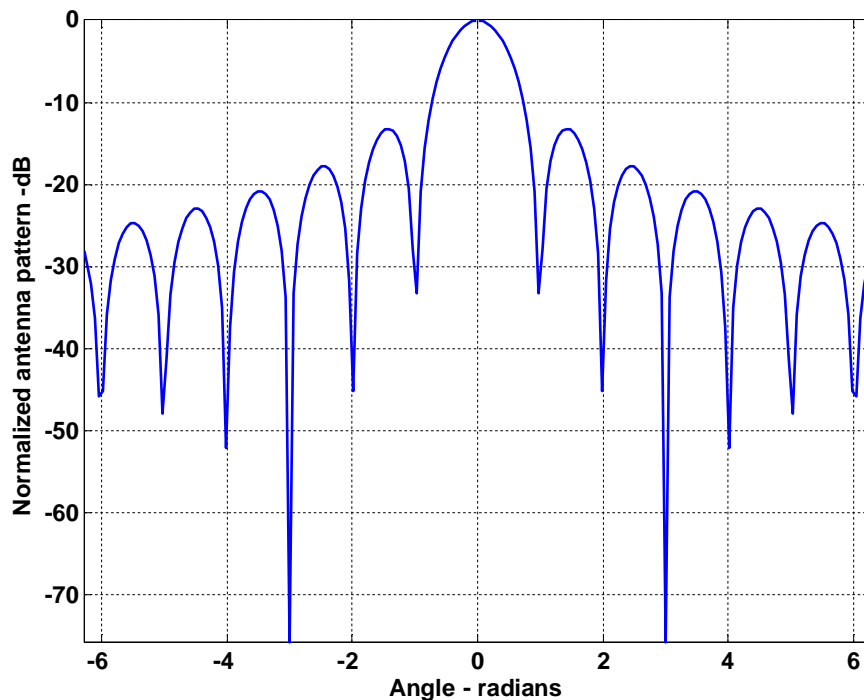
Figure 1.9: Normalized (sin x / x) antenna pattern

When antenna scanning rate is so fast that the gain on receiver is not the same as on transmitter, the loss that occurs is known as scanning loss. Phased array radars are vulnerable to both pattern and scan losses.

1.4.3 Atmospheric Loss

In order to accurately predict radar performance, we must modify free space analysis to include the effects of the earth and its atmosphere. This modification should account for ground reflections from the surface of the earth, diffraction of electromagnetic waves, bending or refraction of radar waves due to the earth atmosphere, and attenuation or absorption of radar energy by the gases constituting the atmosphere.

1.4.4 Collapsing Loss

When the number of integrated returned noise pulses is larger than the target returned pulses, a drop in the SNR occurs. This is called collapsing loss. Radars detect targets in azimuth, range, and Doppler. When target returns are displayed in one coordinate, such as range, noise sources from azimuth cells adjacent to the actual target return converge in the target vicinity and cause a drop in the SNR. This is illustrated in Figure 1.10
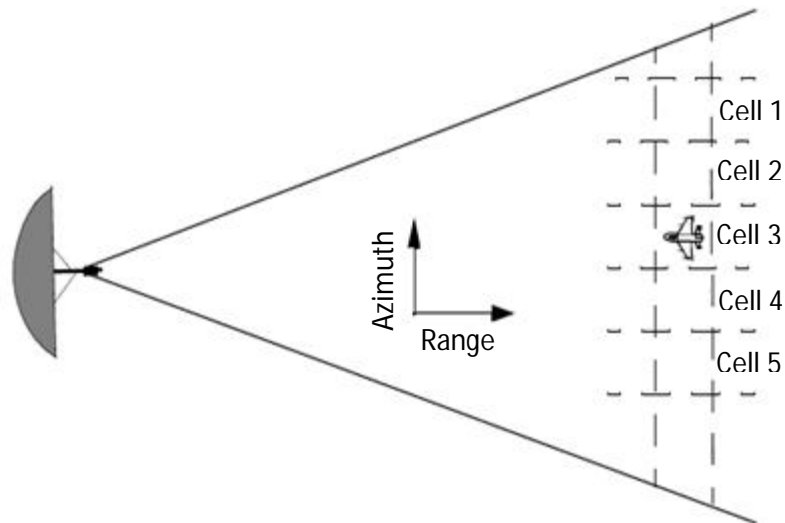
Figure 1.10: Collapsing loss. Noise sources in cells 1, 2, 4, and 5converge to increase the noise level in cell 3.

1.4.5   Signal Processing Loss

These are statistical losses those take place due to following cases

- Detector Approximation
- Constant False Alarm Rate (CFAR) Loss
- Quantization Loss
- Range Gate Straddle
- Doppler Filter Straddle

1.5   Objective of the Thesis

The main objective of this thesis is to analyze the performance of basic mono-static pulse radar system under varying radar cross section and antenna array pattern. The main purposes of the thesis are:

(i)   To develop the equation for basic mono-static pulse radar system from relevant parameters and study the variation of the basic equation under different conditions.

(ii)   To study the variation of radar cross section with respect to aspect angle and frequency.

(iii)   To evaluate the variation of RCS for different shaped objects and its effects over radar performance.

(iv)   To know the atmospheric obstacles for radar wave propagation.

(v)   To determine the significance of the reflection, refraction and diffraction.

(vi)   To evaluate the role of radar antenna for radar wave propagation.

(vii)   To define the basic radar antenna for circular aperture.

(viii)   To evaluate the improvement of the linear array antenna through DFT.

1.6   Organization of the Thesis

Chapter 1 is an introductory chapter. It contains the origin and basic principles of radar. In this chapter, different losses affecting radar performance are also discussed.

In Chapter 2 the basic radar equations for both mono and bi-static radar has been discussed. The impacts of changing various parameters on radar performance are identified with necessary simulation.

In Chapter 3 different parameters that affect the target radar cross section has been studied for different shaped objects.

Chapter 4 deals with radar wave propagation with respect to the earth and its atmospheric attenuation.

Chapter 5 analyzes the characteristics of radar antenna and performance improvement of radiation pattern of linear array antenna.

Chapter 6 contains the concluding remarks the scope of future works as well.

Chapter 2

RADAR EQUATION AND PARAMETERS

2.1 Basic Radar Equation

2.1.1 Mono-static Radar Equation

The basic radar equation has many forms varying according to the parameters being used. The equation parameters vary according to the type and configuration of the radar in use. However, the most common form of the basic radar used is the mono-static radar where the same antenna is used for both transmitting and receiving. The block diagram for such radar system is given in Figure 1.1 in chapter 1. The basic radar equation for such mono-static radar system is developed below. First we consider a noiseless case and then we add the effects of noise to the basic equation.

2.1.2 Noiseless Case

Peak power density (power per unit area), P_D at range R from an omni directional radar with peak transmission power (P_t) is given by

$$P_D = \frac{P_t}{4\pi R^2} \tag{2.1}$$

When using directional antennas with gain G, the power density at a distance R is given by

$$P_D = \frac{P_t G}{4\pi R^2} \tag{2.2}$$

Here, gain depends on the effective aperture A_e of the antenna. Relation between gain and effective aperture area is

$$A_e = \frac{G\lambda^2}{4\pi} \tag{2.3}$$

The reflected power back to the target depends upon the target cross section σ. σ is also called the radar cross section (RCS) which is examined in much detail in the next chapter.

For now it is sufficient to use the fact that σ is the ratio of the power reflected back to the radar (P_r) to the power density incident on the target (P_D),

$$\frac{\sigma}{4\pi R^2} = \frac{P_r}{P_D} \tag{2.4}$$

Using Eq. 2.2 and 2.4, we can find the power delivered to the radar signal processor by the antenna (P_{Dr}) as

$$P_{Dr} = P_r A_e = P_D \frac{\sigma}{4\pi R^2} A_e = \frac{P_t G \sigma A_e}{(4\pi R^2)^2} \tag{2.5}$$

Substituting the value of A_e from Eq. 2.3 we get

$$P_{Dr} = \frac{P_t G^2 \lambda^2 \sigma}{(4\pi)^3 R^4} \tag{2.6}$$

Power delivered is the minimum when target is at maximum range (R_{max}). If we denote the minimum detectable power by S_{min} then from Eq. 2.6

$$R_{max} = \left(\frac{P_t G^2 \lambda^2 \sigma}{(4\pi)^3 S_{min}} \right)^{\frac{1}{4}} \tag{2.7}$$

This is the maximum range that can be achieved if we consider a noiseless medium and a lossless receiver.

2.1.3   In the Presence of Noise

In practical situations the returned signal is corrupted by noise which is a function of radar operating bandwidth, B. The input noise power to a lossless antenna is

$$N_i = kT_e B \tag{2.8}$$

Where, T_e is the receiver effective noise temperature. The effect of receiver fidelity should also be considered. The fidelity of a receiver is its ability to accurately reproduce, in its output, the signal that appears at its input. The broader the band passed by frequency selection circuits, the greater is the receiver fidelity. This gives rise to the noise at receiver input which is defined as the noise figure, F where

$$F = \frac{(SNR)_i}{(SNR)_o} = \frac{\frac{S_i}{N_i}}{\frac{S_o}{N_o}} \tag{2.9}$$

Here $(SNR)_i$ and $(SNR)_o$ are SNR at input and output of receiver. S_i and N_i are input signal and noise power whereas S_o and N_o are output signal and noise power.

Rearranging Eq. 2.9

$$S_i = N_i(SNR)_o = kT_eBF(SNR)_o \tag{2.10}$$

Hence, the minimum detectable signal power can be written as

$$S_{min} = kT_eBF(SNR)_{o_{min}} \tag{2.11}$$

The radar detection threshold is set equal to this minimum output SNR, $(SNR)_{o_{min}}$. Substituting Eq. 2.11 in Eq. 2.7 and considering radar losses (as explained in chapter 1) as L

$$R_{max} = \left(\frac{P_tG^2\lambda^2\sigma}{(4\pi)^3kT_eBFL(SNR)_{o_{min}}} \right)^{\frac{1}{4}} \tag{2.12}$$

Or equivalently,

$$(SNR)_0 = \frac{P_tG^2\lambda^2\sigma}{(4\pi)^3kT_eBFLR^4} \tag{2.13}$$

Eq. 2.13 represents the basic equation for mono-static radar system.

2.1.4   How to increase range

By investigation of the above equations we can decide on how to increase the radar range. Here, the effects of RCS are considered in the next chapter. In short, the use of appropriate RCS prediction methods can contribute into exact target detection at longer ranges.

Minimum detectable SNR depends on the threshold level set during radar design. To increase the range, we need to keep it as low as possible keeping the false alarm under control.

We can increase range by increasing transmitted power. Since the relationship is proportional hence it will be less effective. The effect of increasing transmission power is presented by a MATLAB simulation in the next section.

Range increases as square of antenna gain which makes this parameter a more effective one. In this chapter, we will see how gain is increased by increasing antenna aperture by using MATLAB simulation. More practical measures are suggested in chapter 5 by considering different antenna arrays.

Increasing wavelength or decreasing operating frequency can increase range. We will see the advantage of using low PRF radar later in this chapter by using MATLAB simulation.

Decreasing operating bandwidth is another way to increase the range. But we have already found in chapter 1 that fine resolution requires bandwidth to be as large as possible (or pulse width as small as possible).

 By better design radar losses as mentioned in chapter 1 can also be minimized to give better range. But this is beyond the scope of our thesis work.

Before investigating the effects of changing these parameters on radar range and SNR let us see few variations of the basic mono-static radar equation according to different applications of the radar.

2.2 Variance of Basic Equation

2.2.1 Bi-static Radar Equation

Bi-static radars uses transmit and receive antennas those are placed in different locations. A synchronization link between the transmitter and receiver is necessary to provide following information

- The transmitted frequency in order to compute the Doppler shift.
- The transmit time or phase reference in order to measure the total scattered path.

Frequency and phase reference synchronization can be maintained through line-of-sight communications between the transmitter and receiver. However, if this is not possible, the receiver may use a stable reference oscillator for synchronization.
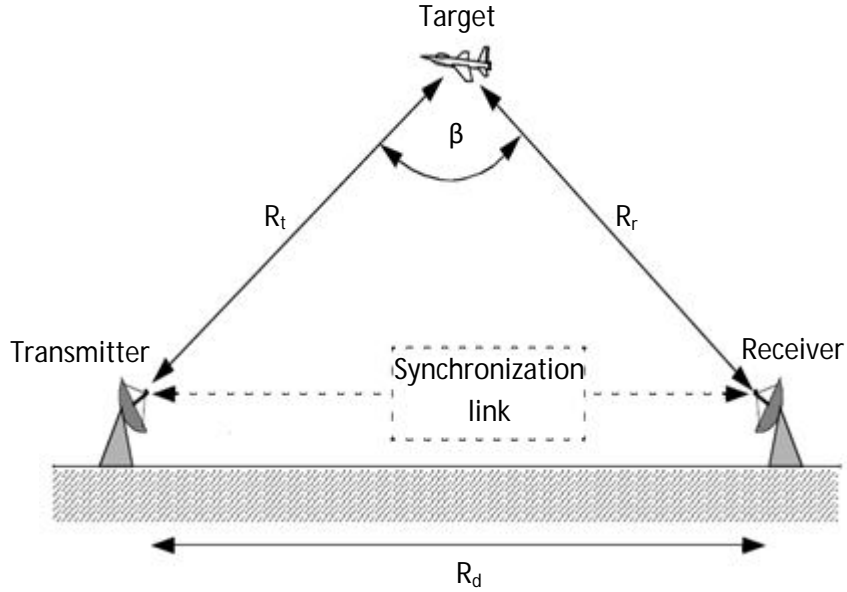
Figure 2.1: Bi-static radar configurations.

Figure 2.1 shows the bi-static radar configuration. The angle β is called the bi-static angle. When β approaches 180^0, the bi-static RCS becomes very large compared to the mono-static RCS which causes a change in the basic radar equation as given below

$$P_{Dr} = \frac{P_t G_t G_r \lambda^2 \sigma_B}{(4\pi)^3 R_t^2 R_r^2 L_t L_r L_p}$$ (2.14)

Here, P_{Dr} = total power delivered to the signal processor by the receiving antenna, P_t = peak transmitted power, G_t = Gain of transmitting antenna, Gr = Gain of receiving antenna, R_t= range from transmitter, R_r = range from receiver, L_t = transmitter losses, L_r = receiver losses, L_p= medium propagation loss. Here, a noiseless condition is assumed.

2.2.2 Low PRF Radar Equation

Once again referring to Figure 1.2, we can define receiving duty factor as

$$d_r = \frac{T-\tau}{T} = 1 - \tau f_r = 1 - \frac{\tau}{T} \tag{2.15}$$

Hence, for low PRF where, $T \gg \tau$, the receiving duty factor $d_r \approx 1$. Hence ignoring the impact of receiving duty factor low PRF radar equation for n_p coherent pulses $(n_p = T_i f_r)$ can be written as following:

$$(SNR)_{n_p} = \frac{P_t G^2 \lambda^2 \sigma (T_i f_r)}{(4\pi)^3 k T_e BFLR^4} = \frac{P_t G^2 \lambda^2 \sigma T_i f_r \tau}{(4\pi)^3 k T_e FLR^4} \tag{2.16}$$

Here T_i = Time on target (time that a target is illuminated by the beam) and bandwidth $B = 1/\tau$. Since transmission duty factor is negligible compared to the receiving duty factor low PRF radars result in maximum unambiguous range thereby increasing overall range of the radar.

We already defined time on target $T_i = n_p / f_r$; Therefore, as the PRF, f_r is decreased time of the scanning beam on target is increased resulting in better output SNR. As a result low PRF radars give better SNR for targets at longer ranges.

2.2.3 High PRF Radar Equation

The central power spectrum line (DC component) for high PRF pulse train contains most of the signal's power. Its value is $(\tau/T)^2$, and it is equal to the square of the transmit duty factor. Thus, using Eq. 2.13, the single pulse radar equation for high PRF radar is

$$(SNR)_0 = \frac{P_t G^2 \lambda^2 \sigma d_t^2}{(4\pi)^3 k T_e BFLR^4 d_r} \tag{2.17a}$$

For high PRF radar, we cannot ignore d_r since $d_r \approx d_t = \tau f_r$. Again, for high PRF radar, $B = T_i$. Additionally, if we replace $P_{ave} = P_t \tau f_r$, then Eq. 2.17a becomes

$$SNR = \frac{P_{ave}T_iG^2\lambda^2\sigma}{(4\pi)^3kT_eFLR^4} \qquad (2.17b)$$

Since $P_{ave}T_i$ in Eq. 2.17b is a kind of energy product therefore it indicates that high PRF radars can enhance detection performance by using relatively low power and longer integration time. Low PRF radars are used primarily for ranging where target velocity is not needed. High PRF radars are used for measuring target velocity (Doppler Shift).

2.2.4 Surveillance Radar Equation

Surveillance or search radars continuously scan a specified volume in space for targets. Search volumes are specified by a search solid angle Ω in steradians. If we define T_{sc} as the time it takes the radar to search a volume defined by the solid angle Ω then we can modify the basic radar Eq. which gives us the search radar equation as

$$SNR = \frac{P_{ave}A\sigma}{16R^4kT_eLF}\frac{T_{sc}}{\Omega} \qquad (2.18)$$

The quantity $P_{ave}A$ in Eq. 2.18 is known as the power aperture product. In practice, the power aperture product is widely used to categorize the radar ability to fulfill its search mission. Normally, a power aperture product is computed to meet predetermined SNR and radar cross section for a given search volume defined by Ω.

2.3   Variation of Radar Parameters and its Effect on Radar Performance

2.3.1   Effect of RCS and Transmitted Peak Power

Here we will perform a MATLAB simulation using basic radar equation. The detail MATLAB code is listed in Appendix A. If we analyze the generated plots we can formulate the following findings for different parameter changes:

- Doubling the peak power improves SNR only a little (3 to 5 dB) in Figure 2.2b.
- Doubling the RCS improves SNR a little better (almost 10 dB) in Figure 2.2a. Although both RCS and the transmitted peak power has a linear relationship with SNR, but since increase in RCS indicates increase in the power reflectivity of the target therefore its effect is more prominent.

- Other radar parameters such as antenna gain variation should be considered to improve SNR or detection range effectively.
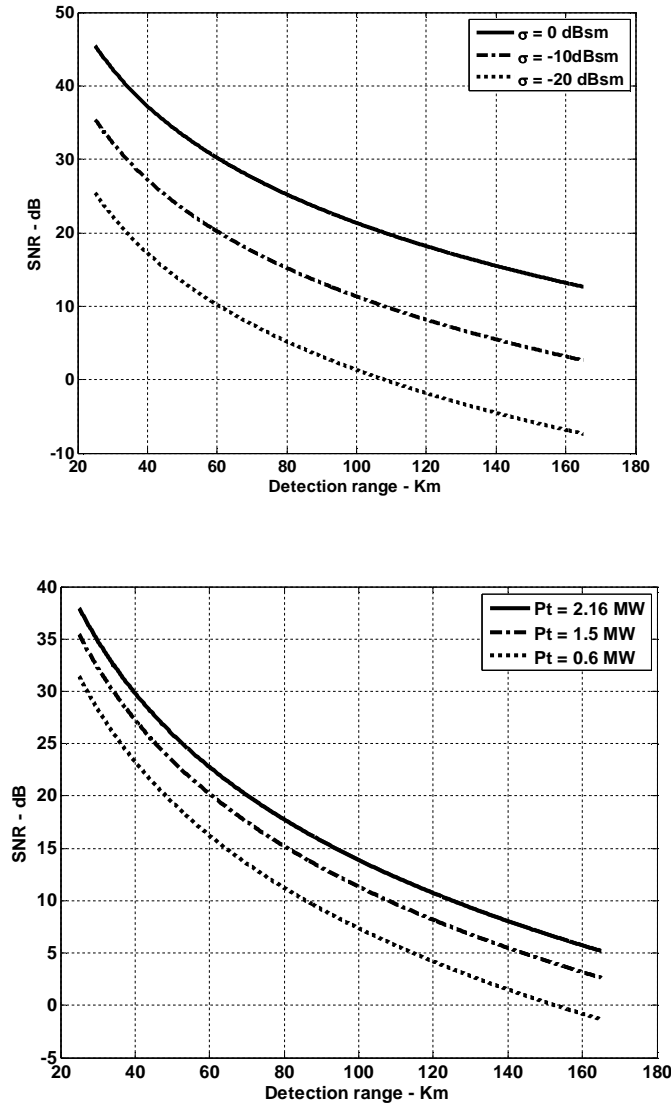
Figure 2.2: (a) Variation of RCS in improving SNR and detection range. (b) Variation of pick power in improving SNR and detection range.

2.3.2 Effect of changing PRF

To show the effect PRF on radar performance let us perform a MATLAB simulation using radar equation. The detail MATLAB code is listed in Appendix A. If we analyze the generated plots we can formulate the following findings for different parameter changes:

- Integrating a limited number of pulses can significantly enhance the SNR;
- However, integrating large amount of pulses does not provide any further major improvement.
- For any variation of RCS or peak power, the effect of change in PRF remains same.
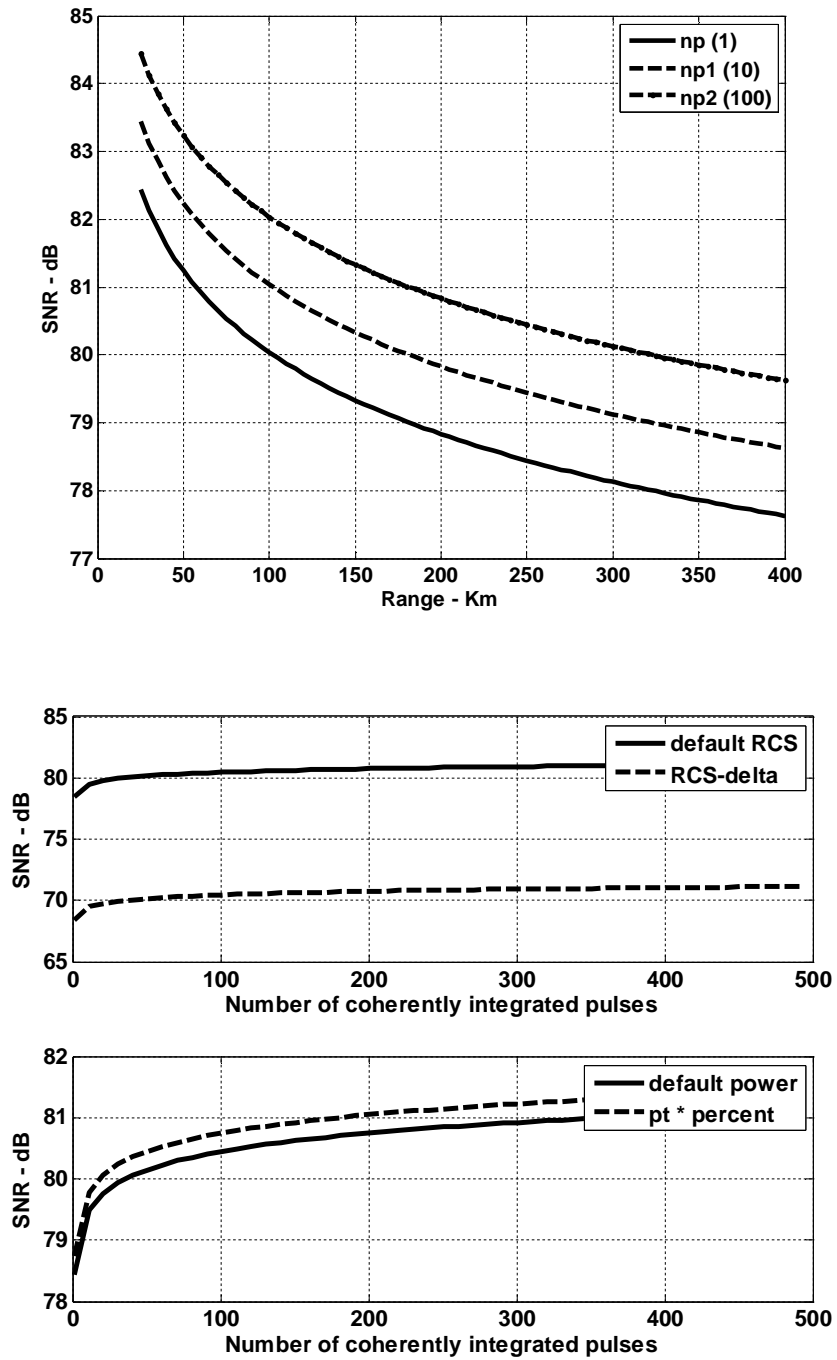
Figure 2.3: Effect of changing PRF on SNR and range

2.3.3 Effect of Power Aperture Product

Let us run a MATLAB simulation that implements the search radar equation. The detail of the MATLAB code is given in Appendix A. The simulation generates two plots. The observation of the plots reveals the following facts

- Figure 2.4a shows that with the increase of power aperture product, the detection range is also increased for all types of target or RCS sizes. This is because the increase in aperture actually increases the antenna gain.
- It means we can increase the antenna aperture to compensate for the lack of power being transmitted to cover a wider range of area for target detection.
- Figure 2.4b shows that different combination of power and aperture area is possible to detect same targets. It also indicates that for the same maximum radar detection range we have a number of options to choose the desired aperture size and the average transmitted power according to the application of the radar.
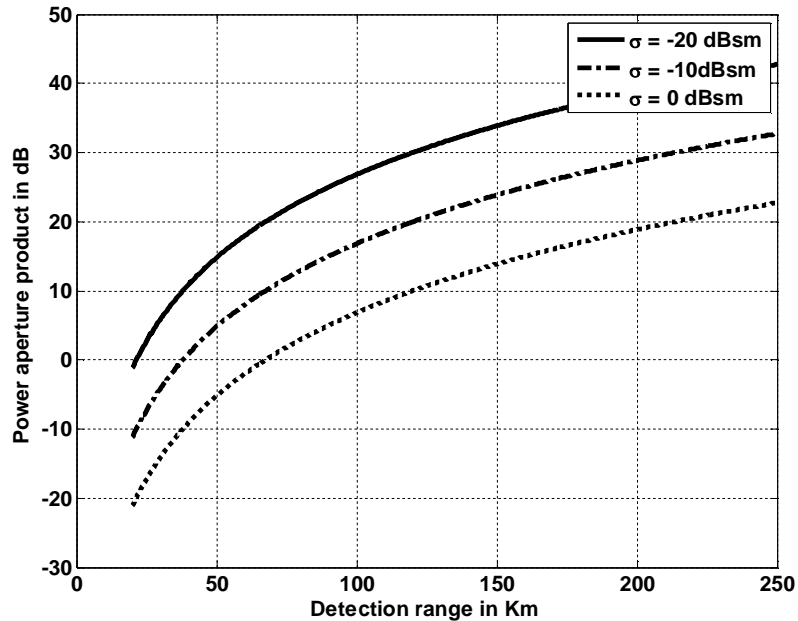
Figure 2.4: (a) Increasing power aperture product to increase detection range
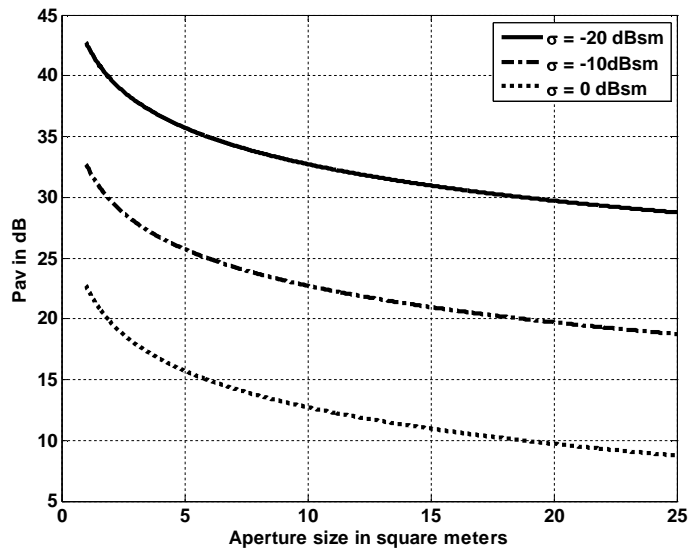
Figure 2.4: (b) Increasing aperture size to decrease average power requirement.

2.4 Radar Performance under Jamming Condition

2.4.1 Radar Jammers

In the presence of jamming or Electronic Counter Measure (ECM), detection capability is determined by receiver signal-to-noise plus interference ratio rather than SNR. And in most cases, detection is established based on the signal-to-interference ratio alone.

Jammers can be classified broadly as shown by Figure 2.5 below
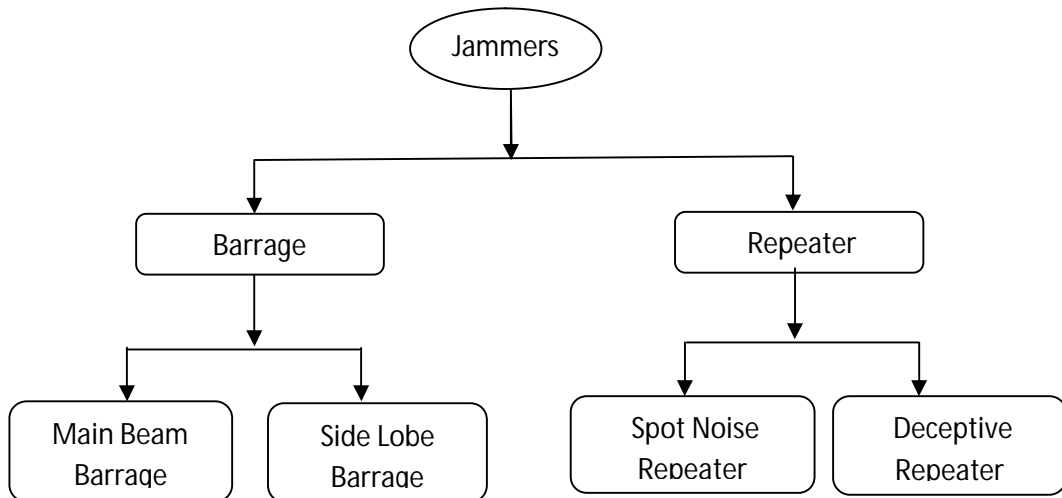
Figure 2.5: Different types of jammers employed against radars

26

Barrage jammer increases the noise level across the entire radar operating bandwidth. It can be deployed in two ways

- If it is located in radar main beam, it can take advantage of the antenna maximum gain to amplify the broadcasted noise signal. Main beam barrage jammers can be deployed either on-board the attacking vehicle, or act as an escort to the target.
- If a barrage jammer is located in the radar side lobe, it must either use more power, or operate at a much shorter range than main beam jammers. Side lobe jammers are often deployed to interfere with specific radar, and since they do not stay close to the target, they have a wide variety of stand-off deployment options.

Repeater jammers carry receiving devices on board in order to analyze the radar's transmission, and then send back false target-like signals in order to confuse the radar. There are two common types of repeater jammers:

- The spot noise repeater measures the transmitted radar signal bandwidth and then jams only a specific range of frequencies.
- The deceptive repeater sends back altered signals that make the target appear in some false position (ghosts).

By not having to jam the entire radar bandwidth, repeater jammers are able to make more efficient use of their jamming power. Radar frequency agility may be the only way possible to defeat spot noise repeaters.

2.4.2   Radar Equation with Jamming

From the discussion of section 2.4.1 it is clear that jammers can primarily be employed as either self-screening jammers (SSJ) or stand-off jammers (SOJ). The effect of jamming on the radar will be different in either case.

a. **Equation for SSJ**   these are carried on the vehicle they are protecting and hence are also known as self-protecting jammers. Escort jammers can be treated as one if they

appear at the same range as that of the target(s). The single pulse power received by the radar from target is

$$P_s = \frac{P_t G^2 \lambda^2 \sigma}{(4\pi)^3 LR^4} \qquad (2.19)$$

where, the symbols carry their usual meaning as mention before. Power received by radar from an SSJ jammer at the same range is

$$P_{SSJ} = \frac{P_J G_J}{4\pi R^2} \frac{\lambda^2 G}{4\pi} \frac{B}{B_J L_J} \qquad (2.20)$$

where, P_J, G_J, B_J, L_J are, respectively, jammers peak power, antenna gain, operating bandwidth and losses. Radar equation for SSJ is thus obtained from Eq. 2.19 and Eq. 2.20 as

$$\frac{S}{S_{SSJ}} = \frac{P_t G_p \sigma B_J L_J}{4\pi P_J G_J R^2 BL} \qquad (2.21)$$

where, G_P is the radar processing gain. The jamming power reaches the radar on a one-way transmission basis, whereas the target echoes involve two-way transmission. Thus, the jamming power is generally greater than the target signal power. In other words, the ratio S/S_{ssj} is less than unity. However, as the target becomes closer to the radar, there will be a certain range such that the ratio is equal to unity. This range is known as the crossover or burn-through range. The range window where the ratio is sufficiently larger than unity is denoted as the detection range. In order to compute the crossover range R_{CO}, we set S/S_{SSj} to unity in Eq. 2.21 and solve for range. It follows

$$(R_{CO})_{SSJ} = \left(\frac{P_t G \sigma B_J L_J}{4\pi P_J G_J BL} \right)^{1/2} \qquad (2.22)$$

b. <u>**Equation for SOJ**</u>   The power received by the radar from an SOJ jammer which is normally along range $(R_{J)}$ is

$$P_{SOJ} = \frac{P_J G_J}{4\pi R_J^2} \frac{\lambda^2 G'}{4\pi} \frac{B}{B_J L_J} \qquad (2.23)$$

Where G' represents radar antenna gain in the direction of the jammer and is considered to be the side lobe gain. The SOJ radar equation is then found from Eq.2.19 and Eq.2.11 as

$$\frac{S}{S_{SOJ}} = \frac{P_t G^2 R_J^2 \sigma B_J L_J}{4\pi P_J G_J G' R^4 BL}$$

(2.24)

Similarly the cross over range is

$$(R_{CO})_{SOJ} = \left(\frac{P_t G^2 R_J^2 \sigma B_J L_J}{4\pi P_J G_J G' BL}\right)^{1/4}$$

(2.25)

And the detection range is

$$R_D = \frac{(R_{CO})_{SOJ}}{\sqrt[4]{\left(\frac{S}{S_{SOJ}}\right)_{min}}}$$

(2.26)

Where, $(S/S_{SOJ})_{min}$ is the minimum signal to jammer power ratio so that target detection is possible.

2.4.3   Range Reduction Factor (RRF)

RRF denotes reduction in radar detection range due to jamming. If R_{dj} and R are the radar detection range with and without jamming then

$$R_{dj} = R \times RRF$$

(2.27)

After a brief calculation it is possible to show that RRF can be expressed as

$$RRF = 10^{\frac{-\Upsilon}{40}}$$

(2.28)

Which is always less than unity since the value of Υ is given by

$$\Upsilon = 10.0 \times \log\left(1 + \frac{T_J}{T_e}\right)$$

(2.29)

Where, T_e is the effective noise temperature in degree Kelvin and T_J is the jammer effective temperature.

The effect of jammers on the reduction of radar range will be clear from the following MATLAB simulation. The simulation implements both Eq. 2.27 and Eq. 2.28.

Related MATLAB codes are given in Appendix A. The simulation generates two plots and the observation of these plots are listed below

- Figure 2.6a is the plot of RRF versus the radar operating frequency. In this plot we see that the value of the RRF decreases with increasing wavelength (i.e. decreasing frequency). It means if the radar operates at higher frequencies value of RRF will be more. Hence, one way to improve radar performance once being jammed is to shift to a higher operating frequency.
- Figure 2.6b is the plot of RRF versus radar to jammer range. In this plot it is observed that the value of RRF increases almost linearly as the distance between the radar and the jammer increases.
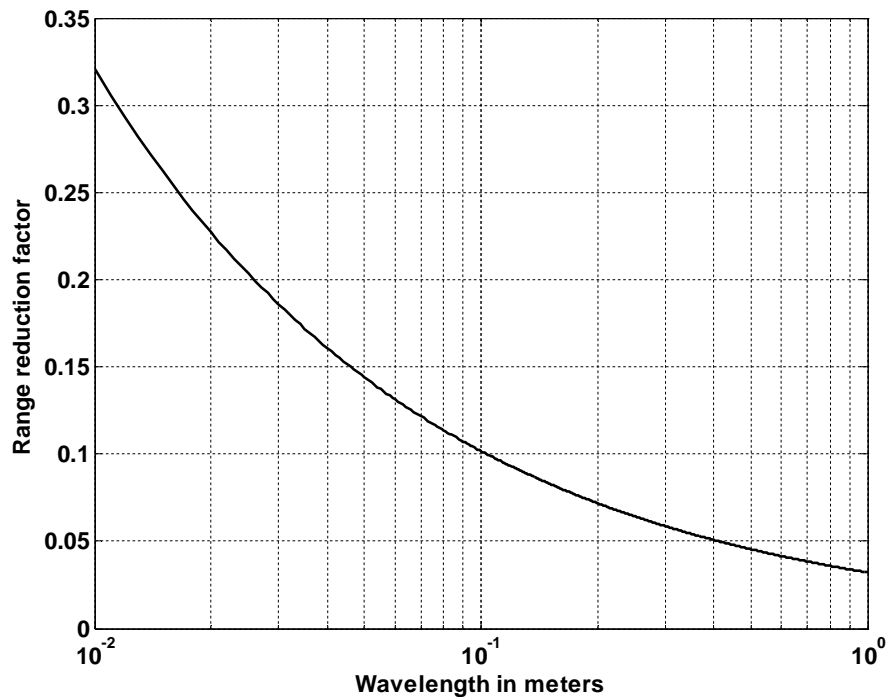
Figure 2.6 (a): RRF versus radar operating wavelength
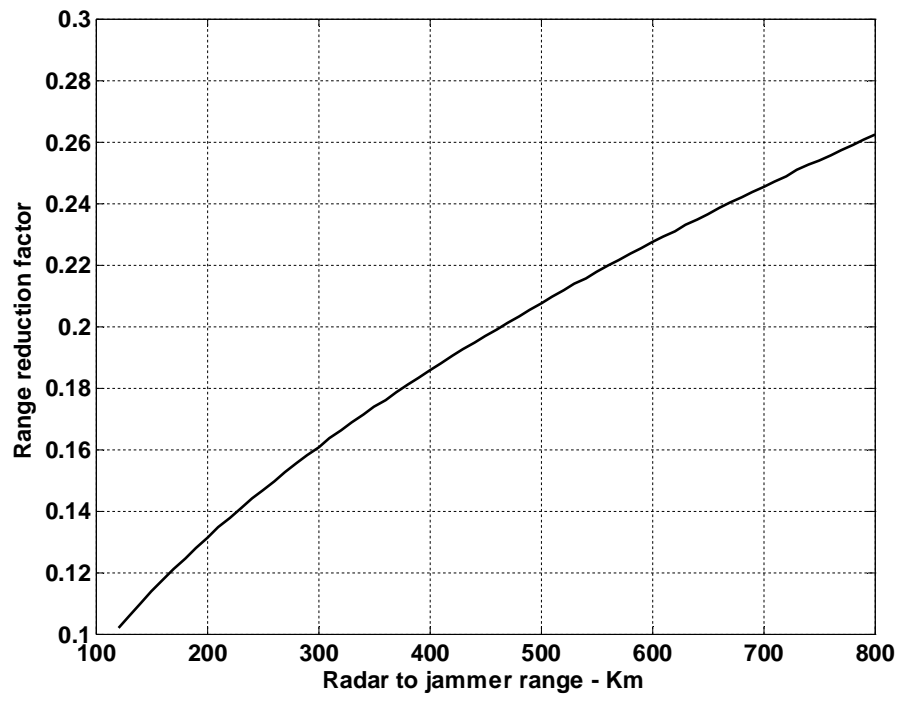
Figure 2.6(b): RRF versus radar to jammer range

Chapter **3**

TARGET RADAR CROSS SECTION

3.1. The concept of polarization

When electromagnetic waves are incident on a target, normally they are diffracted or scattered in all directions. Such scattered waves break down into two parts. One is made of waves that have the same polarization as the receiving antenna. The other portion of the scattered waves will have a different polarization to which the receiving antenna does not respond. The two polarizations are orthogonal and are referred to as the Principle Polarization (PP) and Orthogonal Polarization (OP), respectively. The intensity of the backscattered energy that has the same polarization as the radar's receiving antenna is used to define the target RCS.

3.2. Definition of Radar Target Cross Section or RCS

The radar cross section σ simply represents the amount or magnitude of the echo signals returned to the radar reflected by the target. It is the property of a scattering object or target.The RCS of a target can be viewed as a comparison of the strength of the reflected signal from a target to the reflected signal from a perfectly smooth sphere of cross sectional area of 1 m^2 as shown in Figure 3.1.
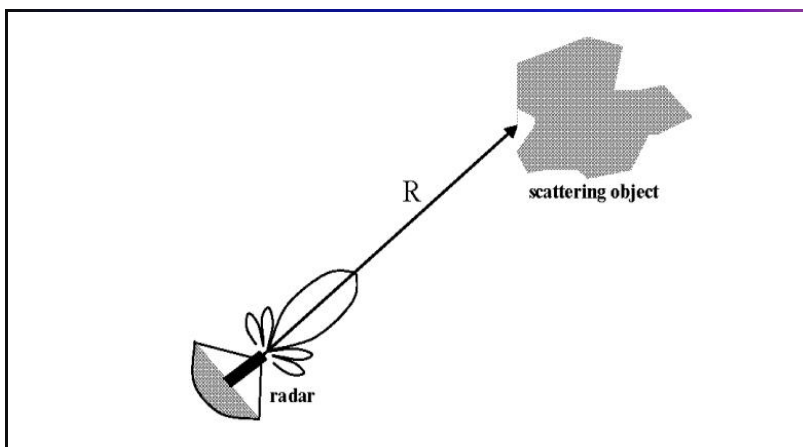
Figure3.1: Detection direction of radar over a target object.

3.3. Measurement of RCS

Sometimes the radar cross section σ is said to be the equivalent area intercepting that amount of power that, when scattering isotropically, produces at the radar a power density, which is equal to that scattered (or reflected) by the actual target. That is

$$P_s = \lim_{r \to \infty} \left[\frac{\sigma P_i}{4\pi r^2} \right]$$

Or, $$\sigma = \lim_{r \to \infty} \left[4\pi r^2 \frac{P_s}{P_i} \right] \tag{3.1}$$

Where P_s *is* the power density of is scattered waves at the receiving antenna and P_i is the power density of incident wave on a target.

So we can say that, RCS is a function of-

- Target geometry and material composition
- Position of transmitter/receiver relative to target
- Angular orientation of target relative to transmitter/receiver
- Frequency or wavelength
- Antenna polarization

The backscattered RCS is measured from all waves scattered in the direction of the radar and has the same polarization as the receiving antenna. It represents a portion of the total scattered target RCS σ_t, where $\sigma_t > \sigma$. The amount of backscattered waves from a target is proportional to the ratio of the target extent (size) to the wavelength, of the incident waves. In fact, radar will not be able to detect targets much smaller than its operating wavelength.

3.4. Significance of RCS

Radar cross section (RCS) is a measure of how detectable an object is with a radar. A larger RCS indicates that an object is more easily detected.

From radar range equation -

$$R_{max} = \left(\frac{P_t \sigma \lambda^2 G^2}{(4\pi)^3 K \sigma T_e BF(SNR)_{0min}} \right)^{\frac{1}{4}} \tag{3.2}$$

Where –

P_t = Peak power.

G = antenna gain.

λ = operating wavelength.

B = bandwidth.

F = noise figure.

SNR = signal to noise ratio.

R = target range.

So radar range at the power of $4(R_{max}^4)$ is directly proportional to the backscattered RCS from the targets.

For a large RCS, the radar range has to be very large for minimum SNR. So it may be said that none of the available radar waveforms may be able to guarantee the minimum required SNR for a particular RCS value at a particular detection range. In this case, the radar has to wait until the target is close enough in range to establish detection.

3.5. Factors that affect RCS

3.5.1. RCS dependency over target size

As a general knowledge the larger the object the greater it's RCS. This is because for a larger size of object the radar reflection is stronger which results in a larger RCS. Also radar constructed at one band cannot detect other band objects.

3.5.2. RCS Dependency on Wavelength

Radar cross section depends on the characteristics dimensions of the object compared to the radar wavelength. When the wavelength is large compared to the objects dimension, scattering is said to be in Rayleigh region. At the other extreme, where the wavelength is small compared to the objects dimensions, it is the optical region.

3.5.3. RCS Dependency on Aspect Angle

RCS surely varies as a function of aspect angle. For any two isotropic scatterers, the composite RCS consists of the superposition of the two individual radar cross sections. Taking any one object as phase reference, when the aspect angle is varied, the composite RCS is modified by the phase that corresponds to the electrical spacing between the two scatterers, that is

$$\text{Elec} - \text{spacing} = \frac{2 \, X \, 1.0 \, X\cos{(\text{aspectangle})}}{\lambda} \quad (3.3)$$

The following figure shows the composite RCS for such two objects. In this case computer simulation using MATLAB was performed for the proposed approximation. The detailed code is listed in the APPENDIX-A.
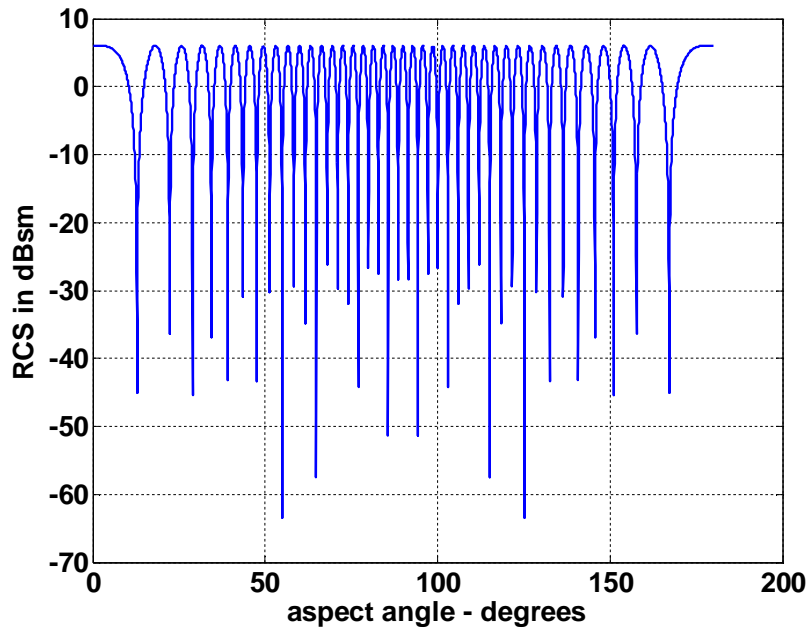
Figure 3.2: Illustration of RCS dependency on aspect angle.

The figure shows that RCS is dependent on radar aspect angle, where the curves represent the composite RCS of two individual scatters. The other parameters were scat_spacing = 1.0, frequency = 3GHz.

Constructive and destructive interference takes place between the RCS of two individual scatteres depending on the aspect angle. When the aspect angle is 0° or 180° constructive interference takes place and the RCS fluctuation is reduced. On the other hand, when the aspect angle is around 90° destructive interference takes place.

3.5.4. RCS Dependency on Frequency

For the demonstration of RCS dependency over frequency, two far field unity isotropic scatterers are aligned with radar line of sight, and the composite RCS is measured by the radar as the frequency is varied from 8 GHz to 12.5 GHz (X-band), the approximation is performed by the computer simulation program MATLAB which is listed in the APPENDIX-A.
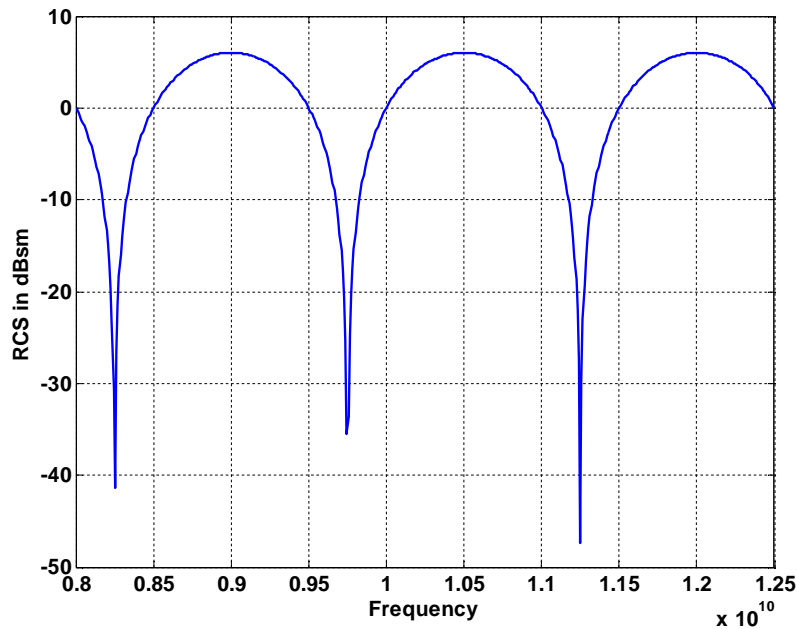
Figure 3.3a: Illustration of RCS dependency on frequency for scattering space 0.1m
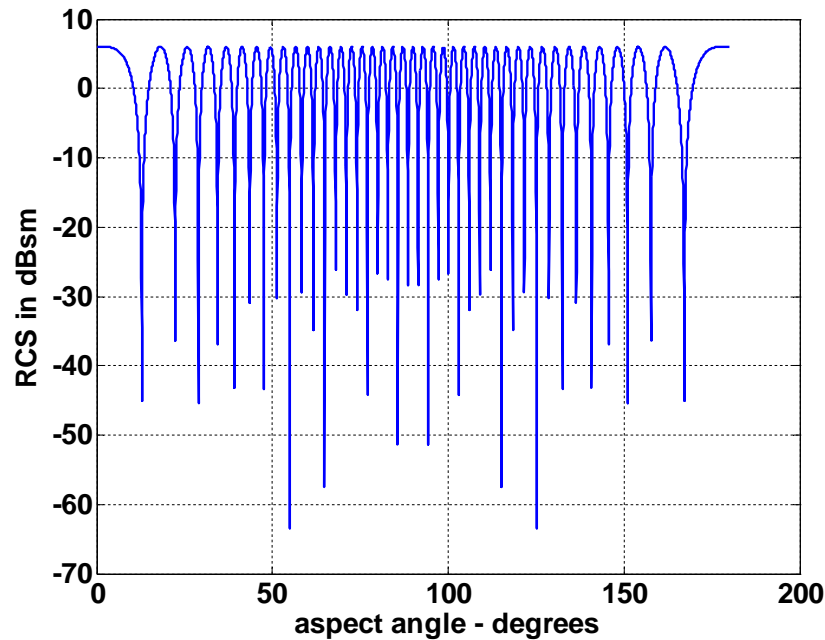
Figure-3.3b: Illustration of RCS dependency on frequency for scattering space 1m.

The plots showing the RCS dependency on frequency represent the RCS fluctuation as a function of frequency. As for little frequency change causes serious RCS fluctuation it is also observed that increase in scattering spacing through .1 m to 1m this fluctuation increases at huge rate. So it can be concluded that more frequency variation produces significant RCS fluctuation at a constant scattering spacing whereas

3.6. RCS of Simple Objects

The RCS of simple targets can be calculated from EM theory. As a part of analysis examples of backscattered radar cross section for a number of simple shape objects. In all cases, except for the perfectly conducting sphere, only optical region approximations are presented.

3.6.1. Perfectly Conducting Sphere

The scattered waves from a perfectly conducting sphere are co-polarized (have the same polarization) with the incident waves. This is because of symmetry and results in zero cross-polarized backscattered wave
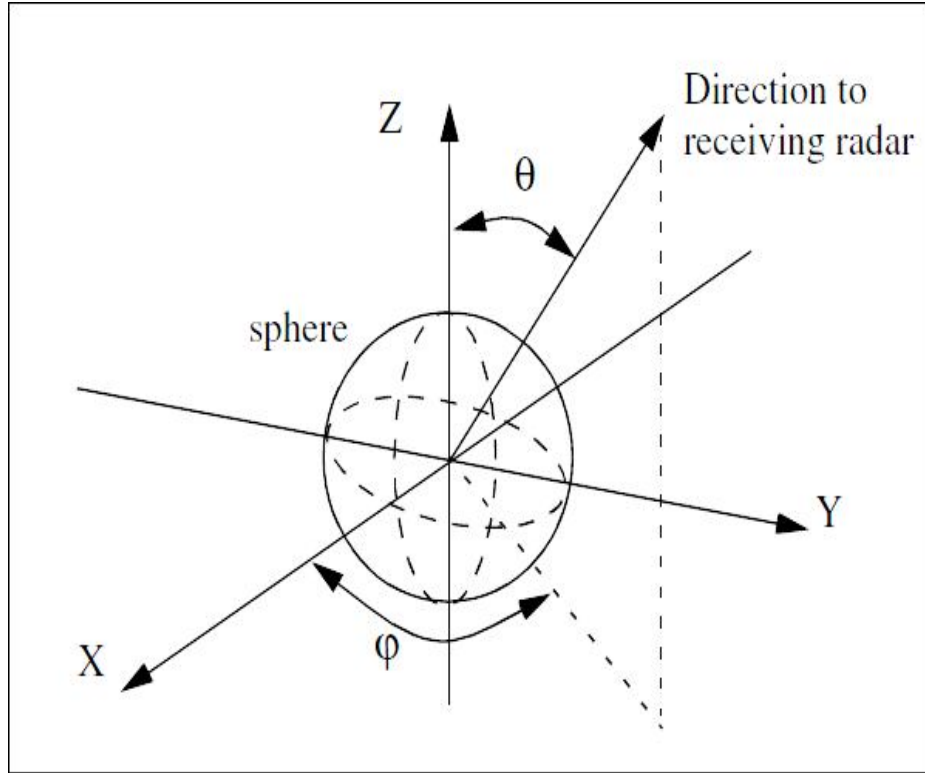
Figure 3.4: Direction of antenna receiving backscattered waves of a sphere.

The normalized exact backscattered RCS for a perfectly conducting sphere is a Mie series given by,

$$\frac{\sigma}{\pi r^2} = \left(\frac{j}{kr}\right)\sum_{n=1}^{\infty}(-1)^n(2n+1)\left[\left(\frac{krJ_{n-1}(kr)-nJ_n(kr)}{krH_{n-1}^{(1)}(kr)-nH_n^{(1)}(kr)}\right)\right.$$
$$\left.-\left(\frac{J_n(kr)}{H_n^{(1)}(kr)}\right)\right]$$

(3.4)

This simulation is very important from the view point of radar designing, which is illustrated in the APPENDIX-A. The result of the simulation shows that the backscattered RCS for a perfectly conduction sphere is constant in the optical region. This is the reason why the designers use spheres of known cross-section to experimentally calibrate the radar system.
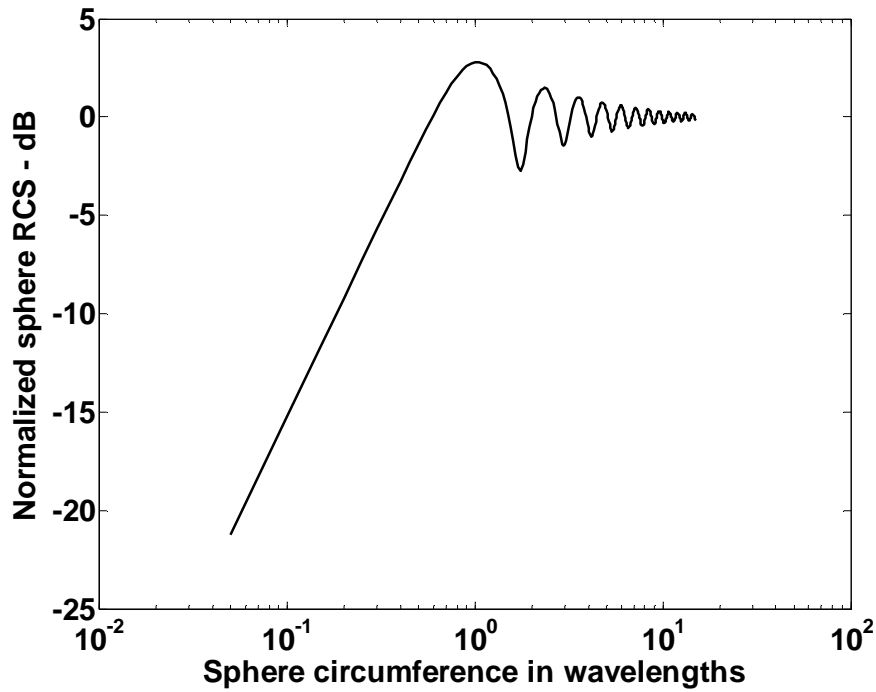
Figure 3.5: Normalized backscattered RCS for a perfectly conducting sphere using semi-log scale.

In the above figure three separate regions are evident:

Firstly, the Rayleigh region where r>>λ

In this case, $\sigma = \pi r^2$

Second, optical region, where λ>>r and $\sigma = 9\pi r^2 (kr)^4$.

And the third one is Mei region, which is a region oscillatory between Rayleigh and optical region.

Where r is the radius of the sphere. $k = \frac{2\pi}{\lambda}$ and λ is the wavelength.

3.6.2. Circular Flat Plate

The RCS of a circular flat plate target is only aspect angle dependent. Due to the circular symmetry, the backscattered RCS of a circular flat plate has no dependency on ɸ.
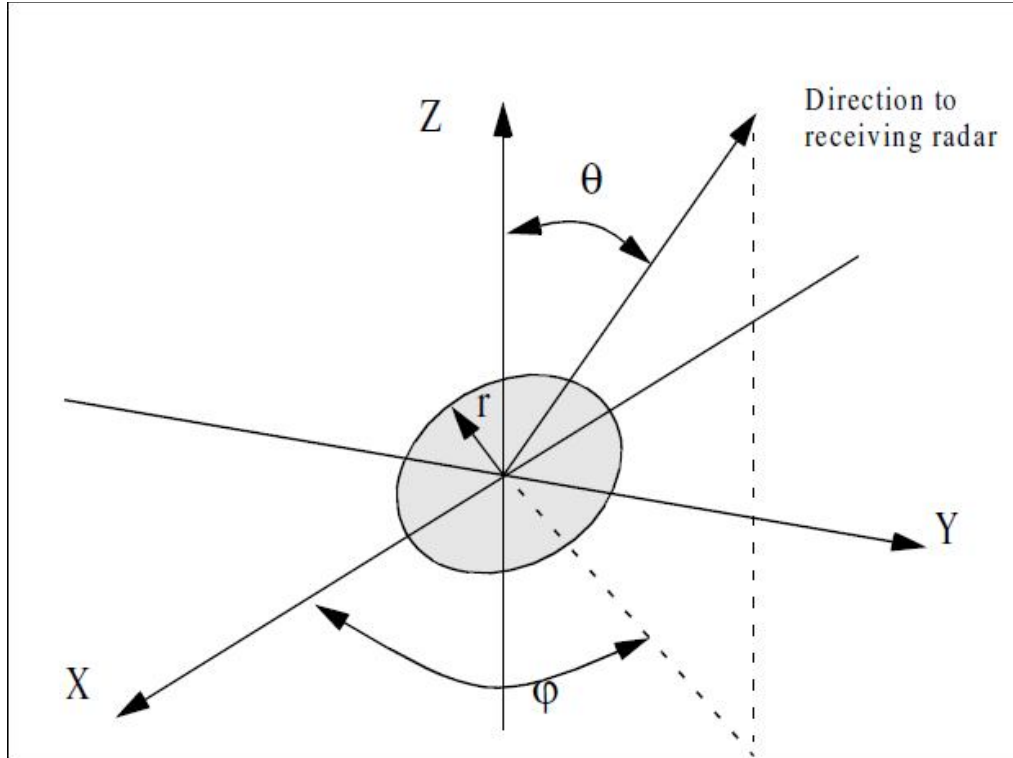
Figure 3.6: antenna receiving waves of a circular flat plate.

For normal incidence that means zero aspect angles the back scattered RCS for a circular flat plate given is,

$$\sigma = \frac{4\pi^3 r^4}{\lambda^2} \Theta = 0° \tag{3.5}$$

For incidence out of $0°$ two approximations for the circular flat plate backscattered RCS are,

$$\sigma = \frac{\lambda r}{8\pi \sin\theta (\tan\theta)^2} \tag{3.6}$$

$$\sigma = \pi k^2 r^4 \left(\frac{2J_1(2kr\sin\theta)}{2kr\sin\theta} \right)^2 (\cos\theta)^2 \tag{3.7}$$

Where $k = \frac{2\pi}{\lambda}$, and $J_1(\beta)$ is the first order spherical Bessel function evaluated at β. The figure below shows the evaluation of RCS versus the corresponding aspect angle. The simulation program code is listed in the APPENDIX-A. The other specifications are, r = 0.125m and f = 8 GHz.
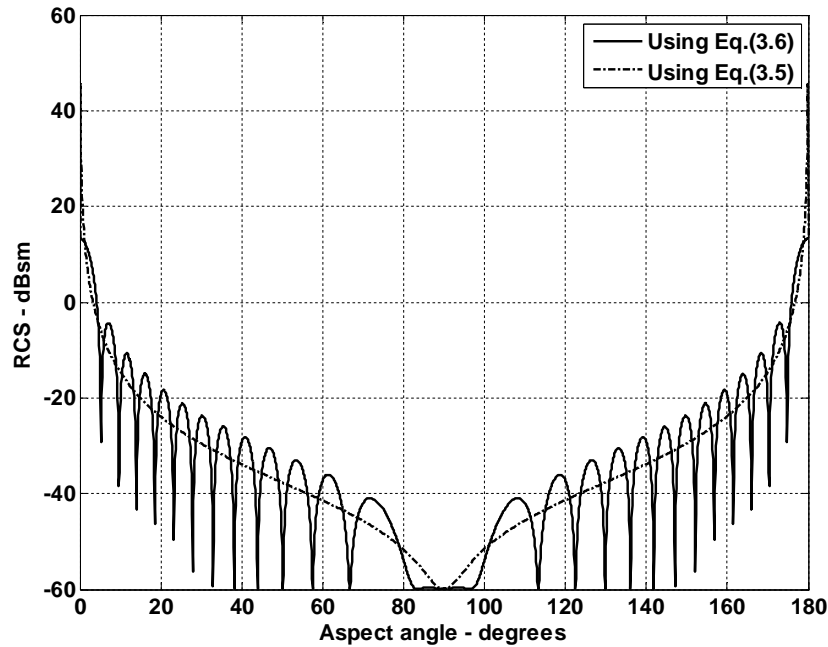
Figure 3.7: Backscattered RCS of a circular flat plate.

In the above figure the solid line corresponds to Eq. 3.7 and the dashed line corresponds to Eq. 3.6.

3.6.3. Circular Cylinder

In the case of evaluating the RCS of a cylinder we are considering a cylinder having circular surface which is referred to as a circular cylinder. For a circular cylinder of radius r and height h, the backscattered RCS is given,

$$\sigma = \frac{2\pi h^2 r}{\lambda} \Theta = 0° \tag{3.8}$$

$$\sigma = \frac{\lambda r sin\theta}{8\pi(\cos\theta)^2} \Theta \neq 0° \tag{3.9}$$

The RCS plot corresponding to the equations using MATLAB is shown in Figure 3.8. The simulation program is listed in the APPENDIX-A. The figure indicates that RCS depends on aspect angle and the broadside speculum occurs at aspect angle of $\frac{\pi}{2}$.
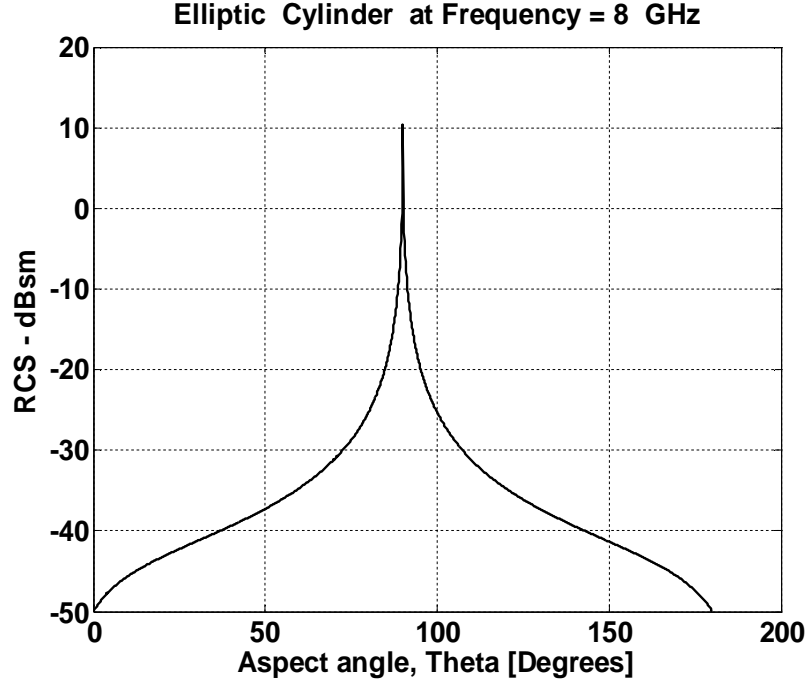
Figure 3.8: Backscattered RCS of a circular cylinder.

In the case of a cylinder it was revealed that the RCS variation as a function of aspect angle is quite equally distributed for values calculated at same distances on both side of 90˚. So it is clear that the normal incidence or maximum RCS occurs at 90˚ aspect angle which is quite high and decreases on both sides.

3.6.4. RCS of a Frustum

Considering the geometry shown in the above figure, the half cone angle α is given by

$$tan\alpha = \frac{r_2 - r_1}{H} = \frac{r_2}{L} \tag{3.10}$$

Where,

r_1 = small end radius.

r_2 = large end radius. and H = height of the frustum.

Considering θ_n as the angle of incidence, one approximation for the backscattered RCS of a truncated cone due to a linearly polarized incident wave is

$$\sigma_{\theta_n} = \frac{8\pi \left(z_2^{3/2} - z_1^{3/2}\right)^2}{9\lambda \, sin\theta_n} \tan\alpha \, (\sin\theta_n - \cos\theta_n \tan\alpha)^2 \tag{3.11}$$

42
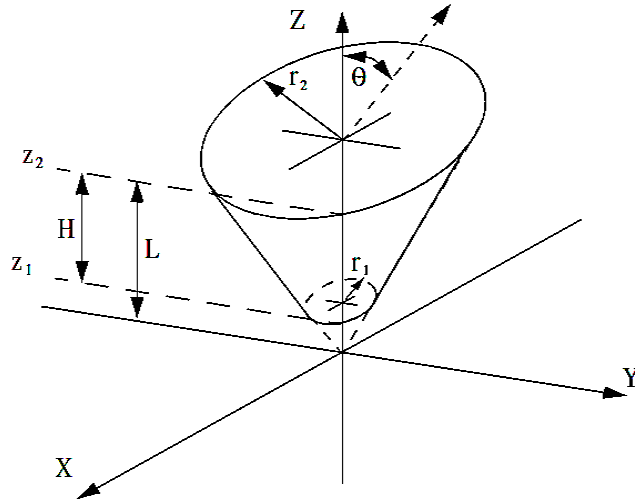
Figure3.9. truncated cone (frustum)

The above equation can also be reproduced as

$$\sigma_{\theta_n} = \frac{8\pi \left(z_2^{3/2} - z_1^{3/2}\right)^2}{9\lambda} \frac{\sin \alpha}{(\cos \alpha)^4} \tag{3.12}$$

For non-normal incidence, the backscattered RCS due to a linearly polarized incident wave is,

$$\sigma = \frac{\lambda z \tan \alpha}{8\pi \sin \theta} \left(\frac{\sin \theta - \cos \theta \tan \alpha}{\sin \theta \tan \alpha + \cos \theta}\right)^2 \tag{3.13}$$

The equation can be simplified as,

$$\sigma = \frac{\lambda z \tan \alpha}{8\pi \sin \theta} (\tan(\theta - \alpha))^2 \tag{3.14}$$

Where z is equal to either z_1 or z_2 depending on whether the RCS contribution is from the small or the large end of the cone.

The RCS plot corresponding to the equations is shown in the figure below. The corresponding MATLAB program is listed in the APPENDIX-A.

43

Viewing from small end

Viewing from large end
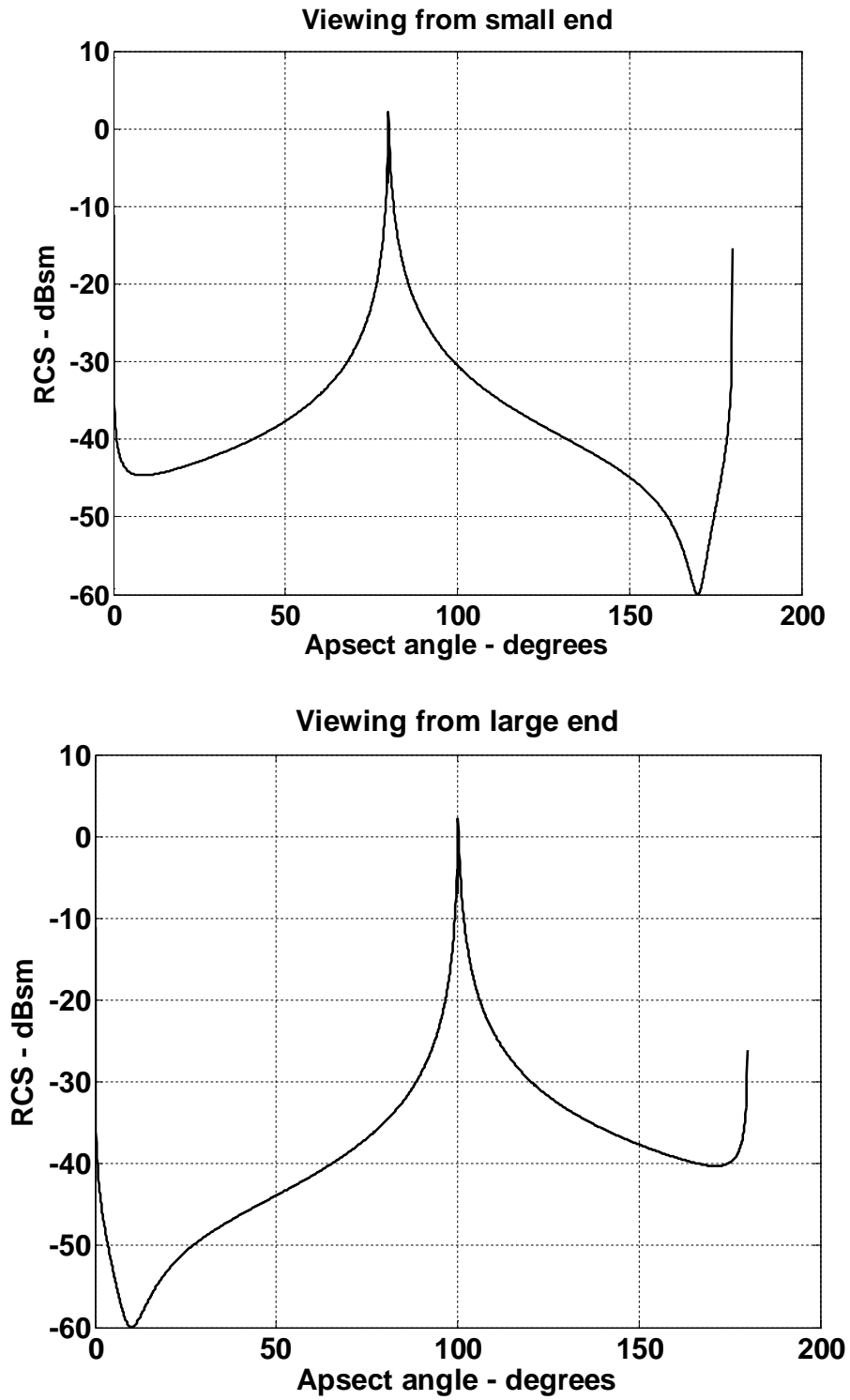
Figure 3.10: Backscattered RCS of a frustum.

In the figures above the one in the up shows a plot of RCS when illuminated by radar in the positive z direction. The one down shows the same thing, except in this case, the radar is in the negative z direction.

For a frustum the RCS variation is for aspect angle and the direction of the radar. Here normal incidence or highest value of RCS at +z direction occurs at 100° aspect angle, while for –z direction it occurs at 80°. On the both side of the normal incidence the RCS decreases symmetrically.

3.6.5. RCS of an Ellipsoid

The most widely accepted equation for the RCS of an ellipsoid is,

$$\sigma = \frac{\pi a^2 b^2 c^2}{\left(a^2(\sin\theta)^2(\cos\varphi)^2 + b^2(\sin\theta)^2(\sin\varphi)^2 + c^2(\cos\theta)^2\right)^2}$$

(3.15)

Where a, b and c are the radius over three axis.

In the above equation when a = b = c, the shape becomes a sphere. Whereas then, $\sigma = \pi c^2$ is the RCS of a sphere.
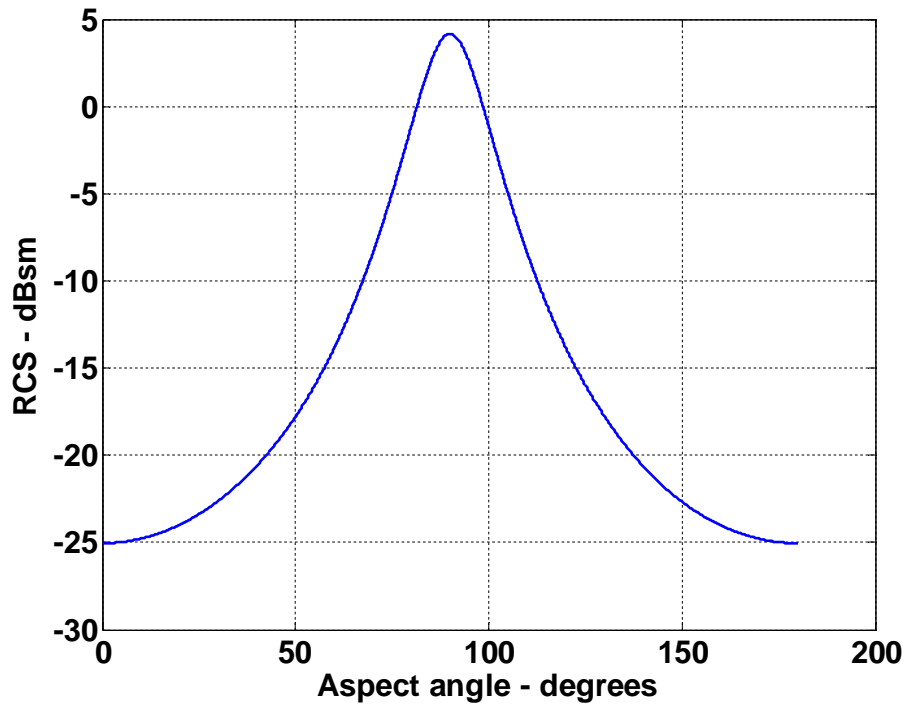
Figure 3.11: Backscattered RCS of an ellipsoid.

The figure shows the backscattered RCS of an ellipsoid versus θ for φ = 45˚. It is seen that the maximum RCS occurs at angle about 90˚ and decreases on the both side of it. At normal incidence (θ = 90˚) the RCS corresponds to that of a sphere of radius c, and is often referred to as the broadside specula RCS value.

3.7. RCS of Complex Objects

Until now we have considered stationary targets for our discussion. This kind of backscattered RCS is often called static RCS. In most practical radar systems there is relative motion between the radar and an observed target. The RCS of complex objects such as aircrafts, missiles, and fabricated structures can vary considerably with viewing aspect and frequency. This observed RCS is referred to as the radar dynamic cross section.

The variability in the complex RCS results from the multiple individual scatterers that constitute the object. Each individual scatterer of a complex target produces an echo signal characterized by amplitude and a phase. Dynamic RCS may fluctuate in amplitude and/or in phase. Phase fluctuation is called glint, while amplitude fluctuation is called scintillation. A complex target RCS is normally computed by coherently combining the cross sections of the simple shapes that make that target. In general, a complex target RCS can be modeled as a group of individual scattering centers distributed over the target.

Complex targets that can be modeled by many equal scattering centers are often called Swerling 1 or 2 targets. Alternatively, targets that have one dominant scattering center and many other smaller scattering centers are known as Swerling 3 or 4 targets.

As an example, consider a circular cylinder with two perfectly conducting circular flat plates on both ends. Assume linear polarization and let H = 1m and r = 0.125 m. The backscattered RCS for this object versus aspect angle is shown in Figure. 3.12. The MATLAB code for the corresponding figure is given in APPENDIX-A.
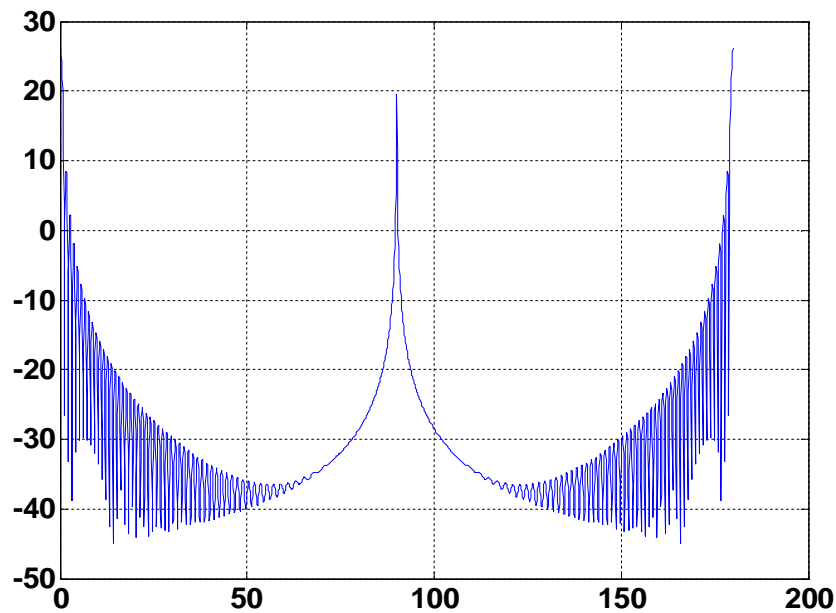
Figure 3.12: Backscattered RCS of a cylinder with flat plates

From the simulation it was revealed that at aspect angles close to 0° and 180° the RCS is mainly dominated by the circular plate, while at aspect angles close to normal incidence, the RCS is dominated by the cylinder broadside specular return.

3.8. Effects of RCS variation

RCS being a measure of how detectable an object is with radar, for a more precise detection of an object by radar, it is important to understand the significance of RCS prediction. Accurate prediction of RCS is critical in order to design and develop robust discrimination algorithms.

3.8.1. Significance of RCS over radar SNR

The significance of RCS in radar performance can be observed by demonstrating the SNR performance of radar for some particular shaped objects. It is revealed from simulation that for a large RCS, for a large radar range the SNR is minimum.

The approximate evaluation is confirmed by comparing the results obtained by the equation with those by computer simulation. Figure 3.13 shows a comparison between the SNR performance of radar for a circular flat plate object and circular cylindrical object, while Figure 3.14 compares the SNR for circular object and rectangular object.
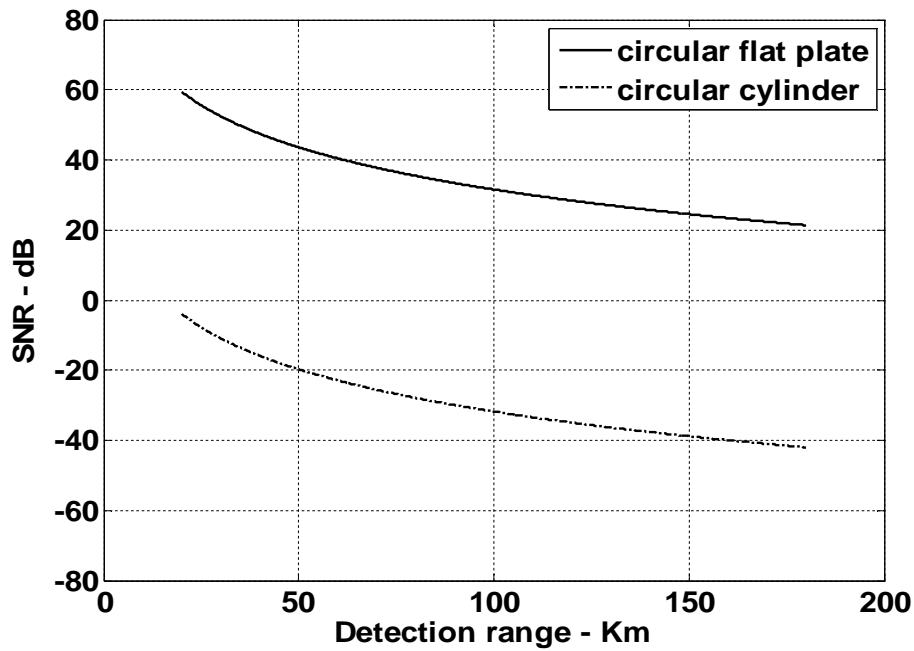
Figure 3.13: composite Range equation of circular plate and circular cylindrical objects fordifferent parameters (r = 0.125 m, h = 1m, P_t = 1.5 $Mwatt$, f = 8 GHz, G = 45 dB, F = 3dB, B = 5MHz, T_e= 290K, L = 6dB, R = 20km ~ 180km.)
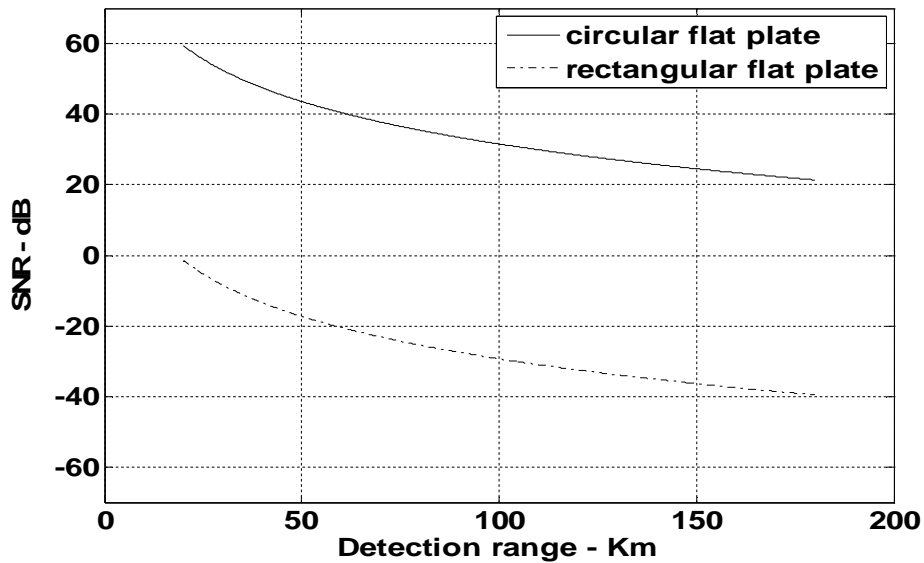
Figure3.14: composite Range equation of circular plate and rectangular flat plate objects for different parameters (r = 0.125m, a = 10.16 cm, b = 5.8 cm, P_t = 1.5 Mwatt, f =8GHz, G = 45dB, F = 3dB, B =5MHz, T_e= 290K, L = 6dB, R = 20km ~ 180km).

From both the simulations shown above it is revealed that for large RCS, SNR degrades with the increase of range, means that for a fixed/ constant range large RCS provides better SNR. The approximate analysis method is applicable to a variety of different objects. This concludes that change in the shape of the target causes huge change in SNR performance.

3.9. Reducing RCS

RCS reduction is chiefly important in stealth technology for aircraft, missiles, ships, and other military vehicles. With smaller RCS, vehicles can better evade radar detection, whether it is from land-based installations, guided weapons or other vehicles. Reduced signature design also improves platforms' overall survivability through the improved effectiveness of its radar counter-measures.

The distance at which a target can be detected for a given radar configuration varies with the fourth root of its RCS. Therefore, in order to cut the detection distance to one tenth, the RCS should be reduced by a factor of 10,000. As this degree of improvement is challenging, it is often possible when influencing platforms during the concept/design stage and using experts and advanced computer code simulations to implement the control options.

Chapter 4

RADAR WAVE PROPAGATION

4.1   Introduction

The wave propagation through the radar system is not done in the free space. To predict the Radar performance accurately we have to consider the signal interference due to earth surface and atmosphere. This includes ground reflections from the surface of the earth, diffraction of electromagnetic waves, bending or refraction of radar waves due to earth's atmosphere, and attenuation or absorption of radar energy by the gases constituting the atmosphere.

4.2   Earth Atmosphere

The earth atmosphere is compromised of several layers, shown in Figure 4.1. The first layer which extends in altitude to about 20 km is known as the troposphere. Electromagnetic waves refract (bend downward) as they travel in the troposphere. The troposphere refractive effect is related to it's dielectric constant which is a function of the pressure, temperature, water vapor, and gaseous content. Additionally due to gases and water vapor in the atmosphere radar energy suffers a loss. This loss is known as the atmospheric attenuation. Atmospheric attenuation increases significantly in the presence of rain, fog, dust and clouds.

The region above the troposphere (altitude from 20 to 50 km) behaves like free space and thus little refraction occurs in this region. This region is known as the interference region.

The ionosphere extends from about 50 km to about 600 km. It has very low gas density compared to the troposphere. It contains a significant amount of ionized free electrons. The ionization is primarily caused by the sun's ultraviolet and X-rays. This presence of free electrons in the ionosphere affects electromagnetic wave propagation in different ways. These effects include refraction, absorption, noise emission and polarization rotation.
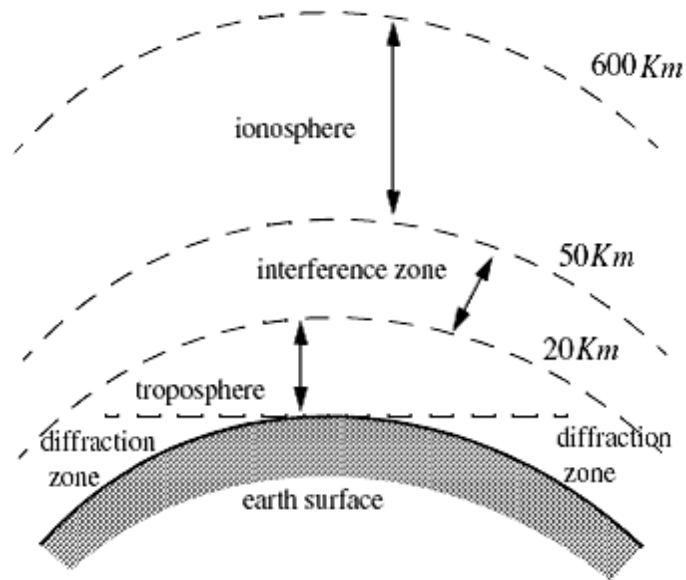
Figure 4.1: Earth atmosphere geometry

The degree of degradation depends heavily on the frequency of the incident waves. For example, frequencies lower than about 4 to 6 MHz, are completely reflected from the lower region of the ionosphere. Frequencies higher than 30 MHz may penetrate the ionosphere with some level of attenuation. In general, as the frequency is increased the ionosphere's effects become less prominent.

4.3   Refraction

In free space, electromagnetic waves travel in straight lines. However, in the presence of the earth atmosphere, they bend (refract). Refraction is a term used to describe the deviation of radar wave propagation from the straight lines. The deviation from the straight line propagation is caused by the variation of the index of refraction. The index of the refraction is defined as

$$n = \frac{c}{v} \qquad (4.1)$$

Where c is the velocity of the electromagnetic waves in free space and v is the wave velocity in the medium. The index of refraction are almost unity close to the earth's surface. With the increasing altitude the index of refraction decreases gradually.

Refraction affects radar waves in two different ways depending on height. For targets that have altitudes, typically above 100 meters, the effect of the refraction is illustrated in Figure 4.2. In this case refraction imposes limitations on the radar's capability to measure target position. Refraction introduces an error in the elevation angle.
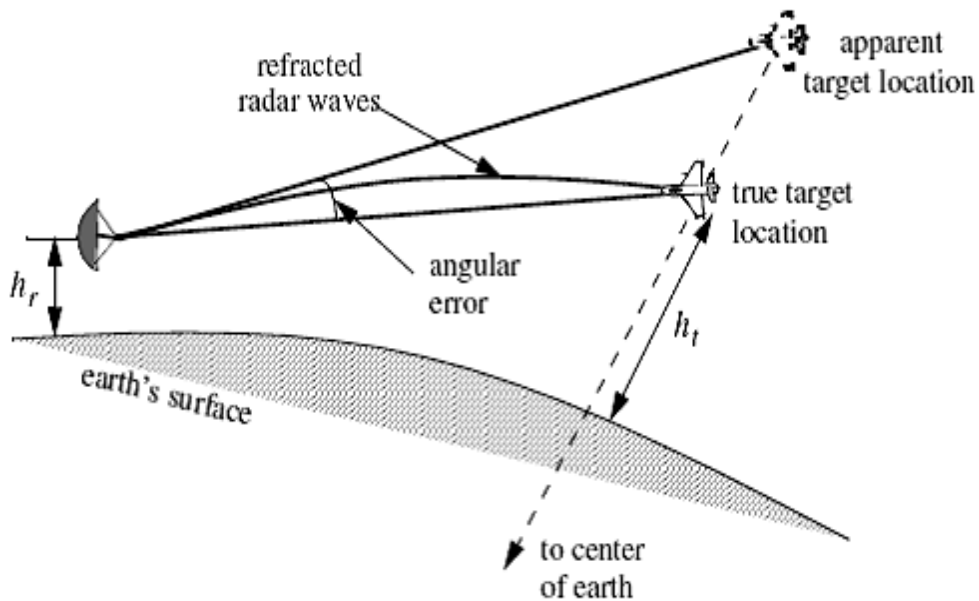
Figure 4.2: Refraction of high altitude waves on electromagnetic waves

In the well mixed atmosphere, the reflectivity gradient close to the earth's surface is almost constant. However, temperature changes and humidity lapses close to the earth's surface may cause serious changes in the refractivity profile when the refractivity index becomes large enough electromagnetic (EM) waves bend around the curve of the earth consequently the radar's range to the horizon is extended this phenomenon is called ducting and is illustrated in Figure 4.3 ducting can be serious over the sea surface particularly during the hot summertime.
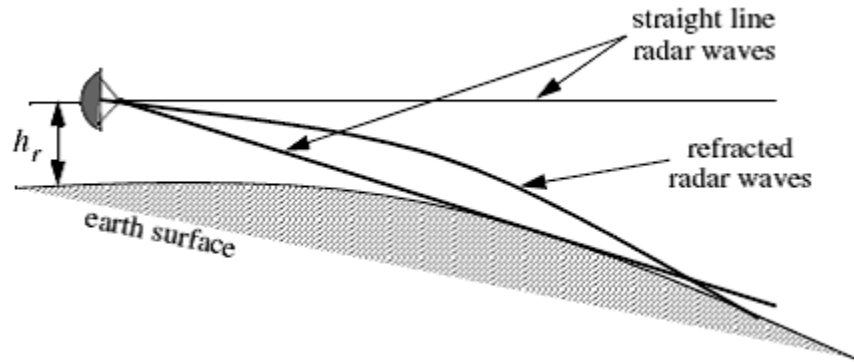
Figure 4.3: Refraction of high altitude waves on electromagnetic waves

Using ray tracing [geometric optics] an integral–relating range–to–target height with the elevation angle as a parameter can be derived and calculated. However, such computations are complex and numerically intensive. Thus, in practice, radar systems deal with refraction in two different ways, depending on height. For targets higher than 3km, actual target heights are estimated from look-up tables or from charts of target height versus range for different elevation angles.

Simpler methods that are valid for altitude less than 3 km, for calculating target height, can also be employed. In this case, the most common way of dealing with refraction is to replace the actual earth with an imaginary earth whose effective radius is $r_e = kr_0$, where r_0 is the actual earth radius, and k can be expressed as,

$$k = \frac{1}{1 + r_0(dn/dh)} \tag{4.2}$$

When the refractivity gradient is assumed to be constant with altitude and is equal to 39×10^{-9} per meter, then $k = {}^4/_3$. Using an effective earth radius $r_e = \left({}^4/_3\right)r_0$ produces what is known as "four third earth model". In general, choosing

$$r_e = r_0\left(1 + 6.37 \times 10^{-3}(dn/dh)\right) \tag{4.3}$$

produces a propagation model where waves travel in straight lines. Selecting the correct value for k depends heavily on the region's meteorological conditions. Blake derives the "height finding equation" for the 4/3 earth. It is

$$h = h_r + 6076 R \sin\theta + 0.6625 (\cos\theta)^2 \tag{4.4}$$
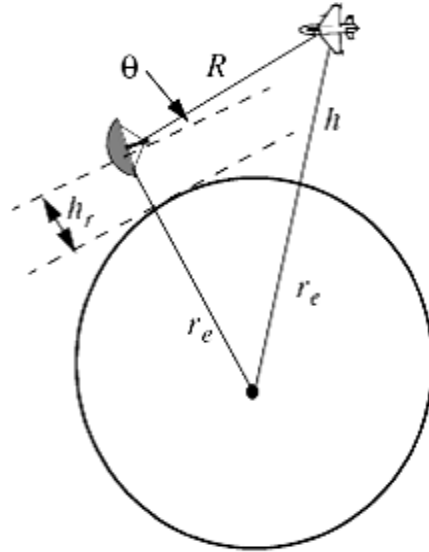
Figure 4.4: Measuring target height for 4/3 earth

Where h and h_r are in feet and R is the nautical miles. All variables are defined in Figure 4.4 The distance to the horizon for a radar located at a height h_r can be calculated with the help of Figure 4.5. For the right-angle triangle OAB we get

$$r_h = \sqrt{(r_0 + h_r)^2 - r_0^2} \tag{4.5}$$

Where r_h is the distance to the horizon. By expanding Eq. 4.5 and collecting terms we can derive the expression for the distance to the horizon as

$$r_h^2 = 2 r_0 h_r + h_r \tag{4.6}$$

Finally, since $r_0 \gg h_r$ Eq. 4.6 is approximated by

$$r_h \approx \sqrt{2 r_0 h_r} \tag{4.7}$$

And when refraction is accounted for, Eq. 4.7 becomes

$$r_h \approx \sqrt{2r_e h_r} \qquad (4.8)$$
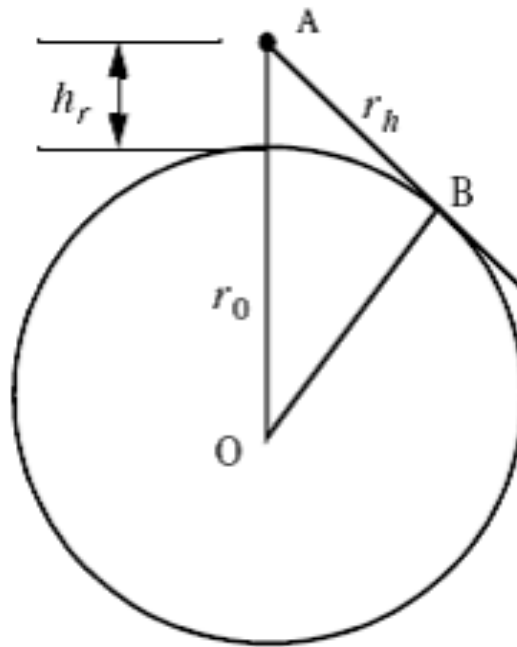
Figure 4.5: Measuring the distance from the horizon

4.4. Ground Reflection:

When radar waves are reflected from the earth's surface, they suffer a loss in amplitude and a change in phase. Three factors that contribute to these changes are the overall ground reflection coefficient for a flat surface, the divergence factor due to earth curvature, and the surface roughness.

4.4.1 Smooth surface reflection coefficient:

The smooth surface reflection coefficient depends on the frequency, on the surface dielectric coefficient and on the radar grazing angle. The vertical polarization and the horizontal polarization reflection coefficients are

$$\Gamma_v = \frac{\epsilon \sin\psi_g - \sqrt{\epsilon - (\cos\psi_g)^2}}{\epsilon \sin\psi_g + \sqrt{\epsilon - (\cos\psi_g)^2}} \qquad (4.9)$$

$$\Gamma_h = \frac{\sin\psi_g - \sqrt{\epsilon - (\cos\psi_g)^2}}{\sin\psi_g + \sqrt{\epsilon - (\cos\psi_g)^2}} \qquad (4.10)$$

Where ψ_g is the grazing angle (incident angle) and ϵ is the complex dielectric constant of the surface and are given by

$$\epsilon = \epsilon' - j\epsilon'' \qquad (4.11)$$

Typical values of ϵ' and ϵ'' can be calculated. For example, seawater at $28°C$ has $\epsilon' = 65$ and $\epsilon'' = 30.7$ at X-band. Figure 4.6 shows the corresponding magnitude plots for Γ_h and Γ_v, while Figure 4.7 shows the phase plots. The plots shown in those figures show the general typical behavior of the reflection coefficient.

Matlab function "ref_coef.m" calculates and plots the horizontal and vertical magnitude and phase response of the reflection coefficient. The syntax is as follows

$$[rh,rv,ph,pv] = ref\_coef(epsp,epspp)$$

Note that when $\psi_g= 90°$ we get

$$\Gamma_h = \frac{1 - \sqrt{\epsilon}}{1 + \sqrt{\epsilon}} = \frac{\epsilon - \sqrt{\epsilon}}{\epsilon + \sqrt{\epsilon}} = -\Gamma_v \qquad (4.12)$$

When the grazing angle is very small ($\psi_g \approx 0$), we have

$$\Gamma'_h = -1 = \Gamma'_v \tag{4.13}$$
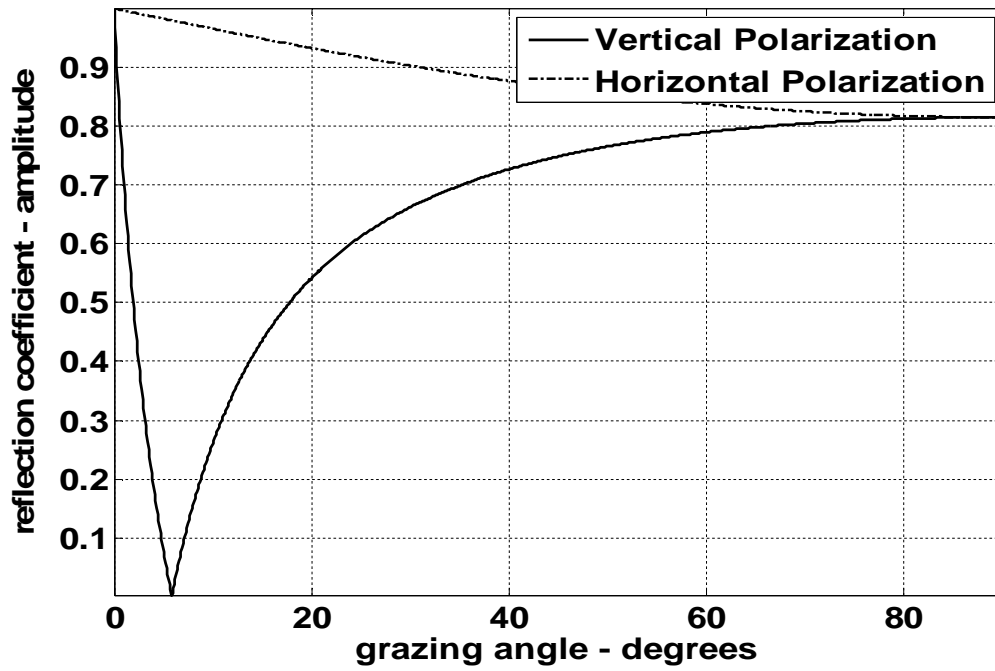
Figure 4.6: Reflection co-efficient magnitude
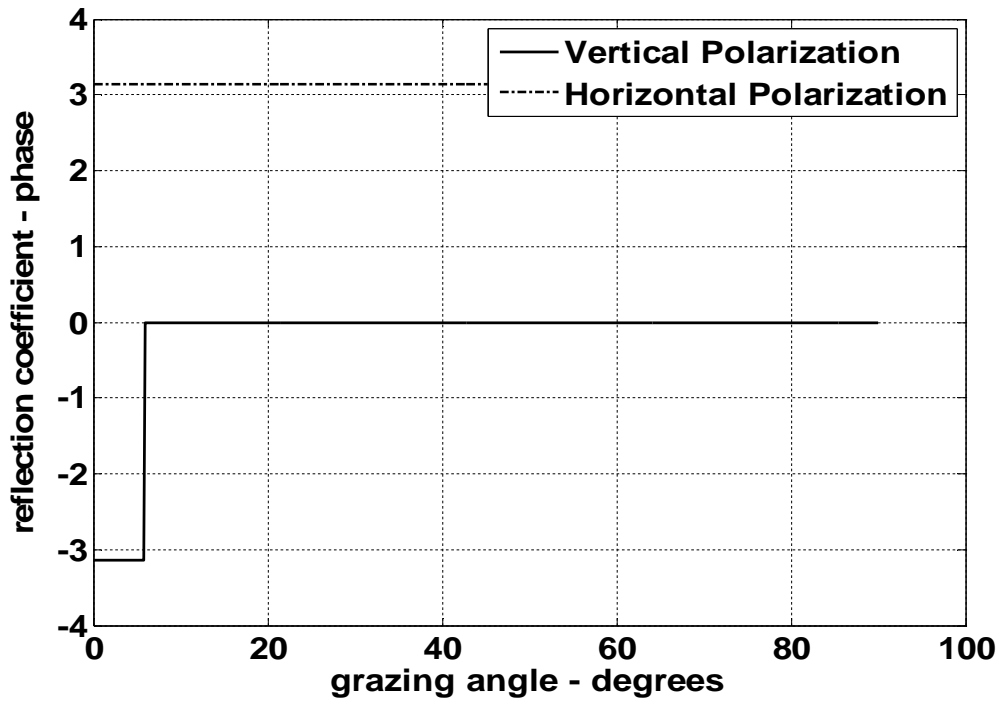
Figure 4.7: Reflection co-efficient phase

Observation of Figure 4.6 and 4.7 yield the following conclusions-

(1) The magnitude of the reflection coefficient with horizontal polarization is equal to unity at very small grazing angles and it decreases monotonically as the angle is increased.

(2) The magnitude of the vertical polarization has a well defined minimum. The angle that corresponds to this condition is called Brewster's polarization angle. For this reason, airborne radars in the look-down mode utilize mainly vertical polarization to significantly reduce the terrain bounce reflections.

(3) For horizontal polarization the phase is almost π. however, for vertical polarization the phase changes to zero around the Brewster's angle.

(4) For very small angles (less than 2°) both $|\Gamma_h|$ and $|\Gamma_h|$ are nearly one and the angle of Γ_h and Γ_v are nearly π. Thus little difference in the propagation of horizontally or vertically polarized waves exists at low grazing angles.

4.5. Diffraction

Diffraction is a term used to describe the phenomenon of electromagnetic waves bending around obstacles. It is of major importance to radar systems operating at very low altitudes. Hills and ridges diffract radio energy and make it possible to perform detection in regions that are physically shadowed. In practice, experimental data measurements provide the dominant source of information available on this phenomenon. Some theoretical analysis of diffraction are also available. However in these cases many assumptions are made and perhaps the most important assumptions is that obstacles are chosen to be perfect conductors.

The problem of propagation over a knife edge on a plane can be described with help of Figure 4.8. The target and radar heights are denoted, respectively h_t and h_r. The edge height is h_e.
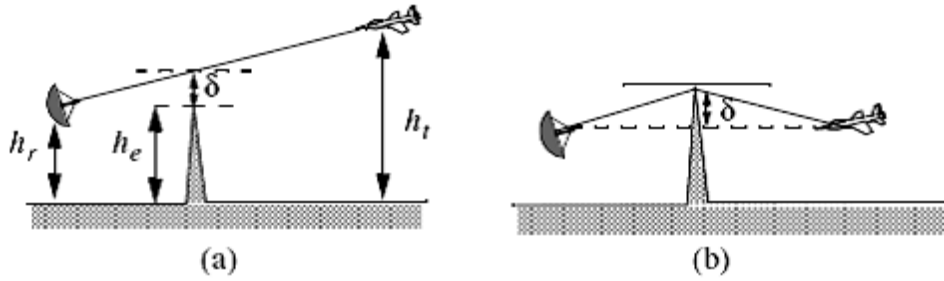
Figure 4.8: Diffraction over knife edge (a)Positive δ (b)Negative δ

Let us, denote the distance by which the radar rays clear (or do not clear) the tip of the edge by δ. As a matter of notation δ is assumed to be positive when the direct rays clear the edge, and is negative otherwise. Because of the fact that ground reflection occurs on both sides of the edge, then the propagation factor is composed of four distinct rays, as illustrated in Figure 4.9.
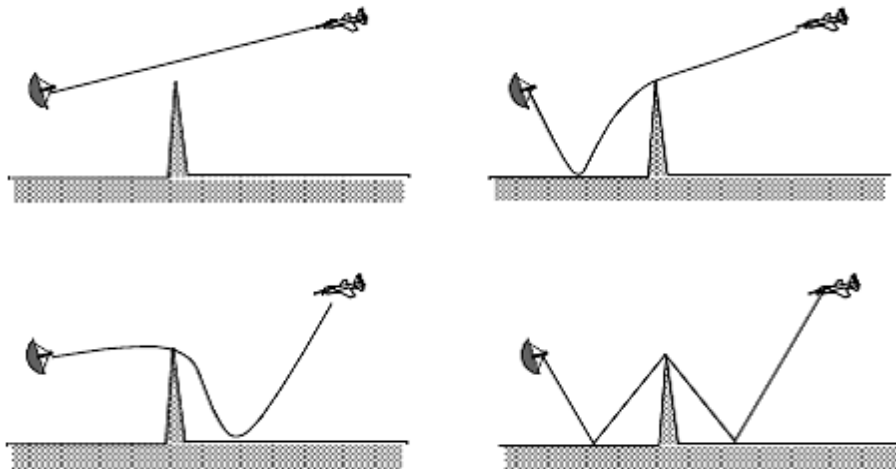
Figure 4.9: Four ray formation

This four ray formation is given by scientist Meek. Here it is shown that how the scattered rays from the target received by the radar antenna. For these echoes, the characteristics of the radar antenna could be, which is discussed in the next chapter.

4.6. Atmospheric Attenuation

Electromagnetic waves travel in free space without suffering any energy loss. Alternatively, due to gases and water vapor in the atmosphere radar energy suffers a los. This is known as

the atmospheric attenuation. Atmospheric attenuation increases significantly in the presence of rain, fog, dust and clouds. Most of the lost radar energy is normally absorbed by gases and water vapor and transformed into heat, while a small portion of this lost energy is used in molecular transformation of the atmosphere particles.

The two-way atmospheric attenuation over a range R can be expressed as

$$L_{atmosphere} = e^{-2\alpha R} \tag{4.14}$$

Where α is the one way attenuation co-efficient. Water vapor attenuation peaks at about 22.3 GHz, while attenuation due to oxygen peaks at between 60 and 118 GHz. Atmospheric attenuation is severe for frequencies higher than 35 GHz.
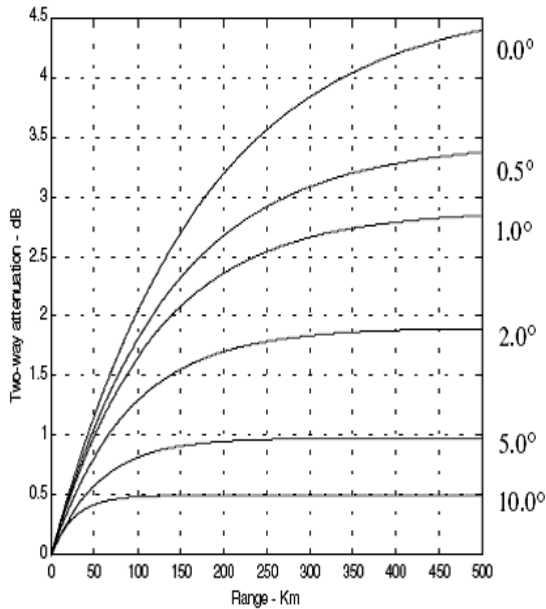
Figure 4.10 (a): Attenuation vs Range at 3 GHz
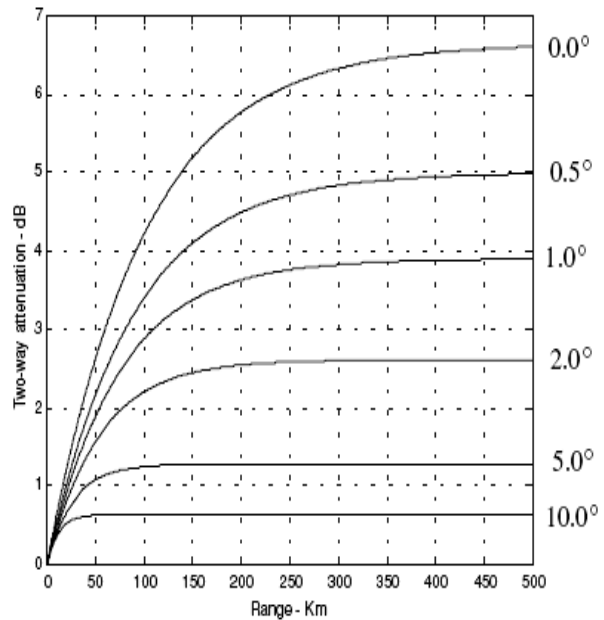
Figure 4.10 (b): Attenuation vs Range at 10 GHz

From the Figure 4.10, it is shown that with the increase of the frequency the attenuation decreases with increase of the elevation angle. At constant elevation angle the more the range the more will be the attenuation.

Chapter **5**

RADAR ANTENNA

5.1   Introduction

An antenna is a radiating device which acts is used to transform the electrical signal in the form of the travelling electromagnetic signal and it acts as a transducer between an electrical signal in a system and a propagating wave.

The Institute of Electrical and Electronic Engineers (IEEE)'s standard definition of terms of Antennas (IEEE std.145-1973) defines an antenna as "a mean for radiating or receiving radio power."

The antenna is needed for two reasons-

- Efficient Radiation
- Matching wave impedance in order to minimize reflection

5.2   Functions of the Radar Antenna

The radar Antenna is a distinctive and important part of any radar. It serves the following functions-

- Acts as the transducer between propagation in space and guided wave propagation in the transmission line.
- Concentrates the radiated energy in the direction of the target (as measured by the antenna gain).
- Collects the echo energy scattered back to the radar from a target (as measured by the antenna effective aperture).
- Measures the angle of arrival of the received echo signal so as to provide the location of a target in azimuth, elevation or both.

- Acts as a spatial filter to separate (resolve the targets) in the angle (spatial) domain and rejects undesired signals from directions other than the main beam.
- Provides the desired volumetric coverage of the radar.
- Establishes the time between radar observations of a target.

5.3   Characteristics of The Radar Antenna

5.3.1   Solid Angle:

Solid angle is the two dimensional angle In the three dimensional space that an object subtends at a point. It is a measure of how large that object appears to an Observer looking from that point. More Precisely, Solid angle is the amount of angle solidly provided by the surface. For a cone, of r radius bounded by the surface S, the solid angle defines as

Figure 5.1: Solid angle of cone

$$\text{solid angle, } \Omega = \frac{S}{r^2}$$

where, r = Radius from the center

S = Area of the surface

For sphere,

$$\text{Solid angle, } \Omega = \frac{4\pi r^2}{r^2} = 4\pi$$

In radar Antenna system, solid angle is important as transmitted signal and the scattered back signal depends upon the solid angle. So the radiation pattern as such as the directionality of the radar antenna is fully dependent upon the solid angle.
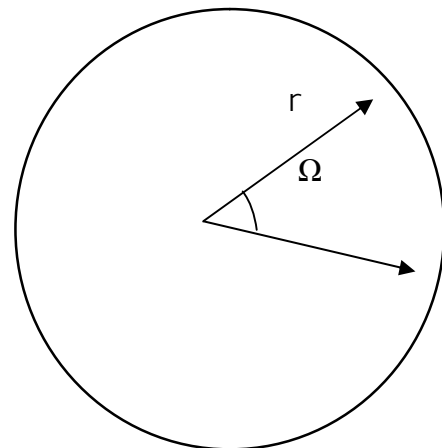
Figure 5.2: Solid angle of sphere

5.3.2 Beamwidth:

Beamwidth is the conical angle measurement between the points where the electric field intensity falls from its maximum value by 3 db. The solid angle is related to beam width in terms of the radiation pattern's principal plane 3 db beam width θ_B and φ_B. For a pattern with one relatively narrow main lobe and negligible side lobes, a rough approximation is, solid angle can be defined as

$$\phi_A \ = \ \theta_B \phi_B.$$

5.3.3 Antenna Gain:

An antenna is a radiating device which is used to transform the electrical signal in the form of the travelling electromagnetic signal and it acts as a transducer between an electrical signal in a system and a propagating wave.

Though radar antenna is a passive element, antenna gain is measured to know that how much power is radiated and how much power we want to radiate. So antenna gain is a measure of how strong a signal is received or transmitted compared to either an isotropic (point source) antenna or to a dipole antenna.

There are two types of antenna gain-

1. Directive Gain (Directivity):

The directive gain is descriptive of the nature of the antenna radiation pattern. The directive gain of a transmitting antenna is defined by,

$$G_D \ = \ \frac{\text{maximum radiation intensity}}{\text{average radiation intebsity}} \tag{5.1}$$

Where the radiation intensity is power per unit solid angle radiated in the direction (θ,φ) and is denoted $P(\theta,\varphi)$ which is watts per sterdian. A plot of the radiation patter intensity as a function of angular co-ordinates I called radiation intensity pattern.

Since the average radiation intensity over the entire solid angle of 4π sterdians is equal to the total power radiated by the antenna divided by 4π .

$$G_D = \frac{4\pi(\text{maximum power radiated per unit solid angle})}{\text{total power radiated by the antenna}} \quad (5.2)$$

2. Power Gain:

The power gain is similar to the directive gain except that it takes account of dissipative loses in antenna and it is defined as-

$$G = \frac{4\pi(\text{maximum power radiated per unit solid angle})}{\text{net power accepted by the antenna}} \quad (5.3)$$

Whenever there is no choice, the power gain should be used in the radar equation since it includes the dissipative losses introduced by the radar.

The directive gain which is always greater than the power gain, is more closely related to the antenna beam width. The difference between the two antenna gains is usually small for the reflector antennas.

5.4 Relationship Between Directivity And Power Gain

The power gain and the directive gain is related by the radiation efficiency ρ_r as follows,

$$G = \rho_r \, G_D \quad (5.4)$$

Eq. 5.2 follows that,

$$G_D = \frac{4\pi P(\beta, \varphi)_{max}}{\iint P(\beta, \varphi) d\beta \, d\varphi} \quad (5.5)$$

As an approximation, it is customary to rewrite Eq. 5.5

$$G_D \approx \frac{4\pi}{\beta_3 \varphi_3} \quad (5.6)$$

Where β_3 and φ_3 are the half-power (3-db) beamwidths in either direction.

Again the antenna effective aperture A_e is related to gain by

$$A_e = \frac{G\lambda^2}{4\pi} \quad (5.7)$$

Where λ is the operating wavelength. The relationship between the antenna's effective aperture A_e and the physical aperture A is

$$A_e = \rho A \qquad (5.8)$$

$$0 \leq \rho \leq 1$$

P is referred as the aperture efficiency, and good antennas require $\rho \rightarrow 1$ (means $A_e = A$)

Using simple algebraic manipulation of Eq. 5.6 and Eq. 5.7 we get,

$$G = \frac{4\pi A_e}{\lambda^2} \approx \frac{4\pi}{\beta_3 \varphi_3} \qquad (5.9)$$

Consequently, the angular cross section of the beam is

$$\beta_3 \varphi_3 \approx \frac{\lambda^2}{A_e} \qquad (5.10)$$

Eq. 5.10 indicates that the antenna beamwidth decreases as $\sqrt{A_e}$ increases.It follows that, in surveillance operation the number of beam positions an antenna will take on to cover a volume V is

$$N_{beams} = \frac{V}{\beta_3 \varphi_3} \qquad (5.11)$$

And when V represents the entire hemisphere Eq. 5.11 is modified to

$$N_{beams} = \frac{2\pi}{\beta_3 \varphi_3} = \frac{2\pi A_e}{\lambda^2} = \frac{G}{2} \qquad (5.12)$$

So for a specified angular region (V) the number of the beams is dependent both on the aperture efficiency and the solid angle.

5.5   Field Regions and Radiation Pattern

Based on the distance away from the face of the antenna, where the radiated electric field is measured, three distinct regions are identified-

1. **Reactive Near Field:** This is the electrostatic field where rays emitted from antenna have spherical wavefront (equi-phase fronts). The range of this region is,

$$R < 0.62\sqrt{D^2/\lambda}$$

2. **Radiative Near Field or Fresnel Region:** Like reactive near field, the emitted rays by antenna in this region are also spherical wave front. The range of this region is,

$$0.62\sqrt{D^2/\lambda} < R < 2D^2/\lambda$$

3. **Far Field or Fraunhofer Region:** This is the region where the angular distribution is dependent on the distance from the antenna

$$R > 2D^2/\lambda$$

In this region, the wavefronts can be locally represented by plane waves.

Where,   D = Largest dimension of the antenna

          R = The distance from the antenna

The near field and Fresnel regions are of little interest in radar system while most radar system operate in the Far or Fraunhofer Region.

The electric field intensity generated from the energy emitted by an antenna is a function of the antenna physical aperture shape and the electric current amplitude and phase distribution across the aperture. This phenomenon is known as Aperture illumination. The plot of the magnitude of the electric field intensity of the emitted radiation $|E(\beta, \varphi)|$ is referred to as the intensity pattern of the antenna. Altenatively, the plot of the square of the electric field intensity $|E(\beta, \varphi)|$ is known as power radiation pattern.

5.6. Circular Dish Antenna Pattern

Depending upon the purpose of the radar, the antennas used in the radar system are different in size and characteristics. Here we concern the circular dish antenna as it is used in microwave and radar applications because of it's simplicity in design and fabrication. So we discuss on the radiation pattern of this circular dish antenna in term of the electric field.

Assume the geometry of the circular aperture antenna shown in Figure 5.3.
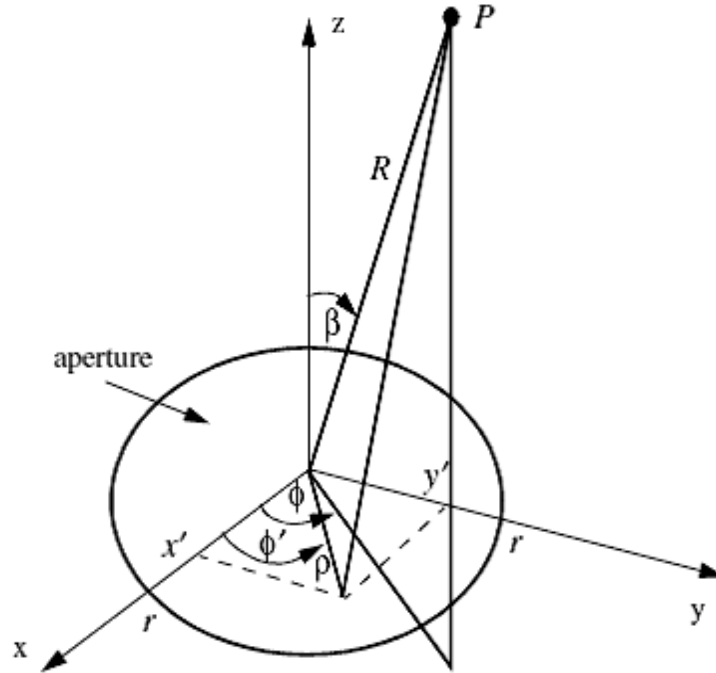
Figure 5.3: Circular aperture geometry

The circular dish antenna is divided into infinitely large number of infinitesimal current elements. The position of the current element in the x-y plane is characterized by $0° < \varphi' < 360°$

The position of the observation point is defined by range R and angular position (β, φ) at far field. Let the circular loop is of ρ radius carrying with a uniform current $I = I_0 \cos\omega t$. The aperture factor at p is given by,

$$E(\beta, \varphi) = \iint D(x'y')e^{j\psi(x'y')}dx'dy' \tag{5.13}$$

And the magnetic vector potential at the point P is,

$$\psi(x', y') = k(x' \sin\beta \cos\varphi + y' \sin\beta \sin\varphi) \tag{5.15}$$

Where,

Propagation constant, $k = \dfrac{2\pi}{\lambda}$, λ is the operating wavelength and $D(x',y')$ is the current distribution over the aperture.

Due to the circular nature of the aperture, it is more convenient to adopt cylindrical co-ordinates which follows that,

$$x^{'} = \rho\cos\varphi^{'} \tag{5.16}$$

$$y^{'} = \rho\sin\varphi^{'} \tag{5.17}$$

$$x^{'}\sin\beta\cos\varphi + y^{'}\sin\beta\sin\varphi = \rho\sin\beta\cos(\varphi - \varphi^{'}) \tag{5.18}$$

$$dx^{'}dy^{'} = \rho d\rho d\varphi^{'} \tag{5.19}$$

$$E(\beta,\varphi) = \int_0^r \rho d\varphi \int_0^{2\pi} e^{jk\rho\sin\beta\cos(\varphi-\varphi^{'})} \tag{5.20}$$

If the current distribution over the aperture is assumed to be unity, then the second integral of the Eq. 5.20 is of the form,

$$\int_0^{2\pi} e^{jz\cos\psi} = 2\pi J_o(z) \tag{5.21}$$

Where J_o is the Bessel function of the first kind of the order zero. Because of the circular symmetry over the aperture, the electric field is independent of φ. For this, $E(\beta,\varphi) = E(\beta)$, then Eq. 5.20 becomes,

$$E(\beta) = 2\pi \int_0^r \rho J_o(k\rho\sin\beta)d\rho \tag{5.22}$$

Using Bessel function identity,

$$\int_0^r \rho J_o(q\rho)d\rho = \frac{r}{q}J_1(qr) \tag{5.23}$$

From Eq. 5.22 and 5.23,

$$E(\beta) = \pi r^2 \frac{2J_1(kr\sin\beta)}{kr\sin\beta} \tag{5.24}$$

Eq. 5.24 is the representation of the electric intensity of the circular aperture antenna in term of the Bessel function. This Eq. is reproduced by the matlab function "circ_aperture.m". This function computes and plots the radiation pattern of the circular aperture antenna. The syntax of the function is as followed,

[emod] = circ_aperture (lamda, d)
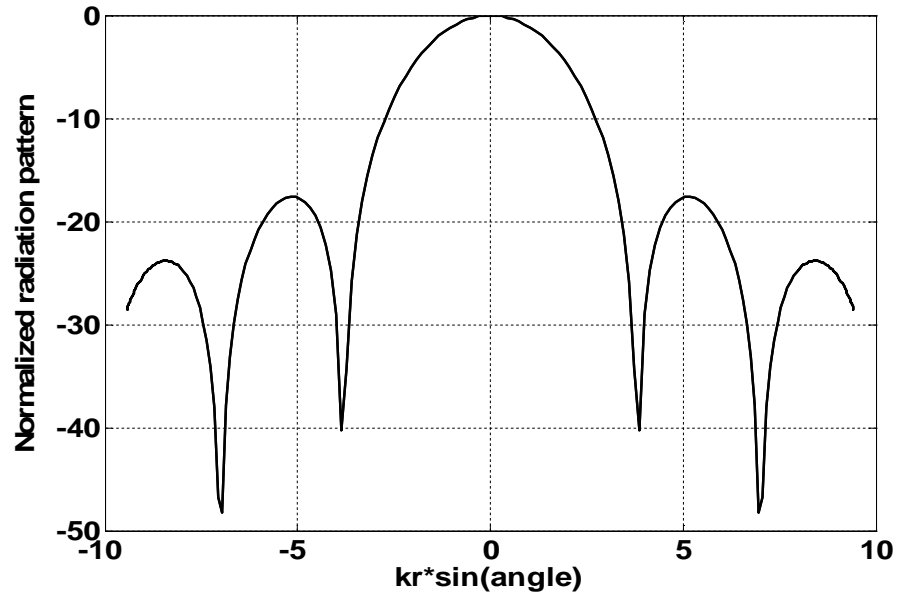
Figure 5.4(a): Radiation pattern of the circular aperture antenna (d=0.3m, λ=0.1m)
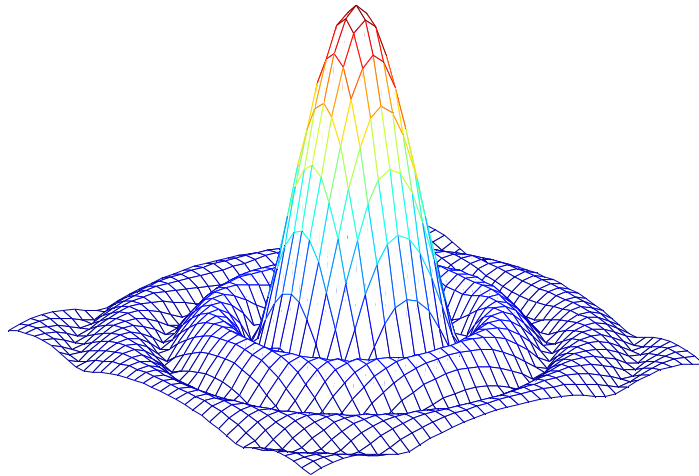
Figure 5.4(b): 3-D plot of the radiation pattern of circular aperture antenna

69

Figure 5.4(a) represents a single peak in one direction in the radiation pattern, this is the direction where the bulk of the radiated power travels. This is the main beam of maximum value. The polar plot and the 3-D plot-Figure 5.4(b) shows that the receiving and the transmitting power by the circular aperture antenna is one directional.
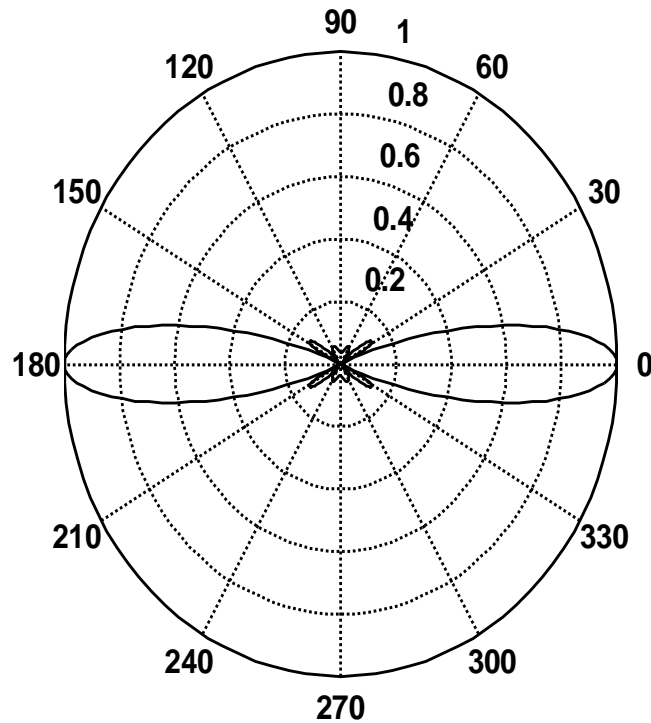
Figure 5.4 (c): Polar plot of the circular aperture

This function concerns the radial distance (R) from the center of the circular aperture and the angle of the aperture (β). With the increase of the angular distance, the intensity decreases from the both side of the center by the law $E \propto \frac{1}{R^2}$ and this is clearly indicated in Figure 5.4(c)

So here it is noticed that, the peak side lobe of the pattern from the sine function is much lower than the peak side lobe from the uniform illumination. Its beamwidth is however increased and its maximum gain is decreased.

5.7 Antenna Array:

It is important to design radar Antennas with more energy radiated in some particular directions and less in other directions. This is tantamount to requiring that the radiation pattern should be concentrated in the actual direction of interest. This is hardly achievable with a single radar Antenna which has a limited radiation pattern. But with the use of the several antennas working together, it is possible to improve the radiation according to some specification.

An antenna array is a group two or more isotropic radiators such that the currents running through them are of different amplitudes and phases. Each radiator is denoted as an element. The elements forming an array could be dipoles dish reflectors, slots in a waveguide or any other type of radiator. Array antennas synthesize narrow directive beams that may be steered mechanically or electronically in many directions. The antenna consists of lines whose elements are fed about a common phase shifter. The antenna which is formed by these numbers of vertically mounted lines is called Linear Array Antenna.

5.7.1 Linear Array:

A linear array antenna is simply the antenna where the antenna elements are arranged along a straight line. Suppose a linear array antenna is consisting of N identical elements spaced by d (normally measured in wavelength units). Let element #1 serves as a phase reference for the array. From the geometry, it is clear that an outgoing wave at the nth element leads the phase at the (n+1) the element by kdsinψ, where k = 2π/λ the combined phase at the far field observation point P is independent of φ is computed as-

$$E\ (p) = E\ (one\ element)*(array\ factor)$$

The array factor (AR) is a general function of the number of elements, their spacing and their relative phases and magnitudes. So the electric field at a far field observation point with direction-sine equal to sinψ (assuming isotropic element) is

$$E\ (\sin\psi)\ =\ \sum_{n=1}^{N} e^{j(n-1)kd\sin\psi} \tag{5.25}$$
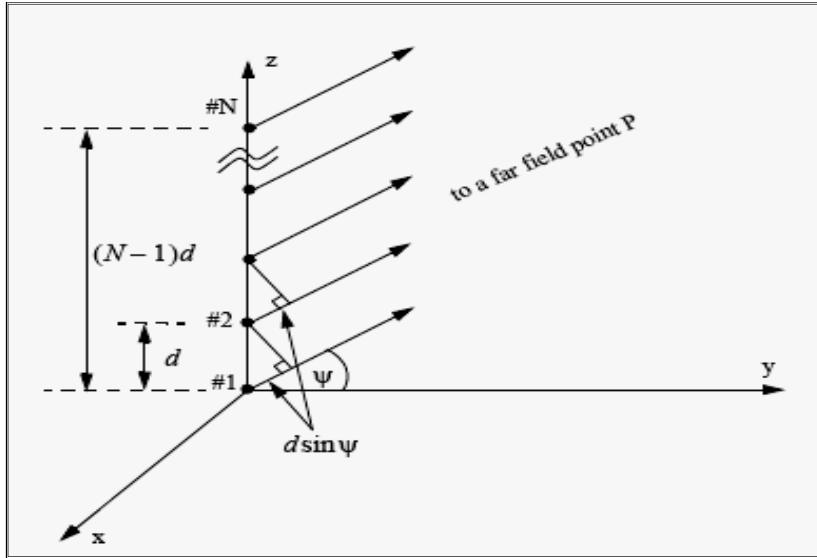
Figure 5.5: Linear array of equally spaced elements

Expanding this equation,

$$E\ (\sin\psi)\ =\ 1 + e^{jkd\sin\psi} + \ldots\ldots + e^{j(N-1)kd\sin\psi} \tag{5.26}$$

The right-hand side of Eq. (2) is a geometric series which can be expressed in the form,

$$1 + a + a^2 + a^3 + \cdots\ldots + a^{(N-1)} = \frac{1-a^N}{1-a} \tag{5.27}$$

Replacing a by $e^{jkd\sin\psi}$ yeilds,

$$|E\ (\sin\psi)| = \frac{1-e^{jNkd\sin\psi}}{1-e^{jkd\sin\psi}}$$

$$= \frac{1 - (\cos Nkd\sin\psi) - j(\sin Nkd\sin\psi)}{1 - (\cos kd\sin\psi) - j(\sin kd\sin\psi)} \tag{5.28}$$

The far field array intensity pattern is then given by

$$|E\ (\sin\psi)| = \sqrt{E(\sin\psi) \times E^*(\sin\psi)} \tag{5.29}$$

Substituting Eq. 5.28 into 5.29,

$$|E\,(\sin\psi)| \;=\; \sqrt{\frac{(1 - \cos N k d \sin\psi)^2 \,+\, (1 - \sin N k d \sin\psi)^2}{(1 - \cos k d \sin\psi)^2 \,+\, (1 - \sin N k d \sin\psi)^2}}$$

$$=\; \sqrt{\frac{1 - \cos N k d \sin\psi)}{1 - \cos k d \sin\psi)}} \qquad\qquad (5.30)$$

And using the trigonometric identity, $1 - \cos\theta = 2(\frac{\sin\theta}{2})^2$ yields

$$|\,E\,(\sin\psi)\,| \;=\; \left|\frac{\sin(N k d \sin\psi/2)}{\sin(k d \sin\psi/2)}\right| \qquad\qquad (5.31)$$

Which is a periodic function of $k d \sin\psi$, with a period equal to 2π.

The maximum value of $|\,E\,(\sin\psi)\,|$ which occurs at $\psi = 0$, is equal to N. It follows that the normalized intensity pattern is equal to,

$$|\,E\,(\sin\psi)\,| \;=\; \frac{1}{N}\left|\frac{\sin(N k d \sin\psi/2)}{\sin(k d \sin\psi/2)}\right| \qquad\qquad (5.32)$$

The normalized two way array pattern (radiation pattern) is given by

$$G\,(\sin\psi) \;=\; |\,E\,(\sin\psi)\,|^2 \;=\; \frac{1}{N^2}\left(\frac{\sin(N k d \sin\psi/2)}{\sin(k d \sin\psi/2)}\right)^2 \qquad\qquad (5.33)$$

Figure 5.6 (a) shows a plot of Eq. 5.33 versus sin for N = 8. The radiation pattern G (sinψ) has cylindrical symmetry about its axis (sinψ = 0) and is independent of the azimuth angle. Thus it is completely determined by its values within the interval ($0 < \psi < \pi$).

The main beam of an array can be steered electronically by varying the phase of the current applied to each array element. Steering the main beam into the direction-sine $\sin\psi_0$ is accomplished by making the phase difference between any two adjacent elements equal to $k d \sin\psi_0$. In this case the normalized radiation pattern is–
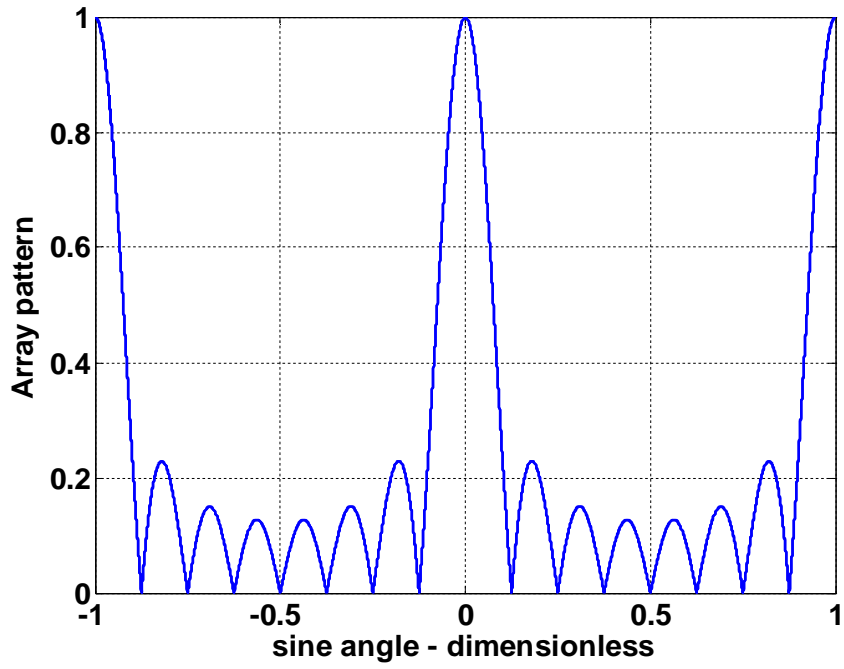
Figure 5.6 (a): Normalized radiation pattern for linear array (N=8 and d=λ)
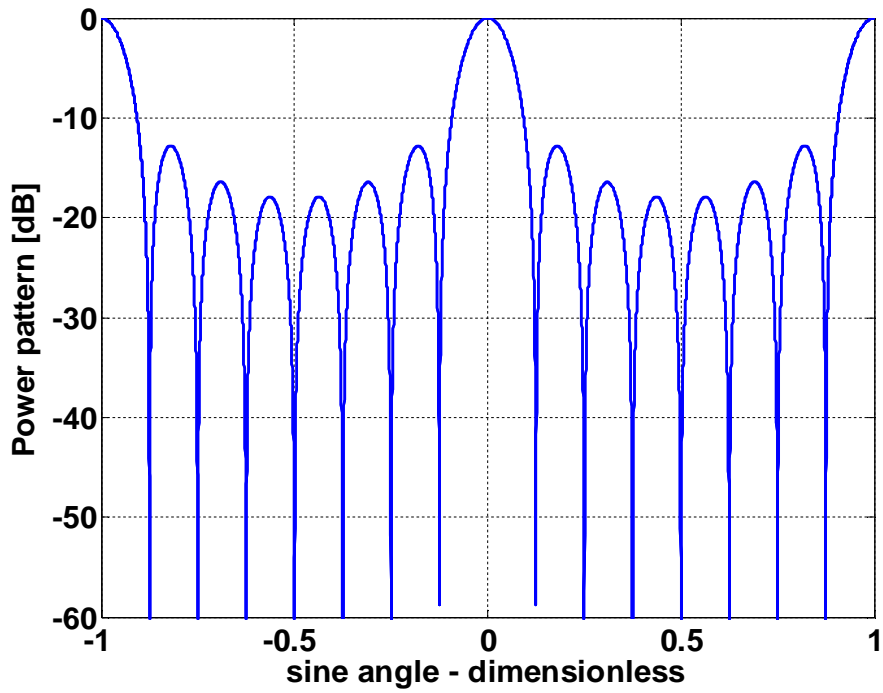
Figure 5.6 (b): Normalized Power Pattern

$$G(\sin\psi) = \frac{1}{N^2}\left(\frac{\sin\left[\left(\frac{Nkd}{2}\right)(\sin\psi - \sin\psi_0)\right]}{\sin\left[\left(\frac{kd}{2}\right)(\sin\psi - \sin\psi_0)\right]}\right)^2 \qquad (5.34)$$

If $\psi_0 = 0$, then the main beam is perpendicular to the array axis and the array is said to be a broadside array. Alternatively, the array is called endfire array when the main beam points along the array axis.

Power pattern [dB]
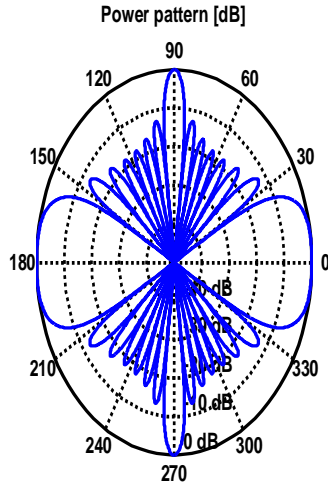
Array pattern

Figure 5.7 (a): Polar Plot of the Power Pattern
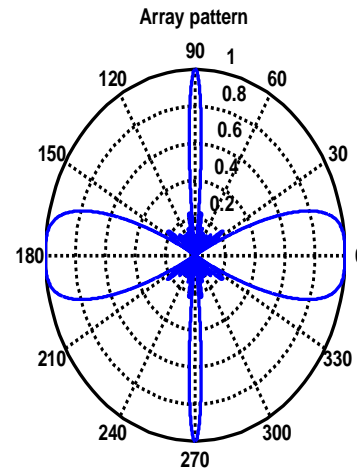
Figure 5.7 (b): Polar Plot of the Array Pattern

The radiation pattern maxima are computed using L'Hospital's rule when both the denominator and numerator of Eq. 5.33 are zeros. More precisely,

$$\frac{kd\sin\psi}{2} = \pm m\pi ; \qquad m = 0,1,2,3\ldots\ldots\ldots\ldots\ldots etc \qquad (5.35)$$

Solving ψ yields,

$$\psi_m = asin\left(\pm\frac{\lambda m}{2}\right) ; \qquad m = 0,1,2,3\ldots\ldots\ldots\ldots\ldots etc$$

Where the subscript m is used as a maxima indicator. The first maxima occurs at $\psi_0 = 0$, known as main beam and the other maxima occurring at $|m| \geq 1$, known as grating lobes which are undesirable and must be suppressed. The grating lobes occur at,

$$\left|\sin\psi - \sin\psi_o\right| = \pm\frac{\lambda n}{d} \; ; \qquad n = 1,2,3\ldots\ldots\ldots\ldots\ldots. \text{etc} \qquad (5.36)$$

The radiation pattern attains the secondary maxima (sidelobes) when the numerator of the Eq. 5.33 is maximum or equivalently,

$$\frac{Nkd\sin\psi}{2} = \pm(2l + 1)\frac{\pi}{2} \qquad (5.37)$$

Solving ψ yields,

$$\psi_l = \text{asin}\left(\pm\frac{\lambda}{2d}\frac{2l + 1}{N}\right) ; \qquad l = 1,2,\ldots\ldots\ldots\ldots. \qquad (5.37)$$

where the subscript l is used as an indication of the side lobe maxima. The nulls of the radiation pattern occure when only the numerator of Eq. 5.34 is zero. More precisely,

$$\frac{Nkd\sin\psi}{2} = \pm n\pi \; ; \qquad n = 1,2,\ldots\ldots\ldots \qquad (5.38).$$

Again solving for ψ,

$$\psi_n = \text{asin}\left(\pm\frac{\lambda n}{dN}\right) ; \qquad n = 1,2,\ldots\ldots.. \qquad (5.39)$$

Where the subscript n is used as a null indicator, define the angle which corresponds to the half power point as ψ_n. It follows that the half power (3-db) beamwidth is $2\left|\psi_m - \psi_n\right|$ and this is occurs when,

$$\frac{Nkd\sin\psi_n}{2} = 1.391 \text{ radians}$$

Thus in order to prevent the grating lobes from occurring between ± 90, the element spacing should be d < λ/2 instead of d < λ. By this the directionality of the radar antenna will be improved.

5.7.2   Radiation Pattern By Computation Method Via DFT:
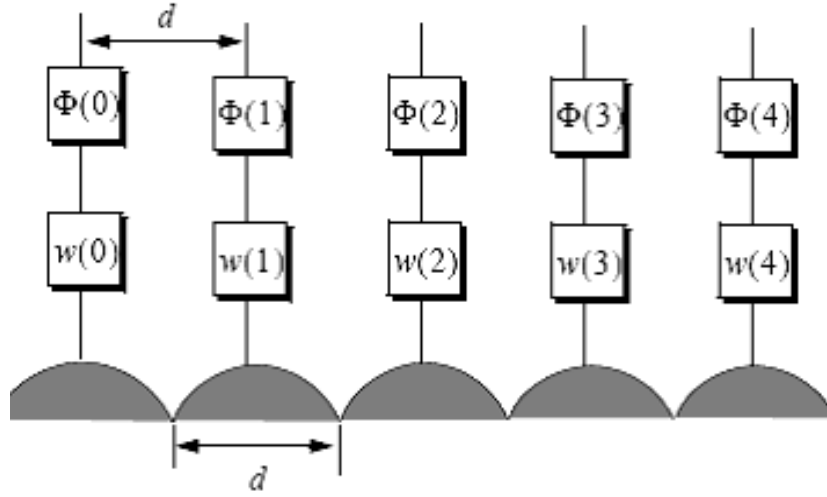
Figure 5.8: Linear Array of size 5 with phase shifting hardware

Figure 5.8 shows a linear array of size N element spacing d and wavelength λ. The radiators are circular dishes of diameter d. Let w(n) and φ(n) denotes the tapering and phase shifting sequences. The normalized electric field at a far field point in the direction-sine $\sin\psi$ is –

$$E(\sin\psi) = \sum_{n=0}^{N-1} w(n)e^{j\Delta\phi\left(n-\left(\frac{N-1}{2}\right)\right)} \tag{5.40}$$

Where in this case the phase reference is taken as the physical center of the array and

$$\Delta\varphi = \frac{2\pi d}{\lambda}\sin\psi$$

Expanding and factoring Eq. 5.40 we get,

$$E(\sin\psi) = e^{j\varphi_0}\{w(N-1)e^{-j\Delta\varphi(N-1)} + w(N-2)\,e^{-j\Delta\varphi(N-2)} + \cdots\ldots\ldots + w(0) \tag{5.41}$$

The discrete fourier transform of the sequence w(n) is defined as

$$W(q) = \sum_{n=0}^{N-1} w(n)e^{\frac{j2\pi nq}{N}} \quad ; \qquad q = 0,1,\ldots\ldots\ldots.N-1 \tag{5.42}$$

The set of $\{\sin\psi_q\}$ which makes $\qquad\qquad \sin\psi_q = \frac{\lambda q}{Nd}$ $\qquad\qquad$ (5.43)

So from Eq. 5.42 and Eq. 5.43,

$$E(\sin\varphi) = e^{j\varphi_0}W(q) \tag{5.44}$$

The one way array pattern is computed as the modulus of Eq. 5.44. It follows that the radiation pattern becomes,

$$G(\sin\psi) = G_e|w(q)| \tag{5.45}$$

Where, G_e is element pattern.
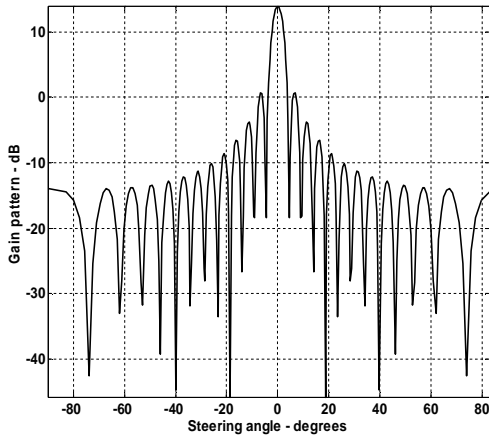
Figure 5.9 (a): Array gain pattern for steering angle 0, win=none
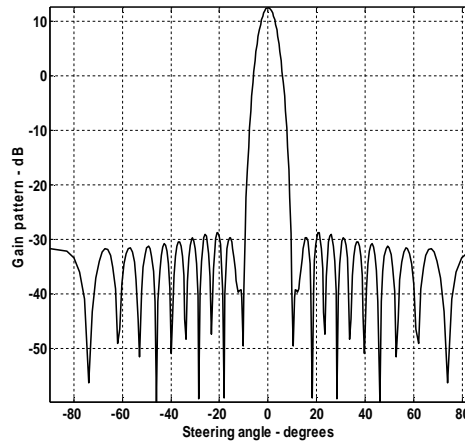
Figure 5.9 (b): Array gain pattern for steering angle 0 ,win=Hamming
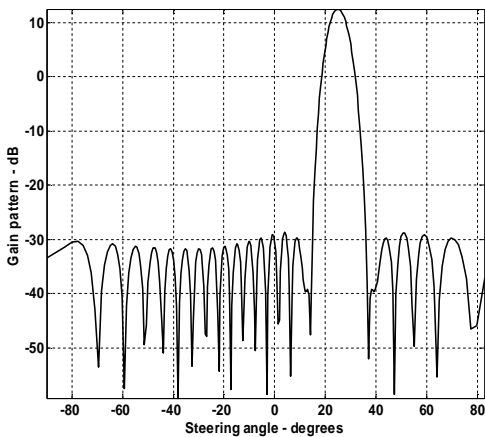
Figure 5.9(c):Array gain pattern for steering angle 25, win=Hamming
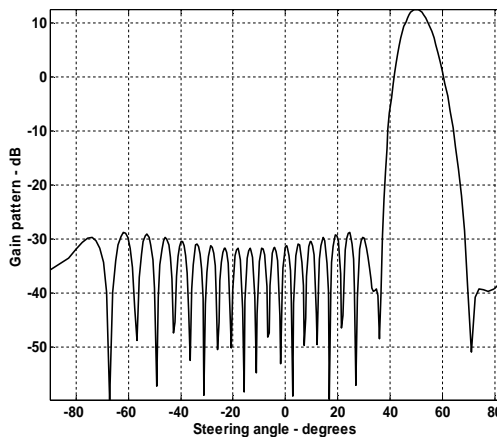
Figure 5.9d:Array gain pattern for steering angle 50,win=Hamming
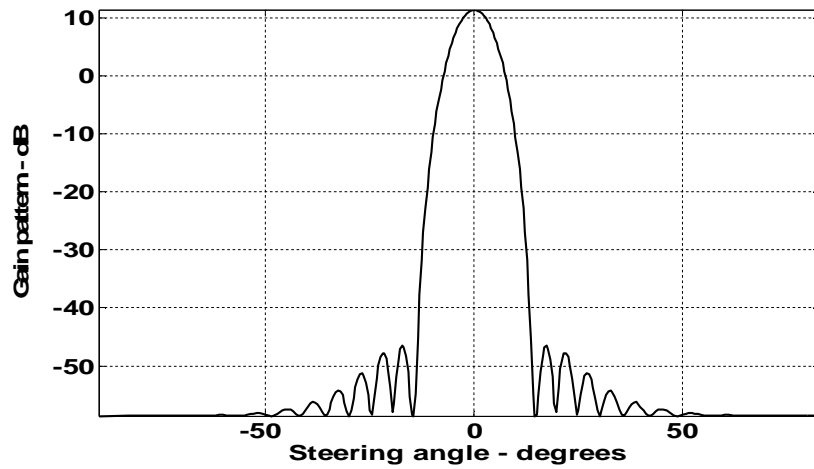
Figure 5.10(a): Array gain pattern for steering angle = 0, win=Blackman
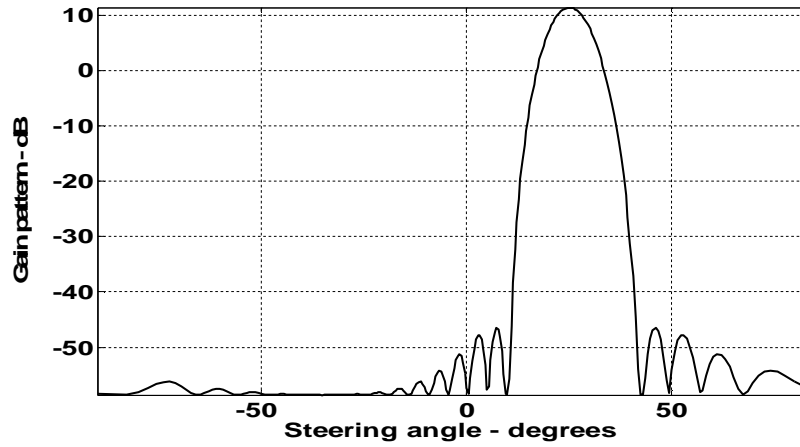
Figure 5.10(b): Array gain pattern for steering angle = 25, win=Blackman
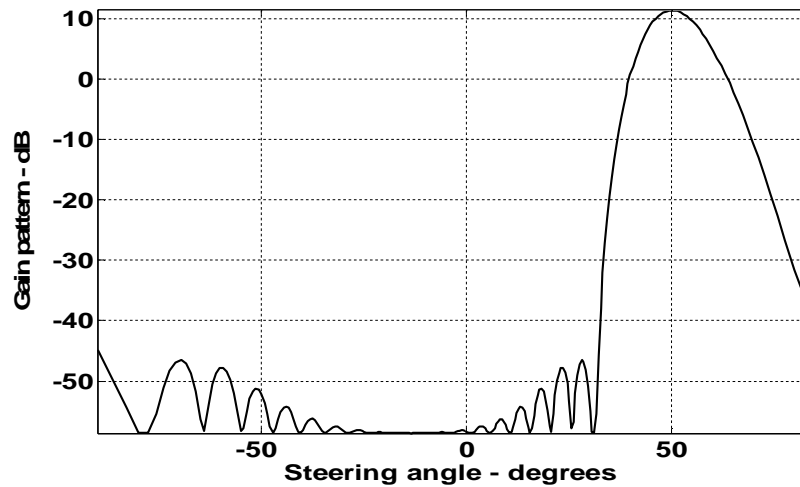
Figure 5.10(c): Array gain pattern for steering angle = 50, win=Blackman

The computer simulation of Eq. 5.42 shows that with the increase of the steering angle (ψ) and the use of the DFT through the various windows (such as hamming, hanning ,blackman etc), the main lobe level is increased lowering the side lobes. At constant steering angle in Figure 5.9(a) there are increased level of the side lobes while in Figure 5.9(b) with the use of the hamming windows the side lobe levels are lowered. In Figure 5.9(c) and 5.9(d), it is shown that the more the steering angle with the windows (hamming window), the less the side lobe levels. Moreover, using the better windows, for example- using Blackman window we get the more better result which is shown in Figure 5.10. Use of the Blackman window increases the directionality spontaneously. By this the gain and the directionality of the radar antenna will be increased.

5.7.3   Array Tapering :

Figure 5.6(a) shows the normalized radiation pattern of a uniformly excited linear array for element spacing d = $\lambda/2$. The first side lobe is about 13.46 db below the main lobe.

In order to reduce the side lobe levels, the array must be designed to radiate more power towards the centre and much less at the edge. Array tapering is nothing, simply the use of the windowing. Windowing reduces the side lobe levels at the expense of widening the main beam. Thus for a given radar application, the choice of the tapering sequence must be based on the trade off between side lobe reduction and main beam widening.

Chapter 6

CONCLUSION AND FUTURE WORKS

6.1   Introduction

"Effects of Changing RCS and Antenna Array Pattern on Radar Performance" concentrates on radar fundamentals, principles, and rigorous mathematical derivations. Computer simulation of the radar system performance is of great importance in the initial research and development (R&D) steps of recognition, detection, and tracking, and in modern radar education. Radar system analysis requires expensive experiments. The task of simulation is to replace such experiments in initial steps.

6.2 Results and Discussions

Chapter 1 begins with the basic radar system, its origination and classification along with the operating frequency bands. In the process, it is shown graphically that increasing the pulse width increases the effective detection range for a pulsed radar system. It is not an economic way to increase the range as it means increasing the transmitted power. However, fine resolution requires pulse width to be as small as possible (or bandwidth as large as possible). Achieving fine range resolution while maintaining adequate average transmitted power can be accomplished by using pulse compression techniques (not part of this thesis). Thereafter, MATLAB simulation is used to observe the effect of pulse integration. The results indicate that single pulse radar has minimum SNR and detection range. Non-coherent Integration (NCI) of number of pulses increases the SNR and the detection range. Coherent Integration (CI) of same number of pulses gives highest SNR and maximum detection range. Therefore, CI of number of pulses optimizes radar performance. At the end, few of the radar losses have been discussed

which affect SNR in a significant way. The remedy for the losses related to atmosphere and antenna are discussed in the subsequent chapters.

In chapter 2, the basic equation for a mono-static pulsed radar system is developed. The analysis was extended to find the equation for the bi-stable radar system. Then different parameters were varied to observe their effects on the radar range by using MATLAB simulation. Doubling the peak power improves SNR only a little where as doubling the RCS improves SNR a little better. Other radar parameters such as antenna gain variation should be considered to improve SNR or detection range effectively. To investigate further in detail we changed the pulse integration number and found that integrating a limited number of pulses can significantly enhance the SNR. However, integrating large amount of pulses does not provide any further major improvement in radar performance. We also found from the simulation that we can increase the antenna aperture to compensate for the lack of power being transmitted to cover a wider range of area for target detection. Then we took a short effort to study different types of jammers employed against radars. We developed the changed radar equations due to different kind of jammers. The effect of jammers on the reduction of radar range was clear from the MATLAB simulation where we found that if the radar operates at higher frequencies, the value of RRF will be more. Hence, one way to improve radar performance under jamming condition is to operate the radar at higher frequency. From another simulation it is observed that plot it is observed that the value of RRF increases almost linearly as the distance between the radar and the jammer increases.

In chapter 3, the methods of RCS calculation are examined. Target RCS fluctuations due to aspect angle, frequency, and polarization are presented. Radar cross section characteristics of some simple and complex targets are also considered. Radar cross section fluctuates as a function of radar aspect angle and frequency. It is evident that RCS fluctuation is more prominent to the variation of frequency. Little frequency change can cause serious RCS fluctuation. Constructive and destructive interference takes place between the RCS of two individual scatteres depending on the aspect angle. Examples of backscattered RCS for a number of simple shape objects (such as sphere, circular flat plate, frustum, ellipsoid, circular cylinder,

triangular flat plate, cylinder with circular plates etc.) were presented. The analysis is done for far field mono-static RCS measurements in the optical region. Near field RCS, bi-static RCS, and RCS measurements in the Rayleigh region were not considered since their treatment falls beyond our intended scope. Again, RCS treatment is mainly concerned with Narrow Band (NB) cases. Wide Band (WB) RCS measurements can be a broader field for further analysis. The effect of changing RCS in radar performance is observed by demonstrating the SNR performance of radar for some particular shaped objects. From simulation it is revealed that for large RCS, SNR degrades with the increase of range, means that for a fixed/ constant range large RCS provides better SNR.

Chapter 4 mainly presents the phenomenology of radar wave propagation. To analyze the radar performance accurately, one must consider the interference and attenuation due to the earth and atmosphere. Here, first the attenuation due to the reflection from the earth surface has been considered with respect to the various frequency bands. Then the interference due to the bending of the electromagnetic waves are considered and the "four third model" is represented to measure the target height accurately. Ground reflection caused a vital effect in radar wave propagation which is measured by reflection co-efficient. The phase and magnitude of the reflection co-efficient is determined for varying grazing angle which results at low grazing angle, the difference between the vertical and horizontal polarization is very low. Finally, it is observed that the diffraction and attenuation due to the atmosphere (rain, fog or clouds) also affect the radar wave propagation.

Chapter 5 presents the relation between directivity and power gain of radar antennas. An analytical solution for the electric field and the radiation pattern with respect to the steering angle and the element spacing has been evaluated. By MATLAB simulation it is shown that the side lobes can be reduced by increasing steering angle and using different windows. This gives an estimation to attain better directivity of the main beam with the optimized gain. The analysis approximates that the linear array antenna improves the directionality and the gain of the radar system.

6.3   Scope of Future Works

The thesis work mostly deals with the mono-static radar and stationary targets. In most practical radar systems there is relative motion between the radar and an observed target. Therefore, the RCS measured by the radar fluctuates over a period of time as a function of frequency and the target aspect angle. This observed RCS is referred to as the radar dynamic cross section. The future concern of the analysis can be to study the dynamic RCS which varies in amplitude and/or in phase. Furthermore, the evaluation process can be extended for the bi-static radar systems following the basic radar equation described in this thesis.

The study on Moving Target Indicator (MTI) gives a broader scope of future work. Future works may develop more around the signal processing techniques to be able to detect the target more specifically, such as shape and type. This will enhance radar capability in terms of target pin point.

Integration of radar system with other military applications such as anti-jamming capability, automatic alarm and fire control may also be a good area for future research and development.

BIBLIOGRAPHY

[1]   Ingo Harre & Bremen, "RCS in Radar Range Calculations for Maritime Targets", V2.0-20040206.

[2]   Lav Varshney, "Radar System Components and System Design", Technical Report by Syracuse Research Corporation, 2002.

[3]   Peebles, Jr., P. Z., "Radar Principles", John Wiley & Sons, 1998.

[4]   Naval Air Systems Command (Aviocnics Department, Washington) "Electronic Warfare and Radar Systems Engineering Handbook", 3rd ed.

[5]   John D Kraus, Ronald J Marhefka, Ahmed S Khan "Antennas for All Applications", 3rd ed, McGraw-Hill Publishing company limited, 2006

[6]   Nathanson F. E., "Radar Design Principles", 2nd ed, Prentice Hall of India, 1999.

[7]   Hamish Meikle, "Modern Radar Systems", 2nd ed, Artech House, 2008

[8]   Yakov D.Shirman, "Computer Simulation of Aerial Target Radar Scattering Recognition, Detection and Tracking", Artech House, 2002.

[9]   Skolnik, M. I., "Introduction to Radar System", 3rd ed, Tata McGraw-Hill, 2001.

[10]   Sadiku, M. N. O., "Elements of Electromagnetics", 4th ed, Oxford University Press, 2007, Chap 13.

[11]   Sergey N. Makarov, "Antenna and EM Modeling with MATLAB" John Wiley & Sons,INC, Piblications, 2002, chap 6, pp. 113~124

[12]   Mahafza, B. R., "Radar Systems Analysis and Design Using MATLAB", 2nd ed, Chapman and Hall/CRC, 2005.

MATLAB Codes for Simulations Used

In each chapter a number of plots have been generated using MATLAB for explaining the effects of varying parameters on radar performance. The details of each code used to generate those figures are listed below as per chapter and figure numbers. Few common parameters used throut the codes are listed below:

Symbol	Description	Unit
Pt	peak power	Watts
Freq	radar operating frequency	Hz
G	antenna gain	dB
Sigma	radar cross section	m^2
Te	effective noise temperature	Kelvins
B	radar operating bandwidth	Hz
Nf	noise figure	dB
Loss	radar losses	dB

Chapter 1

Code for Figure 1.3

```
close all
clear all
pt = 1.e+6;
freq = 5.6e+9;
g = 40.0;
sigma = 0.1;
te =300.0;
nf = 5.0;
loss = 6.0;
range = [75e3,100e3,150e3];  % three range values
snr_db = linspace(5,20,200); % SNR values from 5 dB to 20 dB with 200 points
snr = 10.^(0.1.*snr_db); % convert SNR into base 10
```

```
gain = 10^(0.1*g); %convert antenna gain into base 10
loss = 10^(0.1*loss); % convert losses into base 10
F = 10^(0.1*nf); % convert noise figure into base 10
lambda = 3.e8 / freq; % compute wavelength

% Implement the Eq. shown below in the comment
den = pt * gain * gain * sigma * lambda^2;
num1 = (4*pi)^3 * 1.38e-23 * te * F * loss * range(1)^4 .* snr;
num2 = (4*pi)^3 * 1.38e-23 * te * F * loss * range(2)^4 .* snr;
num3 = (4*pi)^3 * 1.38e-23 * te * F * loss * range(3)^4 .* snr;
tau1 = num1 ./ den ;
tau2 = num2 ./ den;
tau3 = num3 ./ den;

% plot tau versus snr
figure(1)
semilogy(snr_db,1e6*tau1,'k',snr_db,1e6*tau2,'k -.',snr_db,1e6*tau3,'k:')
grid
legend('R = 75 Km','R = 100 Km','R = 150 Km')
xlabel ('Minimum required SNR - dB');
ylabel ('\tau (pulse width) in \mu sec');
```

Comment on code for figure 1.3

Eqn used here is

$$\tau = \frac{(4\pi)^3 k T_e F L R^4 SNR}{P_t G^2 \lambda^2 \sigma}$$ .This Eq. is a variation of the basic radar equation.

Code for Figure 1.7 and 1.8

```
close all
clear all
pt = 4;
freq = 94e+9;
g = 47.0;
sigma = 20;
te = 293.0;
b = 20e+6;
nf = 7.0;
loss = 10.0;
range = linspace(1.e3,12e3,10000); % range to target from 1 Km 12 Km, 1000 points
snr1 = radar_eq(pt, freq, g, sigma, te, b, nf, loss, range);
index = find(snr1>9.99999 & snr1<10.0099);
test = isempty(index);
if(test==1)
```

'Error; Tighten values in line 14, and re-run again'
    break
else
end
snr_ref = snr1(index);
r_ref = range(index);
R_ref_ci = (94^0.25) .* r_ref;
snrCI = snr_ref + 40*log10(R_ref_ci ./ range); % Implements the 1st Eq. given in comments

% plot SNR versus range . generate figure 1.7
figure(1)
rangekm = range ./ 1000;
plot(rangekm,snr1,'k',rangekm,snrCI,'k -.')
axis tight
grid
legend('single pulse','94 pulse CI')
xlabel ('Detection range - Km');
ylabel ('SNR - dB');

% Generate Figure 1.8
% first find the new reference range
snr_b10 = 10.^(10/10);
SNR_1 = 10/(2*94) + sqrt(((10^2) / (4*94*94)) + (10 / 94)); % Implements 2nd Eq. given in
comment
LNCI = (1+SNR_1) / SNR_1;
%snrnci_ref = snrCI -10*log10(LNCI);
NCIgain = 10*log10(94) - 10*log10(LNCI);
R_ref_nci = ((10^(0.1*NCIgain))^0.25) * 2.245e3;
snrNCI = snr_ref + 40*log10(R_ref_nci ./ range); % Implements the 1st Eq. given in comment

figure (2)
plot(rangekm,snr1,'k',rangekm,snrNCI,'k -.', rangekm,snrCI,'k:')
axis tight
grid
legend('single pulse','94 pulse NCI','94 pulse CI')
xlabel ('Detection range - Km');
ylabel ('SNR - dB');

Comment on code for figure 1.7 and 1.8

Eqn used in here are

$$(1) \qquad \text{SNR} = \text{SNR}_{ref} \frac{\tau}{\tau_{ref}} \frac{1}{L_p} \frac{\sigma}{\sigma_{ref}} \left(\frac{R_{ref}}{R}\right)^4$$

$$(2) \qquad n_P \; = \; \frac{\theta_a T_{SC} f_r}{2\pi}$$

Code for Figure 2.2a and 2.2b

```
close all
clear all
pt = 1.5e+6;
freq = 5.6e+9;
g = 45.0;
sigma = 0.1;
te = 290.0;
b = 5.0e+6;
nf = 3.0;
loss = 6.0;
range = linspace(25e3,165e3,1000); % range to target from 25 Km 165 Km, 1000 points
snr1 = radar_eq(pt, freq, g, sigma, te, b, nf, loss, range); % using radar basic Eq.
snr2 = radar_eq(pt, freq, g, sigma/10, te, b, nf, loss, range);
snr3 = radar_eq(pt, freq, g, sigma*10, te, b, nf, loss, range);

% plot SNR versus range
figure(1)
rangekm  = range ./ 1000;
plot(rangekm,snr3,'k',rangekm,snr1,'k -.',rangekm,snr2,'k:')
grid
legend('\sigma = 0 dBsm','\sigma = -10dBsm','\sigma = -20 dBsm')
xlabel ('Detection range - Km');
ylabel ('SNR - dB');
snr1 = radar_eq(pt, freq, g, sigma, te, b, nf, loss, range);
snr2 = radar_eq(pt*.4, freq, g, sigma, te, b, nf, loss, range);
snr3 = radar_eq(pt*1.8, freq, g, sigma, te, b, nf, loss, range);
figure (2)
plot(rangekm,snr3,'k',rangekm,snr1,'k -.',rangekm,snr2,'k:')
grid
legend('Pt = 2.16 MW','Pt = 1.5 MW','Pt = 0.6 MW')
xlabel ('Detection range - Km');
ylabel ('SNR - dB');
```

Code for Figure 2.3a and 2.3b

```
close all;
clear all;
c = 3.0e+8;
pt = 1.5e+6;
freq = 5.6e+9;
g = 45.0;
sigma = 0.1;
te = 290.0;
b = 5.0e+6;
nf = 3.0;
loss = 0.0;
np = 1; % 1 number of coherently integrated pulses
prf = 100 ;        % PRF in Hz
range = 250.0;  % target range in Km
np1 = 10; % choice 1 of np
np2 = 100; % choice 2 of np
rcs_delta = 10.0;   % rcs variation
pt_percent = 2.0;   % pt variation
lambda = c / freq;
p_peak = log10(pt);
lambda_sq = lambda^2;
lambda_sqdb =log10(lambda_sq);
sigmadb =log10(sigma);
for_pi_cub =log10((4.0 * pi)^3);
k_db =log10(1.38e-23);
te_db =log10(te)
b_db =log10(b);
np_db =log10(np);
range_db =log10(range * 1000.0);

% Implementing low PRF radar Eq. (2.16)
snr_out = p_peak + 2. * g + lambda_sqdb + sigmadb + np_db - ...
   for_pi_cub - k_db - te_db - b_db - nf - loss - 4.0 * range_db

% Generate plots in figure 2.3
index = 0;
n1 = np_db;
n2 =log10(np1);
n3 =log10(np2)
for range_var = 25:5:400 % 25 - 400 Km
  index = index + 1;
  rangevar_db =log10(range_var * 1000.0);
  snr1(index) = p_peak + 2. * g + lambda_sqdb + sigmadb + n1 - ...
    for_pi_cub - k_db - te_db - b_db - nf - loss - 4.0 * rangevar_db;
```

```
    snr2(index) = p_peak + 2. * g + lambda_sqdb + sigmadb + n2 - ...
        for_pi_cub - k_db - te_db - b_db - nf - loss - 4.0 * rangevar_db;
    snr3(index) = p_peak + 2. * g + lambda_sqdb + sigmadb + n3 - ...
        for_pi_cub - k_db - te_db - b_db - nf - loss - 4.0 * rangevar_db;
end
figure(1)
var = 25:5:400;
plot(var,snr1,'k',var,snr2,'k--',var,snr3,'k--.')
legend('np = 1','np1','np2')
xlabel ('Range - Km');
ylabel ('SNR - dB');
grid on;
%title ('np = 1, np1 = 10, np2 =100');
% Generate plots in Fig. 1.20
sigma5 = sigmadb - rcs_delta;
pt05 = p_peak + log10(pt_percent);
index = 0;
for nvar =1:10:500 % 500 pulses
    index = index + 1;
    ndb =log10(nvar);
    snrs(index) = p_peak + 2. * g + lambda_sqdb + sigmadb + ndb - ...
        for_pi_cub - k_db - te_db - b_db - nf - loss - 4.0 * range_db;
    snrs5(index) = p_peak + 2. * g + lambda_sqdb + sigma5 + ndb - ...
        for_pi_cub - k_db - te_db - b_db - nf - loss - 4.0 * range_db;
end
index = 0;
for nvar =1:10:500 % 500 pulses
    index = index + 1;
    ndb = log10(nvar);
    snrp(index) = p_peak + 2. * g + lambda_sqdb + sigmadb + ndb - ...
        for_pi_cub - k_db - te_db - b_db - nf - loss - 4.0 * range_db;
    snrp5(index) = pt05 + 2. * g + lambda_sqdb + sigmadb + ndb - ...
        for_pi_cub - k_db - te_db - b_db - nf - loss - 4.0 * range_db;
end
nvar =1:10:500;
figure (2)
subplot (2,1,1)
plot (nvar,snrs,'k',nvar,snrs5,'k --')
legend ('default RCS','RCS-delta')
xlabel ('Number of coherently integrated pulses');
ylabel ('SNR - dB')
grid on;
%title ('delta = 10, percent = 2');
subplot (2,1,2)
plot (nvar,snrp,'k',nvar,snrp5,'k --')
legend ('default power','pt * percent')
```

```
xlabel ('Number of coherently integrated pulses');
ylabel ('SNR - dB');
grid on;
```

Code for Figure 2.4a and 2.4b

```
close all
clear all
tsc = 2.5; % Scan time i s2.5 seconds
sigma = 0.1;
te = 900.0;
snr = 15; % desired SNR in dB
nf = 6.0;
loss = 7.0;
az_angle = 2; % search volume azimuth extent in degrees
el_angle = 2; %serach volume elevation extent in degrees
range = linspace(20e3,250e3,1000); % range to target from 20 Km 250 Km, 1000 points

% implementing Eq. 2.18
pap1 = power_aperture(snr,tsc,sigma/10,range,te,nf,loss,az_angle,el_angle);
pap2 = power_aperture(snr,tsc,sigma,range,te,nf,loss,az_angle,el_angle);
pap3 = power_aperture(snr,tsc,sigma*10,range,te,nf,loss,az_angle,el_angle);

% plot power aperture product versus range
% figure 2.4a
figure(1)
rangekm  = range ./ 1000;
plot(rangekm,pap1,'k',rangekm,pap2,'k -.',rangekm,pap3,'k:')
grid
legend('\sigma = -20 dBsm','\sigma = -10dBsm','\sigma = 0 dBsm')
xlabel ('Detection range in Km');
ylabel ('Power aperture product in dB');

% generate Figure 2.4b
lambda = 0.03; % wavelength in meters
G = 45; % antenna gain in dB
ae = linspace(1,25,1000);% aperture size 1 to 25 meter squared, 1000 points
Ae = 10*log10(ae);
range = 250e3; % rnage of interset is 250 Km
pap1 = power_aperture(snr,tsc,sigma/10,range,te,nf,loss,az_angle,el_angle);
pap2 = power_aperture(snr,tsc,sigma,range,te,nf,loss,az_angle,el_angle);
pap3 = power_aperture(snr,tsc,sigma*10,range,te,nf,loss,az_angle,el_angle);
Pav1 = pap1 - Ae;
Pav2 = pap2 - Ae;
Pav3 = pap3 - Ae;
```

```
figure(2)
plot(ae,Pav1,'k',ae,Pav2,'k -.',ae,Pav3,'k:')
grid
xlabel('Aperture size in square meters')
ylabel('Pav in dB')
legend('\sigma = -20 dBsm','\sigma = -10dBsm','\sigma = 0 dBsm')
```

Code for Figure 2.6a and 2.6b

```
% plots of RRF versus wavelength and radar to jammer range. Implements Eq. 2.28 and Eq.
2.29.
c = 3.0e+8;
k = 1.38e-23;
te = 730.0;
pj  = 15; % jammer peak power in W
gj = 3.0;      % jammer antenna gain in dB
g = 40.0;      % radar antenna gain
freq = 10.0e+9;
bj  = 1.0e+6;   % radar operating bandwidth in Hz
rangej = 400.0;% radar to jammer range in Km
lossj = 1.0;   % jammer losses in dB

lambda = c / freq;
gj_10 = 10^( gj/10);
g_10 = 10^( g/10);
lossj_10 = 10^(lossj/10);
index = 0;
for wavelength = .01:.001:1
   index = index +1;
   jamer_temp = (pj * gj_10 * g_10 *wavelength^2) / ...
      (4.0^2 * pi^2 * k * bj * lossj_10 * (rangej * 1000.0)^2);
   delta = 10.0 * log10(1.0 + (jamer_temp / te));
   rrf(index) = 10^(-delta /40.0);
end
w = 0.01:.001:1;

figure (1)
semilogx(w,rrf,'k')
grid
xlabel ('Wavelength in meters')
ylabel ('Range reduction factor')
index = 0;
for ran =rangej*.3:10:rangej*2
   index = index + 1;
   jamer_temp = (pj * gj_10 * g_10 *lambda^2) / ...
```

```
         (4.0^2 * pi^2 * k * bj * lossj_10 * (ran * 1000.0)^2);
   delta = 10.0 * log10(1.0 + (jamer_temp / te));
   rrf1(index) = 10^(-delta /40.0);
end
figure(2)
ranvar = rangej*.3:10:rangej*2 ;
plot(ranvar,rrf1,'k')
grid
xlabel ('Radar to jammer range - Km')
ylabel ('Range reduction factor')
```

Code for figure 3.2

```
closeall;
clearall;
function [rcs] = rcs_aspect(scat_spacing, freq)
eps = 0.00001;
scat_spacing = 1.0; % Enter scatterer spacing, in meters
freq = 3.0e+9;% Enter frequency
wavelength = 3.0e+8 / freq;
aspect_degrees = 0.:.05:180.;
aspect_radians = (pi/180) .* aspect_degrees; % Compute aspect angle vector
% Compute electrical scatterer spacing vector in wavelength units
elec_spacing = (2.0 * scat_spacing / wavelength) .* cos(aspect_radians);
% Compute RCS (rcs = RCS_scat1 + RCS_scat2)
rcs = abs(1.0 + cos((2.0 * pi) .* elec_spacing) ...
        + i * sin((2.0 * pi) .* elec_spacing)); % Scat1 is taken as phase refernce point
rcs = rcs + eps;
rcs = 20.0*log10(rcs); % RCS in dBsm
% Plot RCS versus aspect angle
figure (1);
plot(aspect_degrees,rcs);
grid;
xlabel('aspect angle - degrees');
ylabel('RCS in dBsm');
```

Code for figure 3.3a and 3.3b

```
close all;
clear all;
function [rcs] = rcs_frequency (scat_spacing, frequ, freql)
```

```
eps = 0.0001;
scat_spacing = 1;
frequ= 12.5*10^9; %upper frequency limit
freql= 8*10^9;%lower frequency limit
freq_band = frequ-freql;
delfreq = freq_band / 500.;
index = 0;
forfreq = freql: delfreq: frequ
index = index +1;
wavelength(index) = 3.0e+8 / freq;
end
elec_spacing = 2.0 * scat_spacing ./ wavelength; % Compute electrical scatterer spacing
vector in wavelength units
rcs = abs (  1 + cos((2.0 * pi) .* elec_spacing) ...
        + i * sin((2.0 * pi) .* elec_spacing));
rcs = rcs + eps; % Compute RCS (RCS = RCS_scat1 + RCS_scat2)
rcs = 20.0*log10(rcs); % RCS ins dBsm
% Plot RCS versus frequency
freq = freql:delfreq:frequ;
figure (1);
plot(freq,rcs);
grid;
xlabel('Frequency');
ylabel('RCS in dBsm');
```

Code for figure 3.5

```
clearall;
eps   = 0.00001;
index = 0;
forkr = 0.05:0.05:15
index = index + 1;
sphere_rcs  = 0. + 0.*i;
  f1    = 0. + 1.*i;
  f2    = 1. + 0.*i;
  m     = 1.;
  n     = 0.;
  q     = -1.;
del =100000+100000*i; % initially set del to huge value
while(abs(del) >eps)
    q   = -q;
    n   = n + 1;
    m   = m + 2;
del = (2.*n-1) * f2 / kr-f1;
f1  = f2;
f2  = del;
```

```
del = q * m /(f2 * (kr * f1 - n * f2));
sphere_rcs = sphere_rcs + del;
end
rcs(index)   = abs(sphere_rcs);
sphere_rcsdb(index) = 10. * log10(rcs(index));
end
figure(1);
n=0.05:.05:15;
plot (n,rcs,'k');
set (gca,'xtick',[1 2 3 4 5 6 7 8 9 10 11 12 13 14 15]);
xlabel ('Sphere circumference in wavelengths');
ylabel ('Normalized sphere RCS');
grid;
figure (2);
plot (n,sphere_rcsdb,'k');
set (gca,'xtick',[1 2 3 4 5 6 7 8 9 10 11 12 13 14 15]);
xlabel ('Sphere circumference in wavelengths');
ylabel ('Normalized sphere RCS - dB');
grid;
figure (3);
semilogx (n,sphere_rcsdb,'k');
xlabel ('Sphere circumference in wavelengths');
ylabel ('Normalized sphere RCS - dB');
```

Code for figure 3.7

```
function [rcsdb] = rcs_circ_plate (r, freq)
eps = 0.000001;
freq=8e9;
lambda = 3.e+8 / freq; % X-Band
index = 0;
foraspect_deg = 0.:.1:180
index = index +1;
aspect = (pi /180.) * aspect_deg;
% Compute RCS using Eq. (3.7)
if (aspect == 0 | aspect == pi)
rcs_po(index) = (4.0 * pi^3 * r^4 / lambda^2) + eps;
rcs_mu(index) = rcs_po(1);
else
    x = (4. * pi * r / lambda) * sin(aspect);
    val1 = 4. * pi^3 * r^4 / lambda^2;
    val2 = 2. * besselj(1,x) / x;
rcs_po(index) = val1 * (val2 * cos(aspect))^2 + eps;
% Compute RCS using Eq. (3.6)
    val1m = lambda * r;
```

```
      val2m = 8. * pi * sin(aspect) * (tan(aspect)^2);
rcs_mu(index) = val1m / val2m + eps;
end
end
% Compute RCS using Eq. (3.5) (theta=0,180)
rcsdb = 10. * log10(rcs_po);
rcsdb_mu = 10 * log10(rcs_mu);
angle = 0:.1:180;
plot(angle,rcsdb,'k',angle,rcsdb_mu,'k-.')
grid;
xlabel ('Aspect angle - degrees');
ylabel ('RCS - dBsm');
legend('Using Eq.(3.7)','Using Eq.(3.6)')
freqGH = num2str(freq*1.e-9);
title (['Frequency = ',[freqGH],'  GHz']);
```

Code for figure 3.8

```
function [rcs] = rcs_cylinder(r1, r2, h, freq, phi, CylinderType)
r1=0.125;
 r = r1;          % radius of the circular cylinder
eps =0.00001;
dtr = pi/180;
phi=pi/4;
phir = phi*dtr;
freqGH = num2str(freq*1.e-9);
lambda = 3.0e+8 /freq;      % wavelength
% CylinderType= 'Elliptic';   % 'Elliptic' or 'Circular'

switchCylinderType
case'Circular'
% Compute RCS from 0 to (90-.5)  degrees
index = 0;
for theta = 0.0:.1:90-.5
index = index +1;
thetar = theta * dtr;
rcs(index) = (lambda * r * sin(thetar) / ...
        (8. * pi * (cos(thetar))^2)) + eps;
end
% Compute RCS for broadside specular at 90 degree
thetar = pi/2;
index = index +1;
rcs(index) = (2. * pi * h^2 * r / lambda )+eps;
% Compute RCS from (90+.5) to 180 degrees
for theta = 90+.5:.1:180.
```

```
index = index + 1;
thetar = theta * dtr;
rcs(index) = ( lambda * r * sin(thetar) / ...
        (8. * pi * (cos(thetar))^2)) + eps;
end
case'Elliptic'
   r12 = r1*r1;
   r22 = r2*r2;
   h2 = h*h;
% Compute RCS from 0 to (90-.5)  degrees
index = 0;
for theta = 0.0:.1:90-.5
index = index +1;
thetar = theta * dtr;
rcs(index) =  lambda * r12 * r22 * sin(thetar) / ...
          ( 8*pi* (cos(thetar)^2)* ( (r12*cos(phir)^2 + r22*sin(phir)^2)^1.5 ))+ eps;
end
% Compute RCS for broadside specular at 90 degree
index = index +1;
rcs(index) = 2. * pi * h2 * r12 * r22 / ...
( lambda*( (r12*cos(phir)^2 + r22*sin(phir)^2)^1.5 ))+ eps;
% Compute RCS from (90+.5) to 180 degrees
for theta = 90+.5:.1:180.
index = index + 1;
thetar = theta * dtr;
rcs(index) =  lambda * r12 * r22 * sin(thetar) / ...
          ( 8*pi* cos(thetar)^2* ( (r12*cos(phir)^2 + r22*sin(phir)^2)^1.5 ))+ eps;
end
end

% Plot the results
delta= 180/(index-1);
angle = 0:delta:180;
plot(angle,10*log10(rcs),'k','linewidth',1.5);
grid;
xlabel ('Aspect angle, Theta [Degrees]');;
ylabel ('RCS - dBsm');
title  ([[CylinderType],'  Cylinder','  at Frequency = ',[freqGH],'  GHz']);
```

Code for figure 3.10

```
function [rcs] = rcs_frustum (r1, r2, h, freq, indicator)
formatlong
index = 0;
eps = 0.000001;
```

```
freq = 5.6e+9;
lambda = 3.0e+8 /freq;
r1 =.02057; % Enter frustum's small end radius
r2 = .05753; % Enter Frustum's large end radius
h = .20945; % Compute Frustum's length
alpha = atan(( r2 - r1)/h); % Comput half cone angle, alpha
z2 = r2 / tan(alpha); % Compute z1 and z2
z1 = r1 / tan(alpha);
delta = (z2^1.5 - z1^1.5)^2;
factor = (8. * pi * delta) / (9. * lambda);
indicator=1;
large_small_end = indicator;
if(large_small_end == 1)
normal_incedence = (180./pi) * ((pi /2) + alpha)   % Compute normal incidence, large end

% Compute RCS from zero aspect to normal incidence
for theta = 0.001:.1:normal_incedence-.5
index = index +1;
theta = theta * pi /180.;
rcs(index) = (lambda * z1 * tan(alpha) *(tan(theta - alpha))^2) / ...
      (8. * pi *sin(theta)) + eps;
end
%Compute broadside RCS
index = index +1;
rcs_normal = factor * sin(alpha) / ((cos(alpha))^4) + eps;
rcs(index) = rcs_normal;
% Compute RCS from broad side to 180 degrees
for theta = normal_incedence+.5:.1:180
index = index + 1;
theta =  theta * pi / 180. ;
rcs(index) = (lambda * z2 * tan(alpha) *(tan(theta - alpha))^2) / ...
      (8. * pi *sin(theta)) + eps;
end
else
% Compute normal incidence, small end
normal_incedence = (180./pi) * ((pi /2) - alpha)
% Compute RCS from zero aspect to normal inicedence (large end of frustum)
for theta = 0.001:.1:normal_incedence-.5
index = index +1;
theta = theta * pi /180.;
rcs(index) = (lambda * z1 * tan(alpha) *(tan(theta + alpha))^2) / ...
      (8. * pi *sin(theta)) + eps;
end
%Compute broadside RCS
index = index +1;
rcs_normal = factor * sin(alpha) / ((cos(alpha))^4) + eps;
```

```
rcs(index) = rcs_normal;
% Compute RCS from broad side to 180 degrees (small end of frustum)
for theta = normal_incedence+.5:.1:180
index = index + 1;
theta =  theta * pi / 180. ;
rcs(index) = (lambda * z2 * tan(alpha) *(tan(theta + alpha))^2) / ...
       (8. * pi *sin(theta)) + eps;
end
end
% Plot RCS versus aspect angle
delta = 180 /index;
angle = 0.001:delta:180;
plot (angle,10*log10(rcs),'k','linewidth',1);
grid;
xlabel ('Apsect angle - degrees');
ylabel ('RCS - dBsm');
if(indicator ==1)
title ('Viewing from large end');
else
title ('Viewing from small end');
end
return
```

Code for figure 3.12

```
clearall;
indes = 0;
eps =0.00001;
a1 =.125;
h = 1.;
lambda = 3.0e+8 /9.5e+9;
lambda = 0.00861;
index = 0;
for theta = 0.0:.1:90-.1
index = index +1;
theta = theta * pi /180.;
rcs(index) = (lambda * a1 * sin(theta) / ...
    (8 * pi * (cos(theta))^2)) + eps;
end
theta*180/pi
theta = pi/2;
index = index +1
rcs(index) = (2 * pi * h^2 * a1 / lambda )+ eps;
for theta = 90+.1:.1:180.
index = index + 1;
theta = theta * pi / 180.;
```

```matlab
rcs(index) = ( lambda * a1 * sin(theta) / ...
    (8 * pi * (cos(theta))^2)) + eps;
end
r = a1;
index = 0;
foraspect_deg = 0.:.1:180
index = index +1;
aspect = (pi /180.) * aspect_deg;
% Compute RCS using Eq. (3.7)
if (aspect == 0 | aspect == pi)
rcs_po(index) = (4.0 * pi^3 * r^4 / lambda^2) + eps;
rcs_mu(index) = rcs_po(1);
else
    x = (4. * pi * r / lambda) * sin(aspect);
    val1 = 4. * pi^3 * r^4 / lambda^2;
    val2 = 2. * besselj(1,x) / x;
rcs_po(index) = val1 * (val2 * cos(aspect))^2 + eps;
end
end
rcs_t=(rcs_po + rcs);

angle = 0:.1:180;
plot(angle,10*log10(rcs_t(1:1801)));
grid
```

Code for figure 3.13

```matlab
function [rcs] = rcs_cmb(r, h, freq, lambda, phi, type)
r = .125;
h=1;
eps =0.00001;
dtr = pi/180;
phi= 100;
phir = phi*dtr;
h=1;%cylinder height
freq=8*10^9;
freqGH = num2str(freq*1.e-9);
lambda = 3.0e+8 /freq;      % wavelength index = 0;
%rcs of circular flat plate
index = 0 ;
foraspect_deg = 0.:.1:180
index = index +1;
aspect = (pi /180.) * aspect_deg;
if (aspect == 0 | aspect == pi)
rcs_po(index) = (4.0 * pi^3 * r^4 / lambda^2) + eps;
rcs_mu(index) = rcs_po(1);
```

```
else
    x = (4. * pi * r / lambda) * sin(aspect);
    val1 = 4. * pi^3 * r^4 / lambda^2;
    val2 = 2. * besselj(1,x) / x;
rcs_po(index) = val1 * (val2 * cos(aspect))^2 + eps;
    val1m = lambda * r;
    val2m = 8. * pi * sin(aspect) * (tan(aspect)^2);
rcs_mu(index) = val1m / val2m + eps;
end
   sigma1 =rcs_mu(index);
end
pt = 1.5e+6; % peak power in Watts
g = 45.0; % antenna gain in dB
phi= 100;
r=.125;%radius of circular cylinder
h=1;%cylinder height

te = 290.0; % effective noise temperature in Kelvins
b = 5.0e+6; % radar operating bandwidth in Hz
nf = 3.0; %noise figure in dB
loss = 6.0; % radar losses in dB
range = linspace(20e3,180e3,1000); % range to target from 25 Km to 165 Km, 1000 points
snr1 = radar_eq(pt, freq, g, sigma1, te, b, nf, loss, range);
figure(1)
rangekm  = range ./ 1000;
plot(rangekm,snr1,'k')
grid;
axissquare;
xlabel ('Detection range - Km');
ylabel ('SNR - dB');
%rcs of cylinder
index=0;
for theta = 0.0:.1:180
index = index +1;
thetar = theta * dtr;
rcs(index) = (lambda * r * sin(thetar) / ...
        (8. * pi * (cos(thetar))^2)) + eps;
pt = 1.5e+6; % peak power in Watts
g = 45.0; % antenna gain in dB

sigma3 = rcs(index);
end
te = 290.0; % effective noise temperature in Kelvins
b = 5.0e+6; % radar operating bandwidth in Hz
nf = 3.0; %noise figure in dB
loss = 6.0; % radar losses in dB
```

```
range = linspace(20e3,180e3,1000); % range to target from 25 Km 165 Km, 1000 points
snr3 = radar_eq(pt, freq, g, sigma3, te, b, nf, loss, range);
figure(3)
rangekm  = range ./ 1000;
plot(rangekm,snr3,'k')
grid
axissquare;
xlabel ('Detection range - Km');
ylabel ('SNR - dB');
%combined rcs plot
figure(4)
plot(rangekm,snr1,'k',rangekm,snr3,'k-.')
legend('circular flat plate','circular cylinder')
axis([0 200 -80 80])
grid
xlabel ('Detection range - Km');
ylabel ('SNR - dB');
```

Code for figure 3.14

```
r = .125;
h=1;
eps =0.00001;
dtr = pi/180;
phi= 100;
phir = phi*dtr;
freq=8*10^9;
freqGH = num2str(freq*1.e-9);
lambda = 3.0e+8 /freq;     % wavelength index = 0;
%rcs of circular flat plate
index = 0 ;
foraspect_deg = 0.:.1:180
index = index +1;
aspect = (pi /180.) * aspect_deg;
if (aspect == 0 | aspect == pi)
rcs_po(index) = (4.0 * pi^3 * r^4 / lambda^2) + eps;
rcs_mu(index) = rcs_po(1);
else
    x = (4. * pi * r / lambda) * sin(aspect);
    val1 = 4. * pi^3 * r^4 / lambda^2;
    val2 = 2. * besselj(1,x) / x;
rcs_po(index) = val1 * (val2 * cos(aspect))^2 + eps;
    val1m = lambda * r;
    val2m = 8. * pi * sin(aspect) * (tan(aspect)^2);
rcs_mu(index) = val1m / val2m + eps;
end
```

```
end
pt = 1.5e+6; % peak power in Watts
g = 45.0; % antenna gain in dB
phi= 100;
r=.125;%radius of circular cylinder
h=1;%cylinder height
sigma1 =rcs_mu(index);
te = 290.0; % effective noise temperature in Kelvins
b = 5.0e+6; % radar operating bandwidth in Hz
nf = 3.0; %noise figure in dB
loss = 6.0; % radar losses in dB
range = linspace(20e3,180e3,1000); % range to target from 25 Km to 165 Km, 1000 points
snr1 = radar_eq(pt, freq, g, sigma1, te, b, nf, loss, range);
figure(1)
rangekm  = range ./ 1000;
plot(rangekm,snr1,'k')
grid;
axissquare;
xlabel ('Detection range - Km');
ylabel ('SNR - dB');
% rcs of rectangular plate
a=10.16*10^-2;
b=5.8*10^-2;
ka = 2. * pi * a / lambda;
fortheta_deg = 0.05:0.1:85;
theta = (pi/180.) .* theta_deg;
angle = ka .* sin(theta);
rcs_po = (4. * pi* a^2 * b^2 / lambda^2 ).*  (cos(theta)).^2 .* ...
   ((sin(angle) ./ angle).^2) + eps;
sigma2 = rcs_po;
end

te = 290.0; % effective noise temperature in Kelvins
b = 5.0e+6; % radar operating bandwidth in Hz
nf = 3.0; %noise figure in dB
loss = 6.0; % radar losses in dB
range = linspace(20e3,180e3,1000); % range to target from 25 Km 165 Km, 1000 points
snr2 = radar_eq(pt, freq, g, sigma2, te, b, nf, loss, range);
figure(2)
rangekm  = range ./ 1000;
plot(rangekm,snr2,'k')
grid
axissquare;
xlabel ('Detection range - Km');
ylabel ('SNR - dB');
grid
```

```
%combined rcs plot
figure(5)
plot(rangekm,snr1,'k',rangekm,snr2,'k-.')
legend('circular flat plate','rectangular flat plate')
axis([0 200 -70 70])
grid
xlabel ('Detection range - Km');
ylabel ('SNR - dB');
```

Code for Figure 4.6 and 4.7

```
function linear_array_gui_OpeningFcn(hObject, eventdata, handles, varargin)

handles.output = hObject;
guidata(hObject, handles);

function varargout = linear_array_gui_OutputFcn(hObject, eventdata, handles)
varargout{1} = handles.output;

function [rh,rv,ph,pv] = ref_coef (epsp,epspp)
epsp = 65.0;
epspp = 30.7i;
eps = epsp - i * epspp; %65.0-30.7i;
psi = 0:0.1:90;
psirad = psi.*(pi/180.);
arg1 = eps-(cos(psirad).^2);
arg2 = sqrt(arg1);
arg3 = sin(psirad);
arg4 = eps.*arg3;
rv = (arg4-arg2)./(arg4+arg2);
rh = (arg3-arg2)./(arg3+arg2);
gamamodv = abs(rv);
gamamodh = abs(rh);
figure(1)
plot(psi,gamamodv,'k',psi,gamamodh,'k -.');
axis tight
grid
xlabel('grazing angle - degrees');
ylabel('reflection coefficient - amplitude')
legend ('Vertical Polarization','Horizontal Polarization')
pv = -angle(rv);
ph = angle(rh);
```

figure(2)
plot(psi,pv,'k',psi,ph,'k -.');
grid
xlabel('grazing angle - degrees');
ylabel('reflection coefficient - phase')
legend ('Vertical Polarization','Horizontal Polarization')

The parameters used here-

Symbol	Description
epsp	Real value of dielectric constant
epspp	Complex value of dielectric constant
rh	Reflection co-efficient (horizontal) $\lvert \Gamma_v \rvert$
rv	Reflection co-efficient (vertical) $\lvert \Gamma_h \rvert$
ph	Angle of reflection co-efficient (horizontal)
vh	Angle of reflection co-efficient (vertical)

Chapter 5

Code for Figure 5.4 (a), (b) and (c)

```
clear all;close all;
clc;
lambda = 0.1;
d=0.3;
eps = 0.000001;
k = 2. * pi / lambda;
r = d /2.;
beta = -pi:pi/200.:pi;
sinbet = sin(beta);
var = k * r .* sinbet; %2.0 * pi * (-2:0.001:2);
pattern = (2. * r^2) .* besselj(1,var) ./ (var);
maxval = max(abs(pattern));
pattern = pattern ./ maxval;
emod = 20. * log10(abs(pattern));

figure(1)
```

```
plot(var,emod,'k')
grid;
xlabel('kr*sin(angle)')
ylabel('Normalized radiation pattern');
minval = fix(min(var));
maxval = fix(max(var));
var3d = minval:.5:maxval;
[X,Y] = meshgrid(var3d,var3d);
U = sqrt(X.^2 + Y.^2) + eps;
z = 2. * besselj(1,U) ./ U;

figure (2)
mesh(abs(z))
axis off

figure(3)
polar(beta,pattern,'k')
```

Comment on code for figure 5.4

The Eq. used here-

$$E(\beta) = \pi r^2 \frac{2J_1(kr\sin\beta)}{kr\sin\beta} \tag{5.24}$$

Code for Figure 5.6 (a & b), 5.7 (a & b)

```
clear all;
close all;
eps = 0.00001;
k = 2*pi;
theta = -pi : pi / 10791 : pi;
var = sin(theta);
nelements = 8;
d = 1;        %   d = 1;
num = sin((nelements * k * d * 0.5) .* var);

if(abs(num) <= eps)
   num = eps;
end
den = sin((k* d * 0.5) .* var);
if(abs(den) <= eps)
   den = eps;
end
```

```
pattern = abs(num ./ den);
maxval = max(pattern);
pattern = pattern ./ maxval;

figure(1)
plot(var,pattern)
xlabel('sine angle - dimensionless')
ylabel('Array pattern')
grid

figure(2)
plot(var,20*log10(pattern))
axis ([-1 1 -60 0])
xlabel('sine angle - dimensionless')
ylabel('Power pattern [dB]')
grid;

figure(3)
theta = theta +pi/2;
polar(theta,pattern)
title ('Array pattern')

figure(4)
polardb(theta,pattern)
title ('Power pattern [dB]')
figurepallete
```

Comment on code for figure 5.6

The Eq. used here-

$$G\,(\sin\psi) = |\,E\,(\sin\psi)\,|^{\,2} = \frac{1}{N^2}\left(\frac{\sin(Nkd\sin\psi/2)}{\sin(kd\sin\psi/2)}\right)^{2} \qquad (5.33)$$

Code for Figure 5.9 (a, b, c & d), 5.10 (a, b & c)

```
function varargout = linear_array_gui(varargin)
gui_Singleton = 1;
gui_State = struct('gui_Name',       mfilename, ...
            'gui_Singleton',  gui_Singleton, ...
            'gui_OpeningFcn', @linear_array_gui_OpeningFcn, ...
            'gui_OutputFcn',  @linear_array_gui_OutputFcn, ...
            'gui_LayoutFcn',  [] , ...
            'gui_Callback',   []);
if nargin & isstr(varargin{1})
```

```
   gui_State.gui_Callback = str2func(varargin{1});
end

if nargout
   [varargout{1:nargout}] = gui_mainfcn(gui_State, varargin{:});
else
   gui_mainfcn(gui_State, varargin{:});
end

global Nr  dolr theta0 nbits

function InitializeToggleButton_CreateFcn(hObject, eventdata, handles)
if ispc
   set(hObject,'BackgroundColor','black');
else
   set(hObject,'BackgroundColor',get(0,'defaultUicontrolBackgroundColor'));
end

function InitializeToggleButton_Callback(hObject, eventdata, handles)
'InitializeToggleButton_Callback'
set(handles.Nr,'String', num2str(25))
set(handles.dolr,'String',num2str(0.5))
set(handles.theta0,'String',num2str(0))
set(handles.nbits,'String',num2str(-1))

function PlotToggleButton_CreateFcn(hObject, eventdata, handles)
if ispc
   set(hObject,'BackgroundColor','black');
else
   set(hObject,'BackgroundColor',get(0,'defaultUicontrolBackgroundColor'));
end

function PlotToggleButton_Callback(hObject, eventdata, handles)

'PlotToggleButton_Callback'
Nr = str2num(get(handles.Nr, 'String'))
dolr = str2num(get(handles.dolr, 'String'))
theta0 = str2num(get(handles.theta0, 'String'))
nbits = str2num(get(handles.nbits, 'String'))
winid = 1
win_type = get(handles.WindowChoice,'Value')
switch win_type
  case 1
    win = ones(Nr,1);
  case 2
    win = hamming(Nr) ;
```

```matlab
   case 3
      win = hanning(Nr) ;
   case 4
       win = kaiser(Nr,pi) ;
   case 5
      win = blackman(Nr) ;
end
[theta,patternr,patterng] = linear_array(Nr,dolr,theta0,winid,win,nbits);
figure(1)
plot(theta,patterng,'k')
grid
xlabel('Steering angle - degrees')
ylabel('Gain pattern - dB')
axis tight

function QuitToggleButton_CreateFcn(hObject, eventdata, handles)
if ispc
   set(hObject,'BackgroundColor','black');
else
   set(hObject,'BackgroundColor',get(0,'defaultUicontrolBackgroundColor'));
end

function QuitToggleButton_Callback(hObject, eventdata, handles)
'QuitToggleButton_Callback'
close all
clear all

function Nr_CreateFcn(hObject, eventdata, handles)
if ispc
   set(hObject,'BackgroundColor','white');
else
   set(hObject,'BackgroundColor',get(0,'defaultUicontrolBackgroundColor'));
end

function Nr_Callback(hObject, eventdata, handles)
Nr = str2double(get(hObject,'String'))
set(handles.Nr,'Value',Nr)

function dolr_CreateFcn(hObject, eventdata, handles)
if ispc
   set(hObject,'BackgroundColor','white');
else
   set(hObject,'BackgroundColor',get(0,'defaultUicontrolBackgroundColor'));
end
```

```
function dolr_Callback(hObject, eventdata, handles)
dolr = str2double(get(hObject,'String'))

function theta0_CreateFcn(hObject, eventdata, handles)
if ispc
    set(hObject,'BackgroundColor','white');
else
    set(hObject,'BackgroundColor',get(0,'defaultUicontrolBackgroundColor'));
end

function theta0_Callback(hObject, eventdata, handles)
theta0 = str2double(get(hObject,'String'))

function nbits_CreateFcn(hObject, eventdata, handles)
if ispc
    set(hObject,'BackgroundColor','white');
else
    set(hObject,'BackgroundColor',get(0,'defaultUicontrolBackgroundColor'));
end

function nbits_Callback(hObject, eventdata, handles)
nbits = str2double(get(hObject,'String'))
function WindowChoice_CreateFcn(hObject, eventdata, handles)
if ispc
    set(hObject,'BackgroundColor','white');
else
    set(hObject,'BackgroundColor',get(0,'defaultUicontrolBackgroundColor'));
end
'WindowChoice_CreateFcn'

function WindowChoice_Callback(hObject, eventdata, handles)
'WindowChoice_Callback'
get(handles.WindowChoice,'Value')
```

Comment on code for figure 5.9 and 5.10

The Eq. used here-

$$W(q) = \sum_{n=0}^{N-1} w(n)e^{\frac{j2\pi nq}{N}} \qquad ; \qquad q = 0,1,\dots\dots\dots.N-1 \qquad\qquad (5.42)$$